Mercury Oxidation over Selective Catalytic Reduction (SCR) Catalysts

Madsen, Karin

Publication date:
2011

Document Version
Publisher's PDF, also known as Version of record

Mercury Oxidation over Selective Catalytic Reduction (SCR) Catalysts

Karin Madsen

Haldor Topsøe A/S and
Department of Chemical and Biochemical Engineering
Technical University of Denmark
Kongens Lyngby, Denmark

Technical University of Denmark
Department of Chemical and Biochemical Engineering
Building 229, DK-2800 Kongens Lyngby, Denmark
Phone +45 45252800, Fax +45 45882258
kt@kt.dtu.dk
www.kt.dtu.dk

ISBN -13: 978-87-92481-50-4
Printed by Frydenberg A/S, Copenhagen, Denmark

Preface

The present thesis is written in accordance with the partial requirements of the Ph.D. degree at the Technical University of Denmark (DTU). The Ph.D. project was carried out between May 2008 and July 2011 at the Department of Chemical and Biochemical Engineering (DTU) within the CHEC (Combustion and Harmful Emission Control) research centre in cooperation with Haldor Topsøe A/S and the Danish Agency for Science, Technology and Innovation, which is an institute under the Danish Ministry of Science, Technology and Innovation. Professor Anker Degn Jensen, Department of Chemical and Biochemical Engineering (DTU), Dr. Joakim Reimer Thøgersen, Haldor Topsøe A/S, and Dr. Flemming J. Frandsen, Department of Chemical and Biochemical Engineering (DTU) were supervisors.

I would like to thank all my supervisors for their guidance, valuable input and continuing support in a project with many experimental challenges.

I would also like to thank all my colleagues at both Haldor Topsøe A/S and DTU for their help in many practical and theoretical aspects. Technicians Kim Rafaelsen, Tais Jeppesen and Jesper Sargent Larsen are gratefully acknowledged for all their help in the laboratory. Furthermore, Sidsel Marie Nielsen has continuously provided assistance with various LateX issues and Michael Lykke Heiredal has performed a number of CFD simulations for me.

Finally, I would like to thank my boyfriend Jonas for his patience and support throughout the whole project. My sister Kristine is also gratefully acknowledged for cooking many meals for me during the last very busy five months.

Summary

The vanadium-based SCR catalyst used for NOx-control promotes the oxidation of elemental mercury Hg^0 to Hg^{2+} in flue gases from coal-fired power plants. Hg^{2+} is water soluble and can effectively be captured in a wet scrubber. This means that the combination of an SCR with a wet FGD can offer an effective control option for mercury.

Laboratory experiments have been carried out to quantify the Hg^0 oxidation that can be achieved over commercial SCR catalysts for different gas compositions, operating conditions and catalyst types. The following three net reactions have been identified as relevant for the mercury chemistry over the SCR:

$$R1.\ \ 2\ HCl + Hg^0 + {}^1/_2\ O_2 \ \leftrightarrow\ HgCl_2 + H_2O$$
$$R2.\ \ 2\ NH_3 + 3\ HgCl_2 \ \leftrightarrow\ N_2 + 3\ Hg^0 + 6\ HCl$$
$$R3.\ \ 2\ NO + 2\ NH_3 + {}^1/_2\ O_2 \ \leftrightarrow\ 2\ N_2 + 3\ H_2O$$

where reaction R1 is the oxidation of Hg^0 by HCl, reaction R2 is the reduction of $HgCl_2$ by NH_3 and reaction R3 is the DeNOx reaction.

The importance of each reaction on the achievable Hg^0 oxidation depends on the SCR operating temperature. At T>325°C, the reduction of $HgCl_2$ will take place when NH_3 is present. The overall Hg^0 oxidation will then reflect the relative rate of the Hg^0 oxidation via reaction R1 and the $HgCl_2$ reduction via reaction R2. For T=250-375°C, the DeNOx reaction will inhibit the kinetics of reaction R1 by consuming active Lewis sites that must be oxidized to regain activity for Hg^0 oxidation.
The experimental data obtained in this study indicate that vanadia Lewis sites on SCR catalysts are active in the catalytic Hg^0 oxidation - possibly as Hg^0 adsorption sites.

A kinetic model for the steady-state Hg^0 oxidation over monolithic SCR reactors has been developed taking both external mass transfer, pore diffusion and reaction on the catalyst wall into account. The mercury chemistry that has been identified and quantified in the experimental investigations is incorporated in the model.
The resulting model successfully reproduces the variations in Hg^0 oxidation over the SCR that have been experimentally observed for different gas compositions and testing conditions. This verifies that the relevant mercury chemistry has been taken into account in order to describe the catalytic Hg^0 oxidation in a simulated flue gas. The validity of the model for describing the mercury chemistry over SCR catalysts in real

flue gases is yet to be explored.

Model predictions suggest that the kinetics of the Hg^0 oxidation over high dust SCR reactors is greatly limited by external mass transfer in the entire SCR operating temperature window if HCl≥13 ppm. For lower HCl concentrations, the surface reactivity of the SCR catalyst towards Hg^0 oxidation can become limiting at the higher operating temperatures T>350^{o}C, because the rate of $HgCl_2$ reduction will be considerable. A higher V_2O_5 load on the SCR catalyst will dampen this effect.

Resumé

Den vanadium-baserede SCR (Selective Catalytic Reduction) katalysator anvendes typisk til reduktion af NOx-forbindelser. SCR reaktorer viser sig desuden også at fremme oxidationen af elementært kviksølv Hg^0 til Hg^{2+} i røggasser fra kulfyrede kraftværker. Dette er hensigtsmæssigt, da Hg^{2+} (i modsætning til Hg^0) er vandopløselig og kan således effektivt opfanges i en våd skrubber til SO_2 kontrol. Derved er kombinationen af en SCR reaktor og et vådt afsvovlingsanlæg en mulig løsning for opfangning af kviksølv i røggasser.

Laboratorieforsøg er blevet udført under dette Ph.D-studie for at kvantificere den Hg^0 oxidation, som kan opnås over kommercielle SCR-katalysatorer ved forskellige gassammensætninger, operationsbetingelser og katalysatortyper. Herved er de følgende tre reaktioner blevet identificeret som relevante for kviksølvkemien over SCR-katalysatorer:

$$R1.\ \ 2\ HCl + Hg^0 + {}^1\!/_2\ O_2 \ \leftrightarrow\ HgCl_2 + H_2O$$
$$R2.\ \ 2\ NH_3 + 3\ HgCl_2 \ \leftrightarrow\ N_2 + 3\ Hg^0 + 6\ HCl$$
$$R3.\ \ 2\ NO + 2\ NH_3 + {}^1\!/_2\ O_2 \ \leftrightarrow\ 2\ N_2 + 3\ H_2O$$

Reaktion R1 er oxidationen af Hg^0 med klor, reaktion R2 er reduktionen af $HgCl_2$ med NH_3 og reaktion R3 er reduktionen af NO med NH_3 (DeNOx reaktionen).

Vigtigheden af de enkelte reaktioner for den samlede Hg^0 oxidation afhænger af SCR operationstemperaturen. For T>325^{o}C vil reduktionen af $HgCl_2$ finde sted så længe NH_3 er til stede. Den samlede Hg^0 oxidation vil derfor afspejle den relative hastighed af Hg^0 oxidationen via reaktion R1 og $HgCl_2$ reduktionen via reaktion R2. For T=250-375^{o}C vil DeNOx reaktionen sænke hastigheden af reaktion R1 ved at forbruge aktive vanadinoxid-sites på overfladen af katalysatoren. Disse sites skal reoxideres for at generhverve aktivitet for Hg^0 oxidationen.

I den anden del af Ph.D. studiet er en kinetisk model blevet opbygget, som beskriver steady-state Hg^0 oxidationen over monolitiske SCR-katalysatorer. Denne model tager højde for både ekstern gas-diffusion, samt pore-diffusion og reaktion i katalysatorvæggen. I reaktionshastighederne for R1 og R2 er inkorporeret den kviksølvkemi, som er blevet identificeret og kvantificeret i det eksperimentelle studie.

Den fremkomne model formår at reproducere alle variationer i Hg^0 oxidationen over SCR-katalysatoren, som er observeret i laboratoriet. Hermed verificeres, at der er taget højde for den relevante kviksølvkemi, som finder sted under betingelserne i laboratoriet.

Modellen forudsiger, at kinetikken for Hg^0 oxidationen over high dust SCR-reaktorer primært afgøres af den eksterne gas-diffusion, når koncentrationen af HCl i gasfasen er højere end 13 ppm. Kun for lavere HCl koncentrationer ved høje SCR operationstemperaturer (T>350°C) vil selve katalysatoraktiviteten blive begrænsende for den samlede Hg^0 oxidation, fordi hastigheden for $HgCl_2$ reduktionen under disse betingelser vil være høj.

Contents

Chapter 1

Background and scope of project

1.1 Background

1.1.1 Mercury emissions, health impacts and legislation

The worldwide anthropogenic emission of mercury to the environment was in 2005 estimated to be 1913 tonnes per year (AMAP/UNEP, 2008). 45% of this was estimated to come from the combustion of fossil fuels.

The emitted mercury will deposit on land or water, where it can transform into methylmercury and thereby enter the food chain. Humans are most likely exposed to methylmercury through the consumption of fish. The primary health effect of methylmercury is an impaired neurological development for fetuses, infants, and children (EPA, 2011a).

The US Environmental Protection Agency (EPA) and UN legislation have determined that mercury emissions from power plants pose a significant hazard to public health and have therefore proposed regulations:
Within the UN, an UNECE Protocol on Heavy Metals (UNECE, 2011) is adopted that requires reduction in mercury, cadmium and lead. Parties within the UN will have to reduce their emissions of these three metals below their levels in 1990. The protocol requires the implementation of best available techniques (BAT) for new and existing stationary sources.
On March 16, 2011, the U.S. EPA has proposed standards to limit mercury, acid gases and other toxic pollutants from power plants in the US. The emission limit will prevent 91% of mercury in coal from being released to the air, which will require upgrading of existing controls in order to achieve the required reduction in emissions. A final rule is to be completed by November 2011. The proposed rule provides up to 4 years for facilities to meet the standards (EPA, 2011b).

1.1.2 Mercury in coal-fired power plants

Mercury is present in coal in the order of 0.1 ppmw, which yields concentrations in combustion gases at power plants in the range of 1-20μg/m^3 (Senior, 2001). The amount of mercury emitted to the atmosphere will depend on the fuel, the operating conditions and the air pollution control devices (APCDs) installed.

Existing APCDs for control of other pollutants is found to remove some mercury. The approach of integrating mercury control with other regulatory actions, such as NOx, particulate and/or SO_2-removal offers a reduced compliance cost compared to introducing dedicated mercury control options.

Mercury speciation and capture in existing APCDs

Available measurement techniques only allow for routine measurements of elemental Hg^0, oxidized Hg^{2+} and particulate bound mercury Hg^p in flue gases. The distribution of mercury between these three form is referred to as the **speciation of mercury** (Kolker et al., 2006).

The speciation of mercury will determine the capture in existing APCDs due to differences in properties (Miller et al., 2006)

- Hg^0 is very volatile and difficult to capture
- Hg^{2+} is water soluble and can be effectively removed in a wet desulphurization device
- Hg^p can be effectively removed in a particulate control device (PCD).

Based on measurements at over 80 coal-fired power plant plants in the US (Senior, 2001), it was shown that mercury removals for plants burning bituminous coals generally were higher than those burning subbituminous and lignite coals. The lower removals were in turn an effect of a larger fraction of mercury being on the elemental form Hg^0.

Mercury control with the combination SCR + wFGD

A wet flue gas desulphurization (FGD) device will capture oxidized mercury Hg^{2+} in the flue gas with an efficiency around 90%, whereas almost no Hg^0 will be captured (Pavlish et al., 2003). An increased fraction of Hg^{2+} will therefore enhance the mercury removal in a wet FGD. The selective catalytic reduction (SCR) catalyst used for NOx-control has been shown to promote the oxidation of Hg^0 to Hg^{2+} in coal-fired power plants.
For bituminous coal combustion, the combination of an SCR with a wet FGD have been shown to give superior mercury removals compared to systems without the SCR (Chu et al., 2003; Miller et al., 2006; Withum, 2006). The total mercury capture ranged

from 43-87% for the FGD alone and 56-97% for the SCR-FGD combination.
This strategy poses an option for mercury capture by a wet FGD for flue gases that would otherwise primarily contain elemental Hg^0.

Mercury oxidation over SCR reactors

The oxidation of Hg^0 over full-scale SCR reactors has been reported in the range of 4-98% (Senior, 2004b) depending on coal rank/type, operating conditions and catalyst type/geometry.
Hg^0 is oxidized by halogens in the flue gas. Chlorine is primarily responsible for the oxidation, since this halogen is typically present in the highest concentrations in coal (Vassilev et al., 2000). The net reaction takes the following form

$$Hg^0(g) + 2\ HCl(g) + 1/2\ O_2(g) \leftrightarrow HgCl_2(g) + H_2O(g) \tag{1.1}$$

The concentration of chlorine in the coal appears to be the major determining factor for the observed Hg^0 oxidation across different SCR applications, where an increasing oxidation is seen for increasing HCl. There is a general tendency of lower oxidation achieved over SCR reactors for subbituminous coal combustion compared to bituminous coals (Serre et al., 2008), which in part is due to a typically lower concentration of chlorine in lower rank coals.
Recent research shows that bromine can be effective for oxidizing Hg^0 even at low concentrations (e.g. Eswaran and Stenger (2008)) and may play a role for the mercury chemistry in flue-gases. That will not be covered here.

In the SCR process, NOx is reduced by reacting with NH_3 over a vanadium catalyst according to the reaction stoichiometry

$$4\ NO(g) + 4\ NH_3 + O_2(g) \leftrightarrow 4\ N_2(g) + 6\ H_2O(g) \tag{1.2}$$

$$2\ NO_2(g) + 4\ NH_3(g) + O_2(g) \leftrightarrow 3\ N_2(g) + 6\ H_2O(g) \tag{1.3}$$

The oxidation of Hg^0 is a lucky side reaction over commercial SCR reactors that are optimized for the NOx-reduction. An interesting controversy is posed for the now two feasible reactions across the SCR as it turns out that the DeNOx reaction inhibits the oxidation of Hg^0.

The promoting effect of HCl and inhibiting effect of the DeNOx reaction has been seen across lab-, pilot- and full-scale experiments (e.g (Hong et al., 2010; Machalek et al., 2003; Senior, 2004a)). The influence of other flue gas constituents, operating conditions and catalyst properties is not as unambiguously reported in literature.
Since there is a considerable scatter in the level of Hg^0 oxidation seen in full-scale, a better understanding of the relevant mercury chemistry over the SCR catalysts is needed in order to optimize the oxidation across different applications.

Research on mercury chemistry over SCR reactors has only taken place in the last decade and a fundamental understanding of the relevant chemistry is still in its early stage. Firstly, the mechanism for the catalytic Hg^0 oxidation by HCl remains poorly

understood. Furthermore, the interplay between the DeNOx reaction and the Hg^0 oxidation under different operating conditions has not been fully clarified.

1.2 Scope of project

This PhD-study focuses on the mercury chemistry over SCR catalysts for coal-fired power plants.

The main objective of the study has been to quantify the Hg^0 oxidation by HCl over commercial SCR catalysts for different gas compositions and operating conditions. Based on this, the second objective has been to develop a predictive model for the Hg^0 oxidation that can be achieved across SCR reactors at different applications.

For the purpose, I have built a laboratory setup at Haldor Topsøe A/S, where the mercury oxidation/chemistry over SCR catalysts has been studied in a simulated flue gas. Experimental investigations are performed to study the effects of relevant flue gas components under different operating conditions and for different catalyst compositions/geometries. By doing this, the work should increase the fundamental understanding of mercury chemistry over SCR catalyst by further elucidating e.g. the mechanism for the catalytic oxidation by HCl and/or the interaction between the DeNOx reaction and mercury.
The experimental methodology is described in chapter 3.

A kinetic model has been set up describing the reactions taking place over a monolithic SCR reactor, where both mass transfer phenomena and surface reactions on the catalyst wall will determine the overall Hg^0 oxidation.
The modelling methodology is described in chapter 4.

This thesis consists of four parts. Chapters 5 and 6 quantifies relevant mercury chemistry over the SCR via experimental investigations. Chapter 7 derives rate expressions for the mercury surface reactions taking place over the SCR via microkinetic modelling. Finally, chapter 8 models the Hg^0 oxidation over the SCR reactor by applying the three latter chapters.

Chapter 2

Literature study

2.1 Introduction

This section introduces to mercury chemistry taking place in flue gases from coal-fired power plants upstream of air pollution control devices.

2.1.1 Mercury and chlorine in coal

The mercury content of coal differs by coal basin, by rank and even within individual coal beds. The average coal concentrations of mercury in US, Russia and China have been estimated to be 0.1, 0.08 and 0.15 ppmw (Kolker et al., 2006).

A summary of coal-data for 40.000 fuels samples delivered to US power plants in 1999 is given in table 2.1.

Table 2.1: Data on selected components in utility coal by region and coal rank. A summary of ICR data from (Pavlish et al., 2003). Average coal analysis, dry basis.

Coal rank	**Bituminous**			**Subbit.**	**Lignite**	
Region	Appalachian	Interior	Western	Western	Fort Union	Gulf Coast
Hg [ppb]	126	90	49	68	90	119
Cl [ppm]	948	1348	215	124	139	221

The average mercury concentrations ranges from 49 ppb in Western bituminous to 126 ppb in Appalachian bituminous coal. Switching from a high Hg-coal to a low Hg-coal could intuitively be a source the decreased mercury emissions. However, the percentage

of mercury that will be emitted to the atmosphere greatly depends on other components in the coal, especially HCl (Pavlish et al., 2003).

The chlorine concentration in coal tends to increase with increasing coal age and rank, but will vary greatly across different regions (Tillman et al., 2009). In the US, eastern bituminous coals contain (average) clorine concentrations in the range 283-1262 ppmw, whereas Western coals (lignite, subbituminous and bituminous) have significantly lower chlorine concentrations in the range 70-149 ppm. The concentration of chlorine in coals outside the US has been seen to vary greatly in the range 80-1090 ppm.

This average mercury concentration of 0.1 ppmw in coal translates into a flue gas concentration of around 1.2 ppb (11 μg/Nm^3), whereas the range of chlorine concentrations in coal 70-1262 ppmw translates into flue gas concentrations in the range 5-89 ppm (8-144 mg/Nm^3). Chlorine will always be present in great excess compared to mercury.

2.1.2 Mercury equilibrium speciation

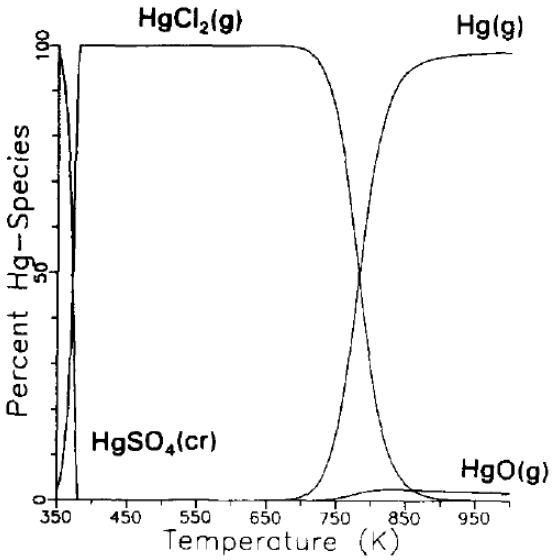

Figure 2.1: Equilibrium distribution of mercury in a typical subbituminous combustion under oxidative conditions assuming global thermodynamic equilibrium (Frandsen et al., 1994). The concentration of chlorine in the coal was set to 300 ppmw $\approx$ 21 ppm in the flue gas.

Global thermodynamic equilibrium calculations find that the oxidized form of mercury in combustion flue gases is primarily mercury(II)-chloride $HgCl_2$. These equilibrium calculations show that $HgCl_2$(g) is the only stable specie of mercury between 380 and 700 K (107-427^{o}C) (Frandsen et al., 1994). The equilibrium distribution of mercury is shown in figure 2.1.

Above 700 K (427^{o}C), the equilibrium will shift gradually towards Hg^0(g) and HgO(g) with Hg^0(g) as the major stable form accounting for more than 90% of the mercury.

The given calculation was performed for a chlorine concentration of 300 ppmw in the coal. Under reducing conditions, only Hg^0 is formed.

It is found that temperature and chlorine concentration are the parameters with greatest impact on mercury speciation under equilibrium conditions (Senior et al., 2000). With decreasing chlorine concentration in the coal, the equilibrium speciation will be shifted towards Hg^0 at lower temperatures.

However, equilibrium will not be attained for mercury in coal-combustion flue gases (Senior et al., 2000). Measurements of mercury speciation in coal-fired power plants show anywhere from 30-95% Hg^{2+} upstream of various APCDs, where all mercury should exist as $HgCl_2$ according to thermodynamics. It is therefore concluded that Hg^0 oxidation in flue gases is limited by kinetics.

2.1.3 Mercury transformations in flue gases

During combustion of coal, all mercury will be released as Hg^0 due to the high temperatures and the volatility of mercury. Only as the flue gas is cooled below 1200 K (927^{o}C) (TOMERED - Deliverable D08, 2006), will mercury speciation towards Hg^{2+} and Hg^p start to take place via homogeneous gas-phase oxidation and by heterogeneous interactions with the fly ash.

2.1.3.1 Homogenous oxidation

The homogeneous oxidation of Hg^0 in flue gases primarily depends on the chlorine concentration and the thermal quench rate of the flue gas after the boiler.

Gaseous chlorine is predicted to primarily be present as HCl in the flue gas (Senior et al., 2000). However, the direct reaction of Hg^0 with HCl is not seen to be of importance to the gas-phase oxidation of Hg^0 due to a very high energy barrier for the reaction (Niksa et al., 2001; Sliger et al., 2000).

The mechanism for the homogeneous oxidation of Hg^0 is via chemical kinetic modelling proposed to take place in a Cl-radical recycle process in the cooling quench of the flue gas (Niksa et al., 2001):

$$Hg^0 + Cl\bullet \rightarrow HgCl \tag{2.1}$$

$$HgCl + Cl_2 \rightarrow HgCl_2 + Cl\bullet \tag{2.2}$$

Sliger et al. (2000) show for a very high HCl concentration (453 ppm) that the reaction primarily takes place in a temperature window between 400-700^{o}C. Here a super-equilibrium concentration of Cl-radicals will be present, while being in a region where $HgCl_2$ is favoured by thermodynamics. The concentrations of both Cl_2-molecules and especially Cl-radicals are therefore of importance to the homogeneous oxidation.

2.1.3.2 Heterogenous interactions with fly ash

Fly ash has both shown the ability to promote Hg^0 oxidation as well as capture mercury by adsorption of Hg^0 and/or $HgCl_2$ on the surface.

Unburned carbon in the fly ash has been demonstrated to play a major role for the adsorption of mercury (Gale et al., 2008; Hocquel, 2004; Huggins et al., 2000; López-Antón et al., 2009). Mercury adsorption (both Hg^0 and $HgCl_2$) is seen to take place on fly ash from combustion of different rank coals (both bituminous, subbituminous and lignite coal) at 120-177^{o}C and the mercury capture will increase with increasing (BET-) surface area (Dunham et al., 2003; López-Antón et al., 2009).
From surface characterisation studies, Huggins et al. (2003) show that adsorbed mercury is probably present as ionic mercury in connection with e.g. sulphide, chlorine or oxygen-anions on the surface, which can explain an increased fraction of Hg^p seen for increasing coal-chlorine concentration (Senior, 2001).

Some fly ashes also have the ability to oxidize Hg^0 (Dunham et al., 2003; Norton et al., 2003). In the work by Dunham et al. (2003), both unburned carbon and Fe_3O_4 in the ash are observed to be active for Hg^0 oxidation at T=121-177^{o}C. However, the composition of the flue gas was seen to affect the heterogeneous Hg^0 oxidation more than the composition of the fly ash from a bituminous coal at 180^o (Norton et al., 2003).
Lee et al. (2000) study the effect of temperature on the heterogeneous oxidation over a fly ash from a bituminous coal. They find a decreasing Hg^0 oxidation with increasing temperature in the range 100-500^{o}C. No oxidation is observed at 500^{o}C. This observation indicates that the heterogeneous oxidation of Hg^0 is mechanistically linked to the adsorption on the fly ash, which is also concluded by Dunham et al. (2003).

Different effects of CaO have been reported based on experimental data. Increasing CaO in the fly ash has been shown to increase mercury capture on fly ash in combustion systems (Gale et al., 2008), but CaO has also been reported to inhibit Hg^0 oxidation in flue gases. Experiments with pure CaO powder show that $HgCl_2$ adsorbs on CaO at 150-300^o. The sorption is apparently accompanied by a reduction of some of the $HgCl_2$ to Hg^0. The sorption rate decreases with increasing temperature, while the reduction rate increases (Hocquel, 2004).
In fixed bed experiments with model fly ashes, Ghorishi et al. (1999) report that CaO inhibits the heterogeneous Hg^0 oxidation by binding gas-phase HCl (producing $CaCl_2$) rendering chlorine unavailable for reactions with Hg^0.
Noticeably, even more different effects of CaO have been stated in literature, where no experimental evidence for it appears to exist. Care must be taken, when applying conclusions on the effect of CaO.

An analysis of full-scale data from 80 power plants shows that the fraction of particulate bound mercury at the inlet to PCDs is influenced by the chlorine concentration and the temperature (Senior, 2001). At temperatures above 260^{o}C, the speciation of mercury appears to be determined by the temperature at the inlet to the PCD, where decreasing temperature favours Hg^p formation. At lower temperature, the effects of other factors such as coal-chlorine and ash composition become evident. At coal-chlorine concentrations greater than 150-200 ppm in the coal, there is a trend of increasing Hg^p from 10%

up to a level of 75%.

2.1.4 Summary

The oxidation of Hg^0 to $HgCl_2$ is limited by kinetics in flue gases from coal-fired power plants.

The mercury chemistry upstream of APCDs has been shown to be dependent on a complex interplay between the time-temperature history, the flue gas composition (especially HCl) and the fly ash composition (especially unburned carbon). This will in term be dependent on the fuel type, the boiler type/operation and the operating conditions in the duct.

The homogeneous oxidation of Hg^0 will cease after the cooling quench at temperatures below 400^{o}C and will therefore be unimportant over and after the SCR. In contrast, the heterogeneous interactions will start to take place around SCR operating temperature (250-450^{o}C) and will become increasingly important in the duct after the SCR, where the temperature will decrease further. A continuous change in mercury speciation after the SCR has been reported in full-scale (e.g. (Chu et al., 2003)) and can probably be accredited to heterogeneous interactions with the fly ash.

The mercury speciation after the SCR is therefore a combined effect of:

- Homogeneous oxidation upstream of the SCR
- Catalytic oxidation over the SCR, and
- Heterogeneous interactions with the fly ash.

2.2 The SCR process

2.2.1 The reactions

Selective catalytic reduction (SCR) is the predominant choice for removal of NOx-species (NO and NO_2) in flue gases. In the SCR-process, NOx is reduced by reacting with NH_3 over a vanadium catalyst according to following reaction stoichiometry:

$$4\ NO(g) + 4\ NH_3(g) + O_2(g) \leftrightarrow 4\ N_2(g) + 6\ H_2O(g) \tag{2.3}$$

$$2\ NO_2(g) + 4\ NH_3(g) + O_2(g) \leftrightarrow 3\ N_2(g) + 6\ H_2O(g) \tag{2.4}$$

The process typically takes place in the range 250-450^{o}C and yields NOx removal rates in excess of 95% (Slabiak, 2005). The reactions will be referred to as the *DeNOx reaction*.

Typical commercial SCR catalysts consist of a porous titanium-dioxide (TiO_2) carrier material in which vanadium pentoxide (V_2O_5) combined with tungsten trioxide (WO_3)

are dispersed. Vanadium pentoxide constitutes the active phase in the SCR process (Gabrielsson and Pedersen, 2008).
Supported vanadium oxides can be present in the differing molecular configurations depending on the load as given on figure 2.2. For low vanadia load, only isolated monomeric species are present on the surface. For increased loading, monomeric vanadia species start reacting producing dimeric or polymeric vanadia species. Both mono and polymeric vanadates are characterised by V=O bands.

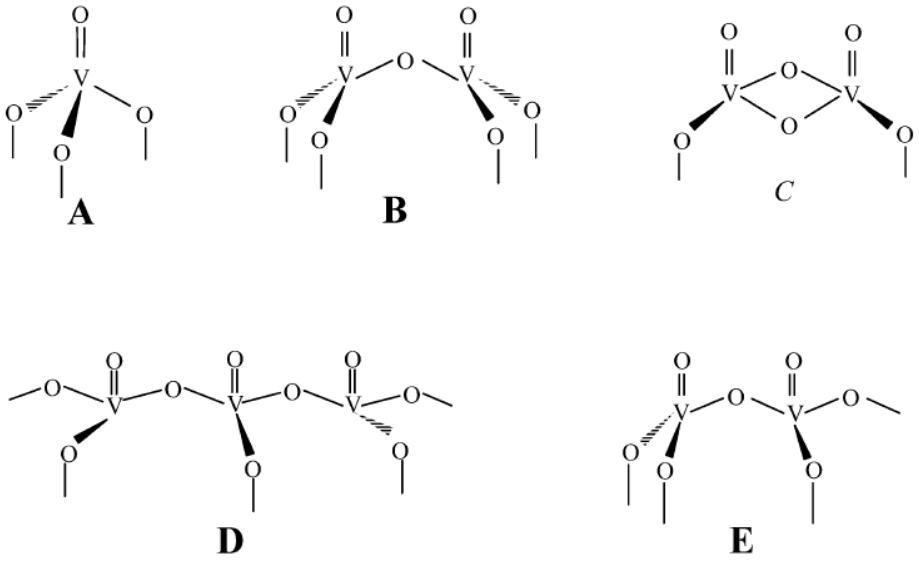

Figure 2.2: Structural models for monomeric (A), dimeric (B and C) and polymeric (D and E) dispersed surface vanadate species. (Giakoumelou et al., 2006).

2.2.2 Process design

Industrial SCR reactors contain up to four catalyst layers with spacing in between. Each layer consists of different catalysts assembled in modules. Monolithic catalysts are used to achieve low pressure drops, large external surface and good resistance to attrition and dust deposition.
Commercial SCR catalysts are normally classified as plate-type, honeycomb (extruded) or corrugated. Figure 2.3(a) shows a typical SCR reactor and figure 2.3(b) shows the Topsøe SCR DNX catalyst, which is classified as corrugated plate-type.

High dust configuration is the most widely used SCR configuration in coal-fired power plants. The name 'high dust' indicates that no particulates have been removed from the flue gas prior to the DeNOx process. The main advantage is that the temperature right after the boiler economizer is in the range suitable for the SCR reaction (Castellino, 2008; Gabrielsson and Pedersen, 2008).

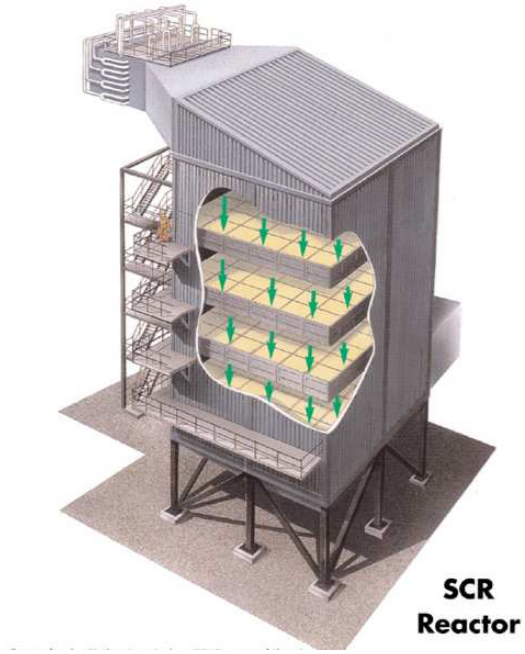

(a) Courtesy of Alstom.

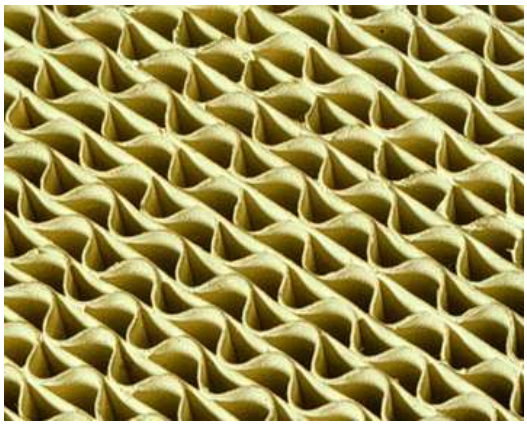

(b) Courtesy of Haldor Topsøe A/S.

Figure 2.3: a: Illustration of SCR reactor, b: Topsoe SCR DNX catalyst.

2.2.3 NO reduction by NH_3

The NOx reduction by NH_3 is regarded by many workers in the field as an Eley-Rideal mechanism under normal SCR operating conditions (Gabrielsson and Pedersen, 2008), where NH_3 adsorbs on the surface and reacts with gaseous NO.
Topsoe (1994) proposes the scheme given in figure 2.4 for the catalytic reduction of NO. The reduction of NO with NH_3 involves both acid- and redox-sites on the catalyst. NH_3 adsorbs on Brønsted acid sites that are supplied by vanadia V^{5+}-OH-sites. The mechanism consists of an initial reduction of the Lewis acid site V^{5+}=O by interaction with adsorbed NH_3, which in turn becomes more activated. This activated NH_3 then reacts with gaseous (or weakly bound) NO releasing V^{4+}-OH. The reduced redox-site can then be reoxidized by O_2 to regenerate V^{5+}=O.

The rate of the surface reaction is dependent on the NO, NO_2 NH_3, O_2 and H_2O concentrations. Complex rate expressions for the catalytic reduction of NO have been proposed based on micro-kinetic modelling (e.g. Dumesic et al. (1996)) in order to describe the kinetics of the reaction under a wide range of reaction conditions.
In the operating window of 300-400^{o}C, a simple Eley-Rideal mechanism is often adopted for describing the kinetics of the reaction (Beeckman and Hegedus, 1991; Beretta et al., 1998). This rate expression takes the form

$$-r_{NO} = k \cdot P_{NO} \cdot \frac{K_{NH_3} \cdot P_{NH_3}}{1 + K_{NH_3} \cdot P_{NH_3}} \tag{2.5}$$

where k is the reaction rate constant and K_{NH_3} is the adsorption coefficient of NH_3.

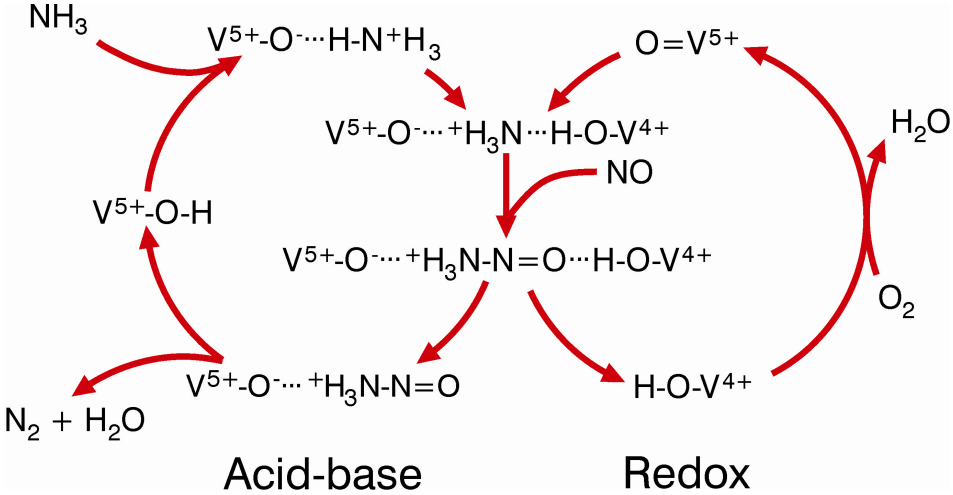

Figure 2.4: The proposed reaction mechanism for NO reduction by NH_3 (Topsoe, 1994).

2.3 Mercury chemistry over SCR catalysts in simulated flue gases

This section will focus on the more fundamental studies of mercury chemistry over SCR catalysts. The study will, therefore, primarily cover laboratory experiments carried out in simulated flue gases. This offers a well-defined system, where important pathways can be identified. Naturally care must be taken to ensure, that the gas compositions tested are relevant for real flue gases.

Only commercial type SCR catalysts for the system $V_2O_5/WO_3/TiO_2$ are considered.

Details on laboratory experiments run in simulated flue gases are given in tables A.1-A.3 in appendix A.

2.3.1 The active phase

The active phase for Hg^0-oxidation over $V_2O_5/WO_3/TiO_2$ SCR catalysts is believed to be vanadia V_2O_5.

In laboratory experiments by Hocquel (2004), the pure metal oxide V_2O_5 is seen to oxidize Hg^0 to $HgCl_2$ for T>170°C in a gas containing 200 $^{mg}/_{m^3}$ HCl. The pure metal oxides TiO_2 and WO_3 are observed to only have negligible influence on the oxidation of Hg^0 by HCl in the temperature range 200-350°C. Analogously, Kamata et al. (2008) show that TiO_2 is essentially inactive for the Hg^0-oxidation by HCl at 150°C.

A linear relationship between vanadia-loading and catalyst activity has been observed (up to a monolayer coverage) showing that both isolated and polymeric vanadate species are active for the Hg^0-oxidation. The effect is seen by Kamata et al. (2008) for V_2O_5/TiO_2

powders and by Struckmann et al. (2008) for two commercial-type catalysts.

2.3.2 Adsorption phenomena of reactants

Studying the adsorption phenomena of mercury and HCl on the SCR can give information on steps in the mechanism for the catalytic Hg^0 oxidation on the SCR catalyst.

2.3.2.1 Mercury adsorption

Elemental mercury Hg^0 is seen to adsorb on SCR catalysts, but the capacity is dependent on the formulation of the catalyst, the temperature and especially the flue gas composition. Hocquel (2004) estimates a mercury adsorption capacity between 1-10 mg/kg catalyst in gases with low HCl ($\approx$ 5 mg/m^3) for commercial SCR catalyst.

The adsorption of Hg^0 on SCR catalysts will primarily take place under oxidative conditions. The adsorption a simple N_2-atmosphere has been shown to be greatly reduced or even eliminated at 300-350°C compared to experiments with O_2 (Eom et al., 2008; He et al., 2009).
The great difference in adsorption capacity indicates that the Hg^0 adsorption taking place in the absence of O_2 may not be representative for real flue gases. Therefore, only experiments performed in the presence of O_2 are considered here (unless otherwise stated).

Hocquel (2004) has reported a major study of mercury sorption in a gas containing HCl, O_2 and H_2O in N_2. The author has studied the Hg^0 adsorption on different commercial SCR catalysts and finds that the adsorption is predominantly influenced by the HCl concentration. The adsorption decreases with increasing HCl concentration up to HCl>50 mg/m^3 (30 ppm), where it is completely eliminated.

The presence of NO and NH_3 in the gas (and thus a concomitant DeNOx reaction) has been seen to decrease the Hg^0-adsorption (Eom et al., 2008; Hong et al., 2010) at 250-350°C.

In terms of catalyst formulation, the study by Hocquel (2004) shows an increasing adsorption with increasing V_2O_5-loading for commercial-type catalysts and only a negligible adsorption was found for an inactive ceramic honeycomb carrier. No adsorption is found on the pure metal oxides TiO_2, WO_3 or V_2O_5 at 330°C.
Thorwarth (2007) finds a continuous adsorption of Hg^0 on both V_2O_5/TiO_2, V_2O_5/WO_3-$/TiO_2$ and WO_3/TiO_2 commercial type catalyst. The study demonstrates the capability of each of the supported metal oxides WO_3 and V_2O_5 to adsorb Hg^0.

Very limited data has been published on the adsorption of $HgCl_2$ on SCR catalyst, which is possibly due to the very low adsorption capacity for this specie. Hocquel (2004) states that $HgCl_2$ does not adsorb on the catalyst, but he shows no data to support this. In a study by Thorwarth (2007), desorption of mercury is seen for a commercial type catalyst that has been exposed to $HgCl_2$. That proves that adsorption

is not completely eliminated for this specie even though it is minor.

2.3.2.2 Transient sorption phenomena

Changes in the gas composition will change the capacity for Hg^0 adsorption on the SCR. The result can be an additional adsorption or desorption of adsorbed mercury. Studying the transient sorption phenomena of mercury that occur by such changes can give information on interaction between mercury and the component that has changed concentration.

Hocquel (2004) impose a stepwise increase in HCl from 3.7-122 mg/m^3 over an SCR catalyst that has been conditioned in a gas with Hg^0 for 30 minutes. The effect is desorption of oxidized mercury rapidly after. Adsorption is eliminated after this point and appears to be replaced by a continuous oxidation of the gaseous Hg^0. The author proposes that the effect of HCl can be explained by:

1. HCl adsorbs on the catalyst on the same site as Hg^0. Mercury is bound in an oxidized form and is displaced from the catalyst surface by HCl, or
2. Adsorbed mercury is volatilized by reaction with HCl producing $HgCl_2$.

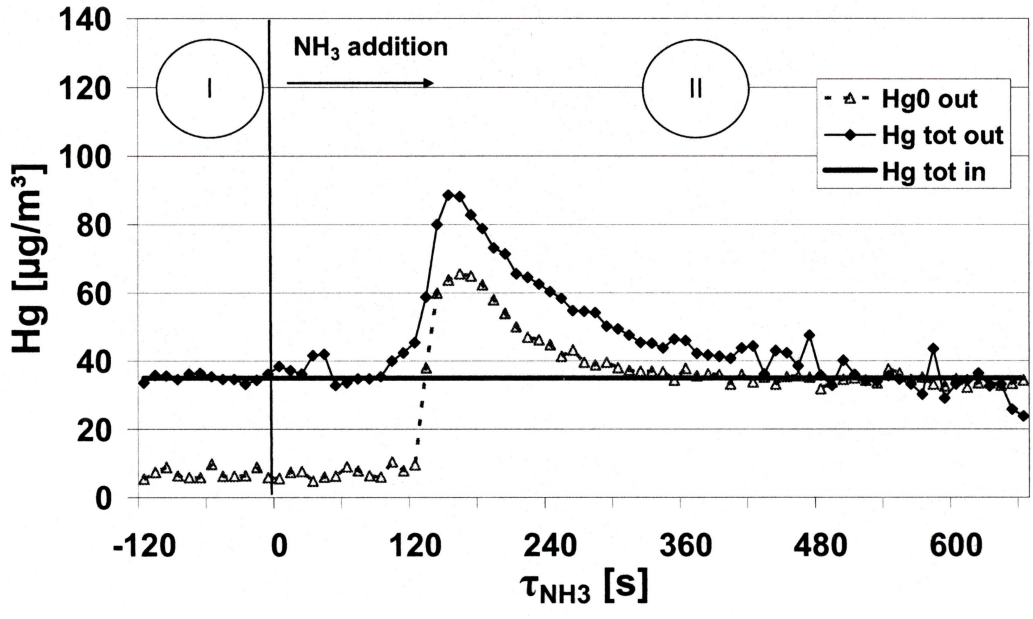

Figure 2.5: The transient mercury sorption behaviour on a $1.8\%V_2O_5/TiO_2$ SCR after a step addition of 620 ppm NH_3 (Thorwarth, 2007). Primarily $HgCl_2$ is present at the SCR inlet and only negligible adsorption is seen in the absence of NH_3. The step addition NH_3 causes a desorption of primarily Hg^0 and a reduction of all $HgCl_2$ to Hg^0.

Thorwarth (2007) studies the effect of a stepwise increase in NH_3 from 0-620 ppm NH_3 on four commercial type catalysts that have been conditioned in a gas with either Hg^0

or $HgCl_2$.
The test with Hg^0 is performed in the absence of HCl. A continuous adsorption of mercury is still taking place after the preconditioning and no oxidation takes place. In contrast, the test with $HgCl_2$ is performed in the presence of 20 mg/m^3 HCl. No adsorption is observed to take place and most of the mercury after the SCR continues to be $HgCl_2$.

For both experiments, the effect of a step increase in NH_3 is desorption of Hg^0. Firstly, this shows that the presence of NH_3 is able to break the coordination between adsorbed mercury (in whatever form) and the catalyst.
Secondly, the fact that Hg^0 is desorbing in both experiments could at a first glance simply suggest that both Hg^0 and $HgCl_2$ binds on the catalyst as Hg^0, but this may not be the case. In the experiment with $HgCl_2$, the presence of NH_3 appears to also remove a fraction of the gaseous $HgCl_2$ over the SCR, which shows that a reduction of gas phase $HgCl_2$ to Hg^0 is taking place with NH_3. The experiment with $HgCl_2$ is shown in figure 2.5. Apparently, NH_3 has the ability to reduce $HgCl_2$, so it is plausible that some of the mercury could bind in an oxidized form. Two hypotheses for the interaction between NH_3 and mercury can be posed:

1. NH_3 binds on the same site as mercury. Mercury is bound as Hg^0 and is displaced from the catalyst surface by NH_3, or

2. Adsorbed mercury is bound in an oxidized form, and is volatilized by a reduction by NH_3 producing Hg^0.

NH_3 is known to primarily adsorb on Brønsted-sites on vanadia on the SCR catalyst (Topsoe, 1994). Hypothesis 1 would then suggest that mercury binds on Brønsted-sites.

The reduction of $HgCl_2$ by NH_3 will be discussed further in section 2.3.3.

2.3.2.3 HCl adsorption

Only a few indirect measurements have been performed to confirm that HCl adsorption is taking place on the SCR catalyst (Eom et al., 2008; He et al., 2009).

He et al. (2009) expose a fresh SCR catalyst to 50 ppm HCl in a N_2-atmosphere for two hours. Subsequently, a gas containing Hg^0 in N_2 is passed over the catalyst. An increased Hg^0 adsorption is now seen to take place over the catalyst compared to adsorption on a catalyst that has not been preexposed to HCl. In the same time period, a minor amount of oxidized mercury (20%) is produced over the SCR for the HCl-treated catalyst. The experimental results are shown in figure 2.6. Notably, the experiment has been performed in N_2 only, which is far from a realistic gas composition.

In extension to the latter experiment, He et al. (2009) perform a surface analysis of an SCR catalyst that has been exposed to 50 ppm of HCl in N_2 for 0, 2 and 10 hours.

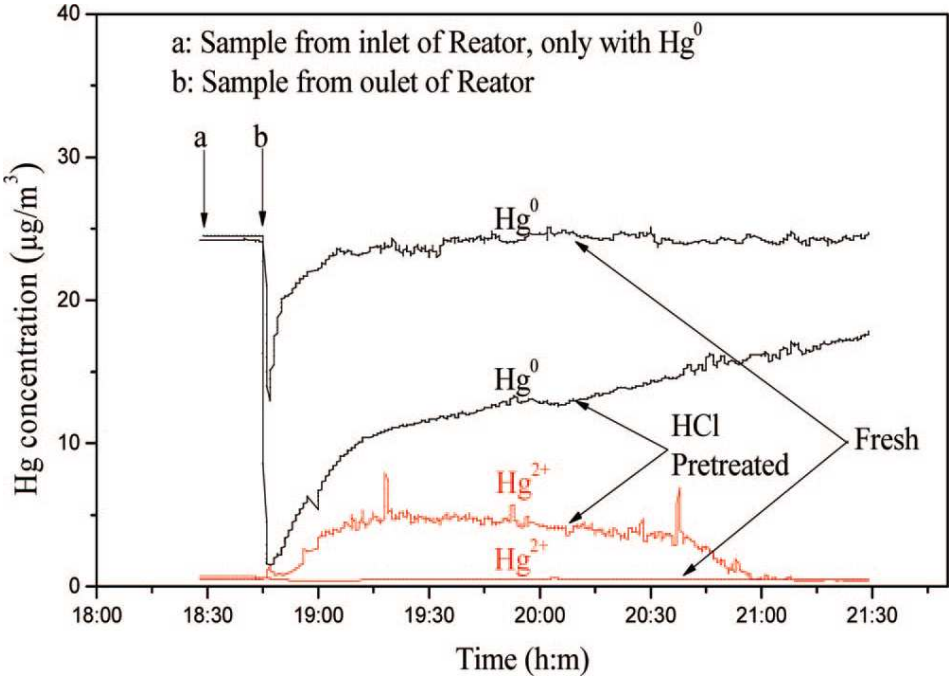

Figure 2.6: Hg^0 adsorption and oxidation in a N_2-atmosphere over a fresh and a HCl pretreated SCR catalyst at 300°C (He et al., 2009).

Both XPS and FT-IR analyses show that the exposure of the catalyst to HCl changes the distribution of vanadia sites on the surface.

The study does confirm that HCl is interacting with the catalyst and possibly the vanadia sites.

2.3.2.4 Mechanism for mercury adsorption

Huggins et al. (2003) perform an XAFS characterization of mercury sorption on a variety of sorbent material from simulated flue gases at low temperatures (<200°C), where mercury is only detected on the sorbents as ionic mercury. Data shows that sorption may occur with iodide, sulphide, chloride and oxygen anions present on the sorbent surface.

The adsorption of Hg^0 on commercial SCR catalysts has been seen to be greatly increased in the presence of O_2 compared to only N_2 and to be increased for catalysts that have been pretreated with HCl. This could indicate that Hg^0 is binding on the SCR catalyst in an oxidized form, analogously to the sorbent interaction.
In the absence of HCl, the adsorption of Hg^0 can continue for days (Zhuang et al., 2007) and no gaseous oxidized mercury is produced over the SCR. This could be due to Hg^0 binding on SCR catalyst in connection with oxygen, possibly as HgO(ads), which is not a volatile specie and will remain bound on the catalyst. In the presence of HCl, mercury will preferentially bind to Cl and produce $HgCl_2$ that is volatile. The result is

a desorption of the adsorbed mercury.

Granite et al. (2000) suggest that the capture of Hg^0 by metal oxides could take place through the oxidation of mercury with lattice oxygen (or chlorine) in a socalled Mars-Maessen mechanism. For vanadium pentoxide the reaction would be:

$$Step\ 1: Hg^0(g) + surface \rightarrow Hg^0(ads) \tag{2.6}$$
$$Step\ 2: Hg^0(ads) + V_2O_5 \rightarrow HgO(ads) + V_2O_4 \tag{2.7}$$
$$Step\ 3: V_2O_4 + {}^1/_2O_2(g) \rightarrow V_2O_5 \tag{2.8}$$
$$Step\ 4: HgO(ads) + V_2O_5 \rightarrow Hg - V_2O_6 \tag{2.9}$$

Step 1 is the collision of Hg^0 with the surface. Step 2 is the reaction of adsorbed mercury with the metal oxide forming adsorbed HgO, while reducing the vanadia. Step 3 is the reoxidation of vanadia by gas-phase oxygen. Finally, step 4 is the reaction between the adsorbed HgO with the surface V_2O_5 producing a binary oxide.

The slight adsorption of Hg^0 in the absence of O_2 coincides with step 1 and 2 in the proposed adsorption mechanism. The increased SCR capacity for mercury adsorption with O_2 corresponds to step 3 and 4 also taking place.

Eom et al. (2008) present XPS data showing that only a weak adsorption of Hg^0 is taking place on SCR catalysts in a N_2-atmosphere. Results indicate that Hg^0 binds on V^{5+}=O-sites producing HgL-O-V^{4+}:

$$Hg^0(g) + O = V^{5+} \leftrightarrow Hg \cdots O - V^{4+} \tag{2.10}$$

which could correspond to step 1 and 2 in the Mars-Maessen mechanism. This suggests that Hg^0 adsorption is coupled to vanadia Lewis-sites on the catalyst.

2.3.2.5 Summary

Both Hg^0 and HCl adsorb on the SCR catalyst, but the amount heavily depends on the gas composition.

Possibly, the adsorbed mercury is predominantly on the form of HgO(ads) on vanadia. If Hg^0 and HCl are adsorbing on the same site on the catalyst is unclear.

The presence of HCl(g) causes a volatilization of Hg(ads), which is released on an oxidized form. Also, the presence of HCl(ads) has been shown to induce an oxidation of Hg^0(g) over the SCR catalyst. This suggests that released oxidized mercury probably is in the form of $HgCl_2$ and that the catalytic Hg^0 oxidation involves the adsorption of both HCl and Hg^0.

If Hg^0 adsorbs in connection with Lewis sites on the catalyst, then it is unlikely that NH_3 simply displaces Hg^0 by its own adsorption on Brønsted sites. More likely is then that NH_3 reduces the adsorbed HgO(ads) to Hg^0, which is released from the catalyst, since it is volatile.

2.3.3 Reduction of $HgCl_2$

The previously described study by Thorwarth (2007) showed that NH_3 has the ability to reduce $HgCl_2$ over commercial SCR catalysts. No reduction was observed in the absence of NH_3. The author, therefore, suggests that $HgCl_2$ could be reduced by NH_3 according to the following reaction:

$$3\ HgCl_2(g) + 2\ NH_3(g) \rightarrow 3\ Hg^0(g) + 6\ HCl(g) + N_2(g) \tag{2.11}$$

Hocquel (2004) also demonstrates a reduction of $HgCl_2$ for different commercial-type SCR catalysts, when adding $HgCl_2$ at 330°C in a simulated flue gas containing NO and NH_3. All catalysts showed an ability to decrease the share of $HgCl_2$ at HCl levels below 10 mg/m^3. The results show a tendency of increasing $HgCl_2$ fraction for increasing HCl concentration, increasing vanadia level and decreasing temperature.

Samples of the pure metal oxides TiO_2 and WO_3 have shown a significant potential to decrease the fraction of $HgCl_2$ even in the absence of NH_3 (Hocquel, 2004). The gas in these experiments contains O_2, H_2O and 1.4-2.8 mg/m^3 HCl in N_2. Experiments were run at 300-330°C, so the only stable form of mercury under these conditions is $HgCl_2$ according to thermodynamic calculations. This can therefore indicate that TiO_2 and WO_3 are binding chlorine and rendering it unavailable for mercury, but no measurements have been made to explore this.

Furthermore, the presence of 76-110 mg/m^3 SO_2 appears to further decrease the share of $HgCl_2$ over the pure metal oxides and the commercial SCR catalysts (Hocquel, 2004). This even takes place in the absence of a catalyst indicating that SO_2 have the ability to reduce $HgCl_2$ homogeneously.

2.3.4 Oxidation of Hg^0

The net reaction for the Hg^0 oxidation by chlorine is typically presented as

$$Hg^0 + 2HCl + {}^1/_2O_2 \leftrightarrow HgCl_2 + H_2O \tag{2.12}$$

since the reaction only takes place under oxidative conditions and chlorine is primarily present as HCl in the flue gas.

2.3.4.1 Establishing steady-state

It has already been established that considerable Hg^0 adsorption/desorption is taking place over SCR catalysts for a potentially very long time period depending on the given conditions. This means that 'steady-state oxidation' implicitly specifies that the Hg^0 oxidation is measured only after these transient sorption phenomena have stabilized.

Many experimental studies are based on an analyzer measuring only elemental mercury Hg^0, since spectrometric methods only detect this specie. In such studies, it is typically assumed that the conversion of Hg^0 to $HgCl_2$ over the SCR catalyst is given by:

$$X = \frac{Hg^0(in) - Hg^0(out)}{Hg^0(in)} \tag{2.13}$$

which is only true if sorption phenomena has ceased. Data taken prematurely can be erroneous. Only a measurement of total Hg can explicitly control for this, but that is not always possible.
Various indirect methods to control the steady-state can alternatively support the hypothesis of steady-state. The validity of experimental data, where such considerations have not been made is highly questionable and will not be considered here.

2.3.4.2 Effect of gas composition

The presence of HCl is crucial for the oxidation of Hg^0 over SCR catalysts. In the absence of HCl, only negligible oxidation is seen (He et al., 2009; Hong et al., 2010).

The effect of increasing HCl concentration in the gas is a promotion of the Hg^0 oxidation over the SCR. The effect is both seen for simple flue gases containing only N_2 and O_2 (Hong et al., 2010) and for more complex gases with NO, NO_2, NH_3 and SO_2 (Eswaran and Stenger, 2008; Zhuang et al., 2007).

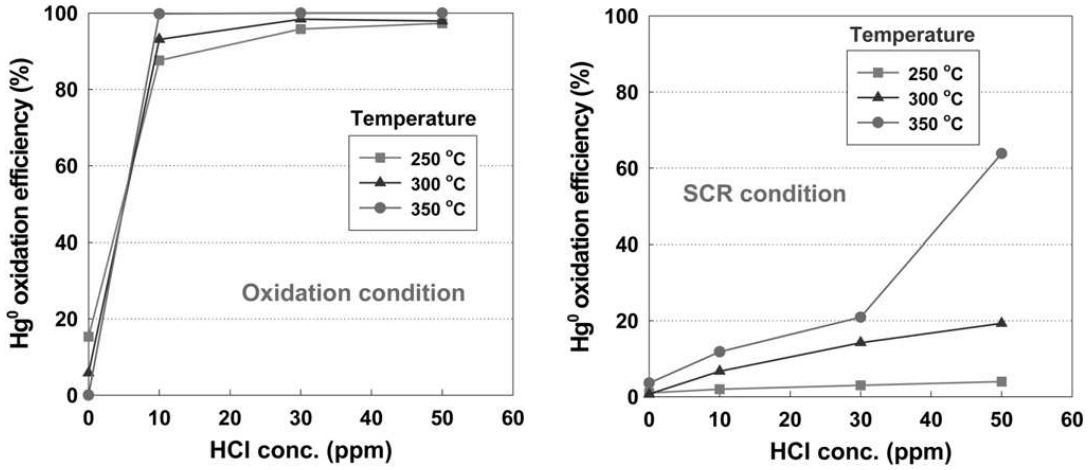

(a) No DeNOx. (b) 500 ppm NO and NH_3.

Figure 2.7: Hg^0 oxidation as function of the HCl concentration over a crushed honeycomb SCR catalyst in a gas containing 50 $\mu g/m^3$ Hg^0 and 3% O_2 in N_2 (Hong et al., 2010).

The presence of NO and NH_3 in the gas inhibits the Hg^0 oxidation (Hocquel, 2004; Hong et al., 2010). Hong et al. (2010) demonstrate that the presence of 500 ppm NO and NH_3 greatly decreases the Hg^0 oxidation to below 20% compared to $\approx$ 100% seen in the absence of NO and NH_3. Both tests are performed for T=250-350°C and are shown in figures 2.7(a)) and 2.7(b).

Further tests on the effect of increasing NH_3/NO ratio show a decreasing oxidation with increasing NH_3/NO (Hong et al., 2010; Struckmann et al., 2008). No inhibition is seen for NO alone. This suggests that NH_3 is the cause for the inhibition, but the possibility of a synergistic inhibition between NO and NH_3 (and a concomitant DeNOx reaction) has not been tested.

The following study by Struckmann et al. (2008) brings further light to the effect of the DeNOx reaction. Here the mercury speciation is measured after one and three layers of catalyst for increasing NH_3/NO ratio for either $HgCl_2$ or Hg^0 at the SCR inlet. Results are shown in 2.8. The concentration of both NO and NH_3 will decrease down through the layers of the SCR reactor as the DeNOx reaction is consuming them.
In the experiment with 100% $HgCl_2$, the fraction of $HgCl_2$ decreases to 40% after catalyst layer 1 for NH_3/NO=1 corresponding to a reduction to Hg^0. The measurement after catalyst layer 3 shows 80% $HgCl_2$, which means that some Hg^0 has been reoxidized over catalyst layers 2 and 3.
The results prove that a $HgCl_2$-reducing reaction is taking place for the particularly DeNOx active catalyst layer 1. The reduction disappears as the concentrations of NO and NH_3 decreases, whereas the Hg^0 oxidation will become relatively more important.
In the experiment with 100% Hg^0, the fraction of $HgCl_2$ in the gas increases down through the catalyst layers. Interestingly, the mercury speciation after catalyst layer 3 is the same for both the experiment starting with $HgCl_2$ and with Hg^0 (80%). This shows that some kind of equilibrium mercury speciation has been established over the three layers of catalyst. Thermodynamic calculation suggests that all mercury should exist at $HgCl_2$ under these conditions, but that thermodynamic equilibrium is not achieved in these experiments.

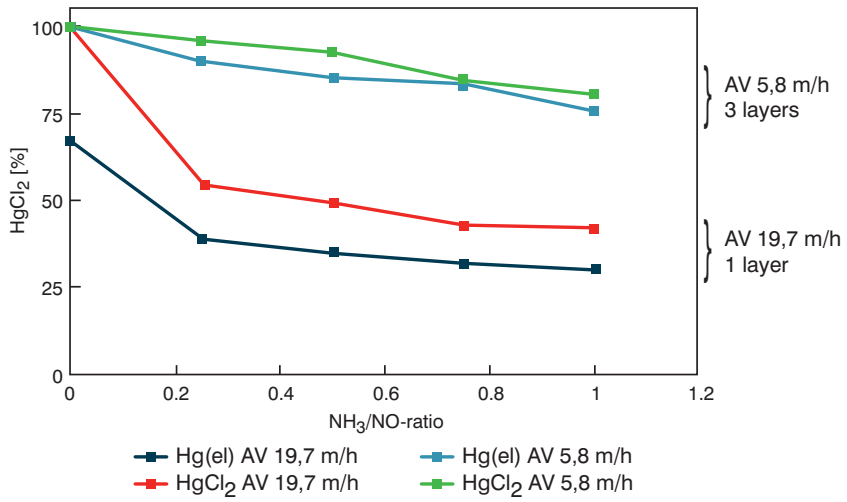

Figure 2.8: The fraction of $HgCl_2$ in the flue gas after one layer of catalyst (AV=19.7 m/h) and after 3 layers (AV=5.8 m/h) with either 100% Hg^0 or 100% $HgCl_2$ in the gas with 400 ppm NO and increasing NH_3/NO-ratio (Struckmann et al., 2008).

Only few studies on the effect of SO_2/SO_3 on the Hg^0 oxidation is found in open literature. Zhuang et al. (2007) report an inhibition by 2000 ppm SO_2 and, especially,

by 50 ppm SO_3 on the Hg^0 oxidation in the presence of 50 ppm HCl.

2.3.4.3 Effect of operating conditions and catalyst type

Studies on the influence of operating conditions and catalyst geometry on the observed Hg^0 oxidation can elucidate the kinetic regime that the catalytic reaction is operating in; Whether the rate of mass transfer of reactants to the surface or the rate of the surface reaction is controlling the overall rate of reaction.

The effect of temperature on the Hg^0 oxidation is studied by Bock et al. (2002) over two honeycomb and one-plate type SCR catalysts at 10-60 ppm HCl and 500 ppm NO and NH_3 in the range 275-420°C. Results are shown in figure 2.9. The geometric surface areas are the same for all three tested catalysts making individual performances comparable.

All catalysts show only a weak dependency of the catalytic Hg^0 oxidation with temperature at HCl=60 ppm. The weak dependency (and especially the negative dependency) on temperature could point at adsorption/desorption phenomena playing a major role for the catalytic oxidation of Hg^0.

For the honeycomb catalysts at HCl=60 ppm, the high-pitch (6.7 mm) catalyst shows an increasing Hg^0 oxidation with temperature, whereas the low-pitch (4.2 mm) catalyst shows a decreasing oxidation above 325°C. Comparatively, the low-pitch catalyst has a superior performance at a level of 90% oxidation, which shows that external mass transfer must limit the overall rate of the Hg^0 oxidation for the high-pitch catalyst. This is supported by the high-pitch catalyst showing a weakly increasing Hg^0 oxidation with temperature corresponding to a weakly increasing diffusion coefficient.

For the plate catalysts, a decreasing oxidation is seen at both 10 and 60 ppm HCl in the entire temperature range 275-410°C. This shows that the surface reaction is mainly determining the overall rate of the catalytic reaction (and not mass transfer to the surface). The surface reaction rate is increased for the higher HCl=60 ppm.
The level of oxidation at HCl=60 ppm is in the same size order as the low pitch honeycomb catalyst, but the observed oxidation decreases more evidently for the plate catalyst indicating a higher surface activity for Hg^0 oxidation of the honeycomb catalyst at temperatures above 350°C.

It was already established in section 2.3.1 that the Hg^0 oxidation increases with increasing V_2O_5. No information is given on the vanadia content of these catalysts, which could have shed further light on the source for the difference in performance between these two catalyst types.

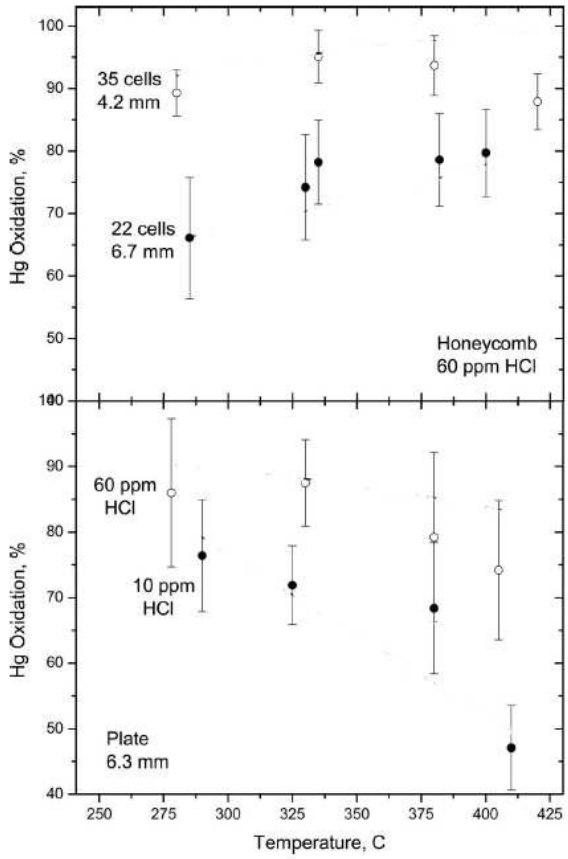

Figure 2.9: The observed Hg^0 oxidation across temperature for two honeycomb catalysts with different pitch and for a plate catalyst at 10 and 60 ppm HCl. The geometric surface are was the same for all three catalysts. Source: Experimental data from (Bock et al., 2002) and plot from (Niksa and Fujiwara, 2005).

2.3.4.4 Mechanism for Hg^0 oxidation

Only He et al. (2009) have proposed a reaction mechanism for Hg^0 oxidation on the SCR surface. The authors suggest a Langmuir-Hinshelwood mechanism as shown in figure 2.10. Here Hg is binding weakly to the oxygen on a Lewis site (as shown by Eom et al. (2008)) and HCl is binding on vanadia sites (as suggested by XPS/FT-IR data in (He et al., 2009)). Mercury then desorbs from the catalyst upon reaction to $HgCl_2$.

A Langmuir-Hinshelwood mechanism does qualitatively best describe the experimental observations, where both Hg^0 and HCl are adsorbing on the catalysts. However, there is only weak experimental evidence to support the suggested adsorption sites and no experimental evidence for the reaction between the adsorbed species. The suggested mechanism is plausible, but must be considered as highly speculative.

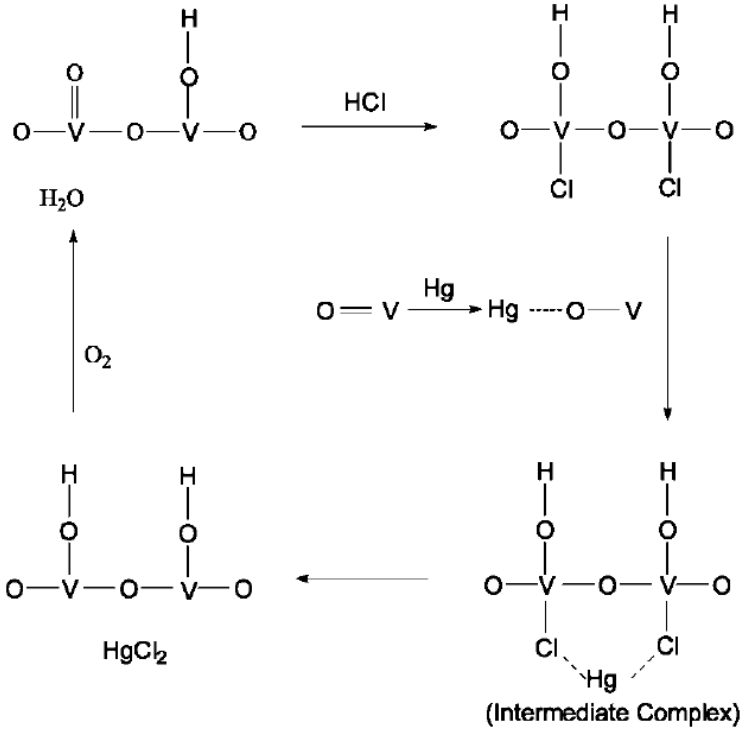

Figure 2.10: Proposed mechanism for Hg^0 oxidation on vanadia (He et al., 2009).

2.3.5 Summary on mercury reactions

Commercial type SCR catalysts have shown a potential to both oxidize Hg^0 and reduce $HgCl_2$.

The reduction of $HgCl_2$ takes place in the presence of NH_3 (with NO). Increasing V_2O_5 seem to dampen the effect, which indicates that the reduction by NH_3 may take place over TiO_2 and/or WO_3, since the two pure metal oxides have shown the ability to reduce $HgCl_2$. An increased reduction is seen in the presence of SO_2.

The active specie for the oxidation of Hg^0 is V_2O_5. HCl is responsible for the catalytic Hg^0 oxidation. The rate of the Hg^0 oxidation over commercial monolithic SCR catalysts is both governed by mass transfer and reaction on the catalyst surface.
The mechanism for the surface reaction possibly involves

- The adsorption of Hg^0 on vanadia in connection with oxygen and/or chlorine on the surface
- A Langmuir-Hinshelwood reaction between Hg(ads) and HCl(ads)
- The reaction product $HgCl_2$ is volatile and is readily released from the catalyst surface to the gas-phase.

The low dependency of the catalytic Hg^0 oxidation on temperature suggests that at adsorption phenomena are limiting the rate of the surface reaction.

The cause for the inhibition of the DeNOx reaction on the Hg^0 oxidation can come from the ability of NH_3 to reduce oxidized mercury as $HgCl_2$(g) or as HgO(ads).

The details on the presented experiments are summarized in tables A.1-A.3 in appendix A.

2.4 Mercury oxidation over SCR reactors in real flue gases

A simulated flue gas cannot duplicate all conditions present in a real gas. The presence of e.g. fly ash can directly or indirectly influence the mercury chemistry over the SCR catalyst by heterogeneous interactions with the gaseous components in the flue gas. The importance of experiments run in simulated flue gases comes from the ability to isolate different effect in a very complex system. However, in order to gain confidence that the effects are relevant to full-scale SCR conditions, the data must be compared to studies in real flue gases.

2.4.1 Pilot-scale data

This section will deal with studies of Hg^0 oxidation over SCR reactors in slipstreams from real coal-fired utility boilers or from pilot-scale combustors. A number of studies exist, where the effect of coal type/rank has been tested for different operating conditions and for SCR installations from different vendors. Typically, the performance of SCR catalysts in flue gases from different bituminous coals is tested, but a few studies on the performance for subbituminous coals (mostly Powder River Basin (PRB)) do exist.

The Hg^0 oxidation over SCR catalysts has been observed to be very dependent on both coal rank and type, but the crucial parameter for the oxidation has repeatedly been demonstrated to be the concentration of HCl. Figures 2.11(a) and 2.11(b) show a summary of the Hg^0 oxidation achieved over SCR reactors for three different slipstream facilities (Machalek et al., 2003; Serre et al., 2008; Sibley et al., 2008) and a pilot-scale combustor (Lee et al., 2004).

The promotion by HCl is evident from figure 2.11(a). The general tendency across these studies is that a lower Hg^0 oxidation is achieved for lower rank coals, which tends to correlate with lower chlorine in these coals. Serre et al. (2008) demonstrate the potential in coal blending of bituminous coals with PRB coals, where e.g. the Hg^0 oxidation for a 70% PRB/30% bituminous coal blend achieved a 40% Hg^0 oxidation compared to an only negligible oxidation for 100% PRB coal. The difference in oxidation correlates with the different Cl-contents of the two coal types.

The summarized data also shows that the Hg^0 oxidation increases with decreasing space velocity as would be expected for a larger catalyst and longer residence time.

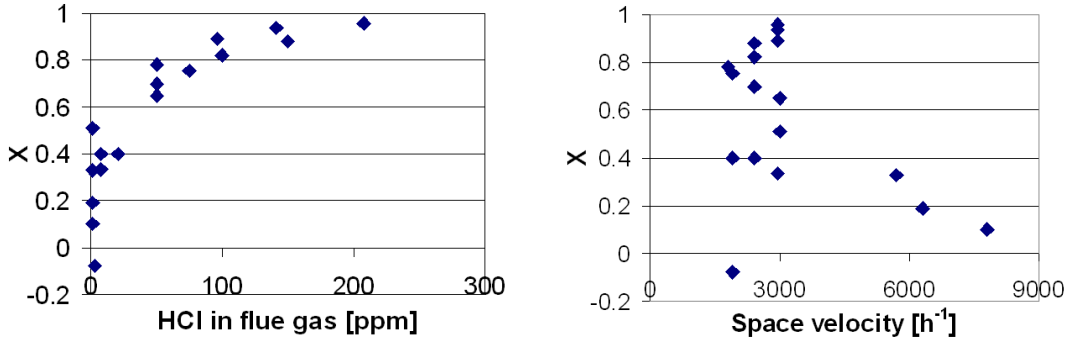

(a) Effect of HCl in the flue gas.

(b) Effect of space velocity.

Figure 2.11: Pilot-scale Hg^0 oxidation over SCR reactors calculated as $X = \frac{Hg^0(in)-Hg^0(out)}{Hg^0(in)}$. Data from Sibley et al. (2008) give $HgCl_2$ fraction at the SCR outlet. Sources: (Lee et al., 2004; Machalek et al., 2003; Serre et al., 2008; Sibley et al., 2008).

Pilot-scale experiments (Machalek et al., 2003; Richardson et al., 2002; Sibley et al., 2008) have shown an inhibiting effect from NH_3 addition on the Hg^0 oxidation. Sibley et al. (2008) demonstrate a lower catalyst activity over the first catalyst layer compared to the second layer, where lower NO and NH_3 concentrations will be present.

The effect of aging of the catalyst remains unclear. Aging was not found to have a significant impact on the Hg^0 oxidation in a bituminous coal combustion (Lee et al., 2004), whereas Richardson et al. (2002) show data from a single experiment indicating that the catalyst activity significantly decreased with time in a PRB combustion gas.

Only few and scattered observations are made on the effect of fly ash properties on the Hg^0 oxidation over SCR catalysts. These will not be covered here.

2.4.2 Full-scale data

Senior (2004b,c,a) has reviewed the available data on Hg^0 oxidation in full-scale power plants. The available data primarily come from combustion of bituminous coals in the US. Figure 2.12(a) displays the Hg^0 oxidation over the SCR as function of coal Cl concentration, where an oxidation in the range of 4-98% is observed. Data suggest that a positive correlation between Hg^0 oxidation and coal chlorine exist, but there is considerable scatter in the data. The sulphur content does not appear to have an influence on the Hg^0 oxidation.

Furthermore, a tendency of decreasing Hg^0 oxidation for increasing temperature was shown in the range 315-425^{o}C as shown in figure 2.12(b). This effect coincides with the lower Hg^0 fraction observed in flue gases upstream of particulate control devices for decreasing temperature, see section 2.1.3.2. Lower temperatures appear feasible for transformations of Hg^0 into Hg^{2+} and Hg^p.

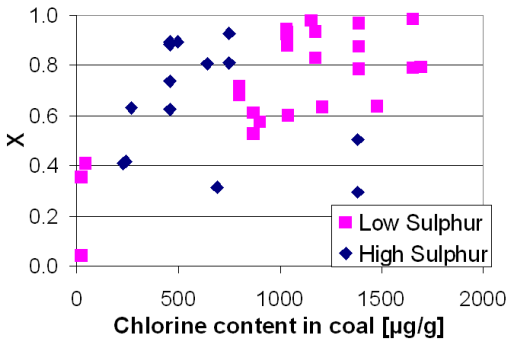

(a) Effect of coal-Cl. Low sulphur entails <1wt % S in the coal and high sulphur >1wt % S in the coal.

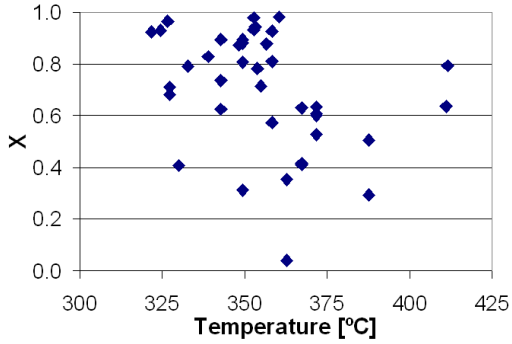

(b) Effect of temperature.

Figure 2.12: Full-scale Hg^0 oxidation over SCR reactors calculated as $X = \frac{Hg^0(in) - Hg^0(out)}{Hg^0(in)}$. Source: (Senior, 2004b).

Various sources to the scatter in Hg^0 oxidation for different SCR applications can be mentioned in this context. Firstly, the space velocity for these SCR installations vary from 1380-5250 h^{-1}, which gives considerable differences in contact time between the flue gas and the catalyst.
Secondly, a consideration of the total mercury speciation after the SCR and not just the conversion of inlet Hg^0 over the SCR also offers an explanation for the scatter. Figure 2.13 shows the mercury speciation after the SCR as function of coal Cl concentration. In this plot, a very evident correlation between coal chlorine and total Hg^0 oxidation appears. Comparing figures 2.12(a) and 2.13 shows that the performance of the SCR reaction is dependent on the inlet speciation of mercury, where an increased conversion X can be expected for a lower inlet fraction of $HgCl_2$. The concentration of chlorine appears to majorly influence the total $HgCl_2$ achievable over the SCR.

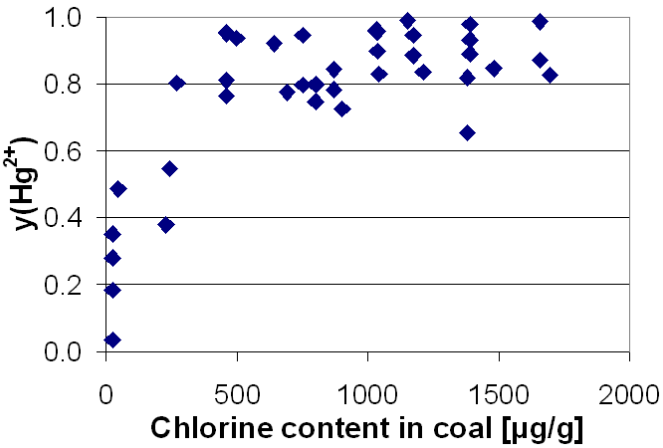

Figure 2.13: Fraction of $HgCl_2$ at SCR outlet as function of coal chlorine. Source of data: (Senior, 2004b).

Full-scale data only contain few measurements without ammonia, since the SCR reactors are in operation for DeNOx control. The general tendency for individual plants that have tested this is an increased Hg^0 oxidation when NH_3 is turned off (Senior, 2004a).

An example of available full-scale data in open literature can be found in Chu et al. (2003).

2.5 Modelling of mercury oxidation over SCR reactors

The Hg^0 oxidation over monolithic SCR reactors has been modelled by both Senior (2006) and Niksa and Fujiwara (2005) including both the effect of external mass transfer and pore diffusion and reaction in the catalyst wall.

Both authors model the surface reaction as a simple Eley-Rideal mechanism, where either adsorbed Hg reacts with gaseous HCl (Senior, 2006) or adsorbed HCl reacts with gaseous Hg^0 (Niksa and Fujiwara, 2005). The models incorporate the inhibiting effect of NH_3 by assuming that Hg^0/HCl and NH_3 competitively adsorb on the same active site on the catalyst, which may not be the true mechanistic cause for the inhibition (e.g. it appears unlikely that acidic HCl and alkaline NH_3 adsorb on the same site).
The rate expressions for the surface reaction will therefore take one of the following forms:

$$-r_s = \frac{k_{Hg} \cdot K_{Hg} \cdot P_{Hg} \cdot P_{HCl}}{1 + K_{NH_3} \cdot P_{NH_3}} \tag{2.14}$$

$$-r_s = \frac{k_{Hg} \cdot P_{Hg} \cdot K_{HCl} \cdot P_{HCl}}{1 + K_{NH_3} \cdot P_{NH_3} + K_{HCl} \cdot P_{HCl}} \tag{2.15}$$

where k_{Hg} is the reaction rate constant, K_{HCl} and K_{NH_3} are the adsorption coefficients of HCl and NH_3, respectively.
The NO reduction must be considered in the model framework in order to simulate the NH_3 concentration profile in the wall, since the concentration of NH_3 influences the Hg^0 oxidation.

By fitting the parameter $k = k_{Hg} \cdot K_{Hg}$ (Senior, 2006) or k_{Hg} and K_{HCl} (Niksa and Fujiwara, 2005) to each type of catalyst, they both manage to describe the overall trends in Hg^0 oxidation across different operating conditions (T, SV, NH_3/NO) and catalyst geometries.

Both these simple mechanistic models give plausible qualitative results.

2.6 Conclusion

It has been demonstrated across both lab-, pilot- and full-scale experiments in both simulated and real flue gases that the two major flue gas components influencing the Hg^0

oxidation over SCR catalysts are HCl and NH_3. The effects of other flue gas components, operating conditions and catalyst types/geometries have not been as unambiguously reported in literature.

The fundamental understanding of the catalytic Hg^0 oxidation and the relevant chemistry over the SCR catalyst is in its early stage. Furthermore, the available experimental investigations on the effect of the two pivotal parameters, HCl and the DeNOx reaction, only seem to cover a narrow range of conditions for each individual study.
Combined, this makes the means to optimize the Hg^0 oxidation over SCR catalysts for different applications unclear.

A study of other (secondary) effects can seem valueless until the effects of HCl and the DeNOx reaction have been further elucidated in the entire SCR operating range.

Chapter 3

Experimental methods

In this chapter the experimental methods and materials are discussed.

3.1 The catalyst

Commercial corrugated-type monoliths obtained from Haldor Topsøe A/S are used in this study. The catalysts are based on V_2O_5 and WO_3 dispersed on a fibre reinforced TiO_2 carrier.

Two types of monolithic geometries across three levels of vanadia in the catalyst have been tested. Table 3.1 shows the specifications for each catalyst geometry and level of vanadia.

Table 3.1: Geometry of monolithic SCR catalyst tested

	Hydraulic diameter [D_h]	Wall thickness [h]	V_2O_5-level
Type A	6.5 mm	1 mm	Typical
Type B	3.4 mm	0.4 mm	Low, typical, high

The type A catalyst is typical for 'high dust'-applications both in terms of geometry (high D_h) and vanadia content.

3.2 The laboratory setup

The mercury chemistry over the SCR catalyst is studied in a laboratory setup at Haldor Topsøe A/S. Here a simulated flue gas containing Hg^0 or $HgCl_2$ is passed through an SCR reactor and the change in mercury speciation after the reactor is measured under different operating conditions, gas compositions and catalyst types.
A schematic illustration of the experimental setup is shown in figure 3.1. The setup roughly consists of

- A module where all gases are mixed and preheated
- An SCR reactor
- A mercury analyzer for measurements of Hg^0
- A reduction unit for reducing all Hg^{2+} to Hg^0 in order to get a total mercury (Hg^T) measurement .

All tubing in contact with mercury consists of pyrex glass, which is heated to 140^{o}C (indicated in red in the illustration). This eliminates precipitates of NH_4Cl forming on the surface and minimizes mercury adsorption.

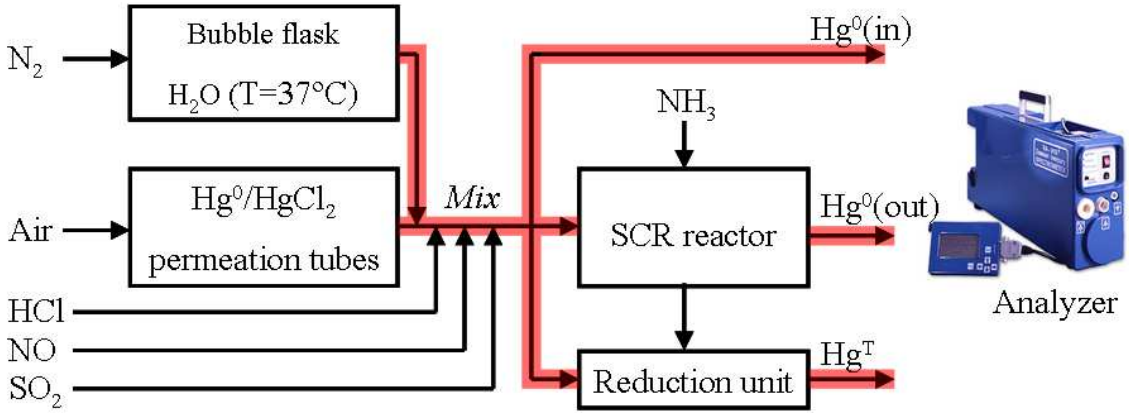

Figure 3.1: Schematic illustration of experimental setup.

3.2.1 Gases

Hg^0 or $HgCl_2$ are introduced into the gas via a VICI Metronics Dynacal ® Permeation Device, where a fixed rate of the component is released depending on the temperature. The permeation tube is a sealed permeable silicon membrane containing liquid Hg^0 or $HgCl_2$. The device is maintained at a constant temperature (T=30 or 50°C) to establish constant vapor pressure inside the device. This results in an equilibrium

between liquid and vapor phase Hg^0 or $HgCl_2$ and the vapor escapes through the walls of the membrane at a constant rate. A constant flow of 15 NL/h of dry air is passed through the permeation tube.

All gas flows of the individual components (except NH_3) are added in the mixing module maintained at 140°C. The gas flow is then heated to test temperature in the reactor via a long pyrex spiral just upstream of the SCR catalyst. NH_3 is added to the heated gas just before the inlet to the catalyst.

H_2O is introduced in the gas by bubbling the N_2 through a 250 mL bubble flask containing H_2O at 37°C, where the N_2 will become (close to) saturated with water at the given temperature.

HCl is added from a gas mixture of HCl (>99.8% pure) in N_2 (>99.999% pure) containing 2500 ppm HCl. NH_3 (>99.8% pure), NO (>99.0% pure) and SO_2 (>99.98% pure) are added from gas bottles containing the pure components. NH_3 is supplied by Brenntag Nordic, while the other gases are supplied by Air Liquide.

The simulated flue gas contains the components and concentration ranges given in table 3.2.

Table 3.2: Range of component concentrations for the simulated flue gas

Component	**Concentrations**
Hg^0	0-25 $\mu g/Nm^3$
$HgCl_2$	0-53 $\mu g/Nm^3$
O_2	0-7.1%
H_2O	2-6.4%
HCl	0-55 ppm
NH_3	0-350 ppm
NO	0-350 ppm
SO_2	0-360 ppm
Total flow	80-550 NL/h

3.2.2 SCR reactor

The reactor consists of 1-2 monolithic channels of SCR catalyst of up to full cassette length in a pyrex glass reactor. Pictures of the reactor are shown in figure 3.2. Each tested catalyst is initially fixed in a seperate glass tube, where cement surrounds the volume between the glass and the outer surface of the catalyst (figure 3.2(a)). The entire SCR/glass tube is inserted in the reactor, where the polished edges of the glass insert and the reactor ensures that bypass does not take place.

In the reactor, a frit is located 1 cm from the entry to the SCR catalyst (figure 3.2(b)). This contributes to the gas mixing and ensures that a similar flow field is entering the catalyst across different tests.

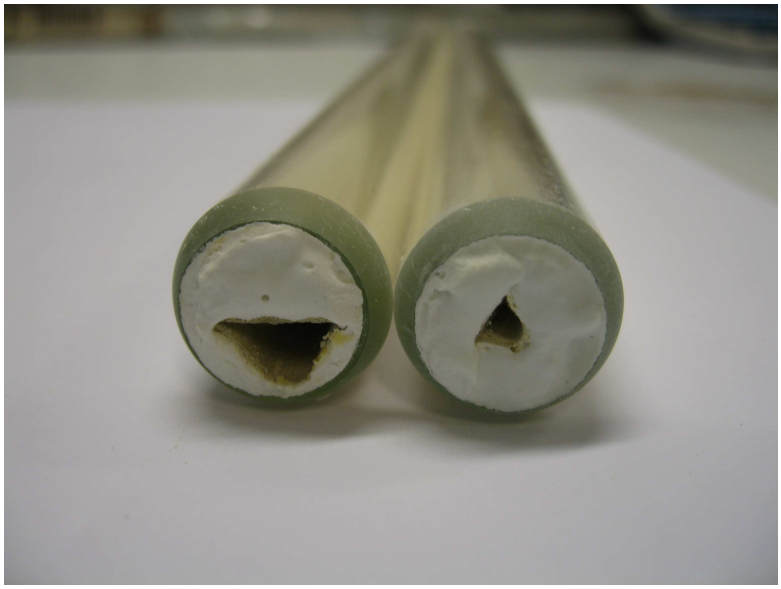

(a) SCR catalysts in glass inserts. SCR type A (left) and type B (right).

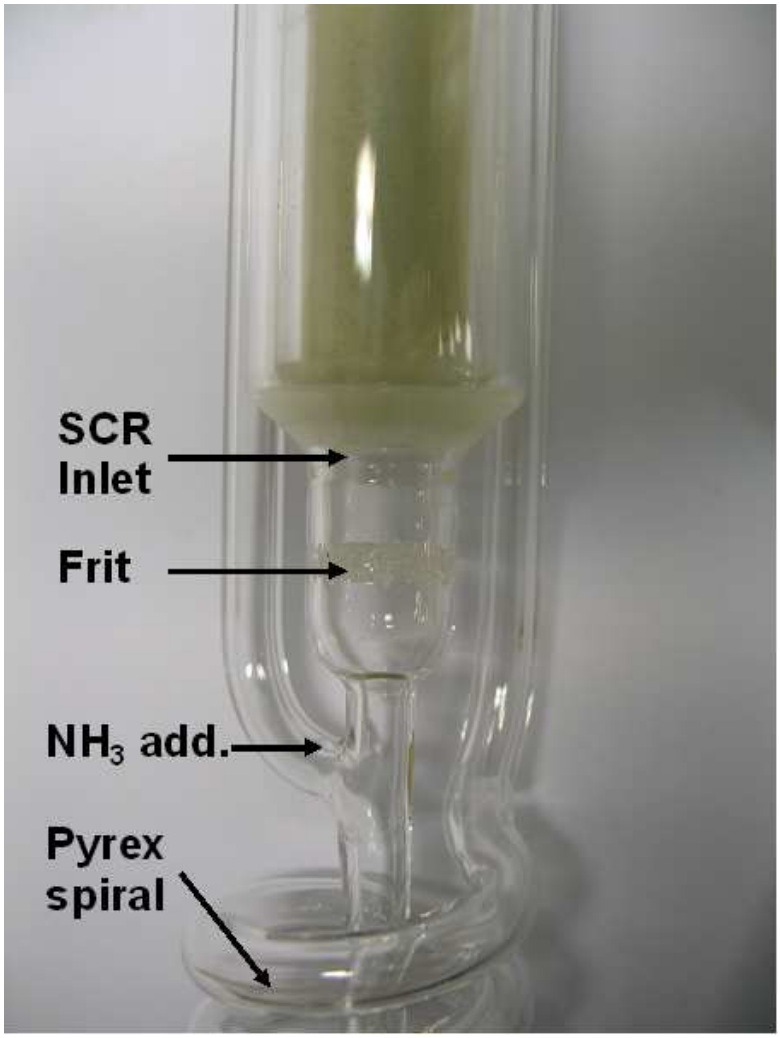

(b) Reactor with SCR catalyst inserted.

Figure 3.2: The SCR reactor consists of a glass spiral for initial heating of the gas, a glass line for addition of NH_3, a frit for mixing/flow aligning and the SCR catalyst.

Experiments over the SCR are run isothermally. Temperature measurements in the monolithic channel show a maximum +/- 2^{o}C deviation from the setpoint in the range T=250-425^{o}C.

3.2.3 Mercury analyzer

Mercury is analyzed in the Lumex RA-915+ analyzer, which uses cold vapor atomic absorption spectrometry to measure gaseous elemental mercury Hg^0 continuously. The analysis is based on differential Zeeman atomic absorption spectrometry using high frequency modulation of light polarization. The analyzer produces real-time data. A description of the analysis technique is given in the appendix B.

The analysis is performed in a heated (140^{o}C) quartz-cell with a detection limit of 48 ng/m^3. The accuracy of the measurement is specified as +/- 20% of the detection limit ($\approx$ 10 $^{ng}/_{m^3}$).

3.2.4 Reduction unit

This unit reduces all oxidized mercury Hg^{2+} to Hg^0 in order to get a total Hg measurement, when the gas consists of a mixture of Hg^{2+} and Hg^0.

The reduction unit is homemade and consists of a quartz reactor with soda lime powder at 730^{o}C. The typical main constituents of soda lime are: $Ca(OH)_2$, H_2O, NaOH and KOH. Soda lime from SKC Soda Lime sorbent tubes (Cat. No. 226-28) is applied for this purpose. The contents of one sorbent tube is applied in the reactor. The soda lime is replaced, when full reduction to Hg^0 is no longer achieved. The lifetime of the reactor varies greatly depending on e.g. gas composition.
The mechanism for the mercury reduction is not clear. Possible explanations are that chlorine from $HgCl_2$ binds to the alkaline hydroxides or that the soda lime just provides a surface for thermodynamically feasible reduction of $HgCl_2$ at 730^{o}C.

A complete reduction of Hg^{2+} over this reactor is only achieved for low H_2O concentrations ($\leq$ 3%) and at low flows ($\leq$ 250 NL/h). The task of reducing $HgCl_2$ is not trivial and no successful attempts have been made to expand this range of applicability.

With the limited applicability of the reduction unit, the mass balance across the system can only been controlled for certain experiments.

The criterion for mass balance closure is +/- 10%.

3.3 Testing procedure

Fresh catalysts are initially preconditioned overnight at T=350^{o}C in a gas flow containing 20 $^{\mu g}/_{Nm^3}$ Hg^0, 4 ppm HCl, 5% O_2, 2%H_2O, 50 ppm NO and NH_3 in balance N_2. SCR catalysts have a capacity for mercury adsorption in a size order that is very dependent on the gas composition and temperature. This means that when a change in e.g. gas composition is imposed on the reactor, an adsorption/desorption of mercury can start to take place. The time-scale for such transient sorption phenomena over the SCR is very different depending on the change in adsorption capacity. The preconditioning serves the purpose of saturating the catalyst with adsorbed mercury under conditions that are similar to the experiments.
A control of the mass balance of total Hg over the catalyst confirms that no more adsorption is taking place after the preconditioning.

3.3.1 Experiments with Hg^0

Experiments are carried out, where Hg^0 is the only source of mercury. The conversion of Hg^0 to Hg^{2+} over the SCR is then measured using different flue gas compositions, operating conditions (linear velocity and temperature) and catalyst composition/geometry.

The steady-state conversion **X** of Hg^0 to Hg^{2+} over the SCR is calculated as

$$X = \frac{Hg^0_{in} - Hg^0_{out}}{Hg^0_{in}} \tag{3.1}$$

The Hg^0 concentration is measured at the SCR reactor outlet after steady-state is achieved under the given test condition. The Hg^0 concentration at the inlet is measured immediately after.
The form of the equation presupposes that all Hg^0 disappearing across the SCR has been oxidized to Hg^{2+}, which only will be true at steady-state, where no transient sorption phenomena are occurring. The criteria for steady-state is given in section 3.3.3.

3.3.2 Experiments with $HgCl_2$

Experiments are carried out, where $HgCl_2$ is the only source of mercury. The fraction of Hg^2+ at the SCR outlet is at steady-state calculated as

$$y_{Hg^{2+}} = \frac{Hg^T_{in} - Hg^0_{out}}{Hg^T_{in}} \tag{3.2}$$

This type of experiment can only be run at conditions, where the reduction unit is applicable in order to get a total mercury measurement.

3.3.3 Criteria for steady-state

For the tested gas compositions, adsorption/desorption transients over the SCR have been observed to last up to a day, when imposing great changes to the system. When only minor changes (as defined below) are imposed on the gas composition and/or operating condition, a steady-state mercury speciation has been found to be present already within 1.5 hour, see section 3.4.

For the experiments in this study, steady-state is assumed to be present after 1.5 hour, when only 'minor changes' are imposed on the gas composition and/or operating conditions. Minor changes include the following:

- Small step increase/decrease in concentrations of HCl, NH_3, NO, SO_2, O_2 or H_2O.
- A temperature change of maximum 25^oC

All experiments that fall under this category will have stabilized for at least 1 hour before the measurement.

Experiments where greater changes are imposed on the system will be left overnight to stabilize, since longer sorption transients are possibly occurring. An example of such a change could be the complete removal of NH_3 from the gas, since NH_3 only slowly desorbs from the SCR catalyst.

3.4 Validation of testing procedure

3.4.1 Mercury contamination

The setup is regularly controlled for mercury contamination. The measurement of Hg^0 in the setup/analyzer must decrease to a value below 100 ng/Nm^3, when the mercury is turned off from the gas stream. Contamination with $HgCl_2$ is also occasionally tested.

3.4.2 Background oxidation

Oxidation of Hg^0 in the tubing (140^oC), the empty SCR reactor (350^oC) and the quartz analyzer cell (140^oC) has been measured in the presence of 4.3 ppm HCl and 100 ppm NO in a gas containing 12.5 $\mu g/m^3$ Hg^0, 3.9% O_2 and 5% H_2O in N_2. The background oxidation is measured to be only 2% and is thus neglected.

3.4.3 Background reduction

Reduction of $HgCl_2$ in the tubing (140^{o}C), the empty SCR reactor (350-400^oC) and the quartz analyzer cell (140^{o}C) has been measured in the presence of 4.3 ppm HCl and 100 ppm NH_3 in a gas containing 144 $\mu g/m^3$ $HgCl_2$, 3.9% O_2 and 5% H_2O in N_2. The background reduction is measured to be 2% and 8% for 350^oC and 400^oC, respectively. It appears to become increasingly important at elevated temperature. The background reduction is yet neglected up to temperatures of 425^{o}C.

3.4.4 Control of the steady-state criteria

3.4.4.1 Control of mass balances

The mass balance has consistently been controlled for all experiments with $HgCl_2$ as the mercury source. Figure 3.3 shows the fraction of total mercury leaving the SCR reactor as function of the stabilization time for the experiments. For the given data points, 'minor changes' in HCl and NH_3 have been imposed on the system at temperatures of 300-400^{o}C. At the time point t=1.5 hours, it can be seen that a mass balance closure +/- 10% is achieved.

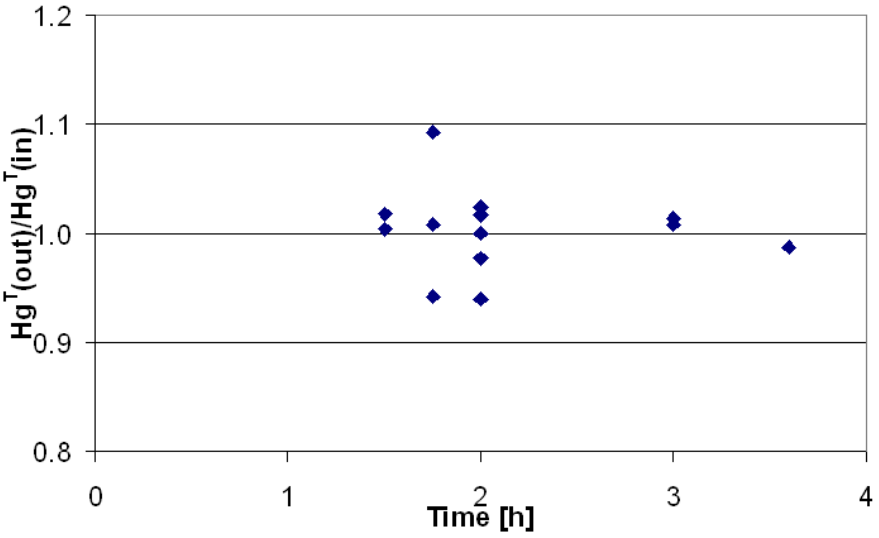

Figure 3.3: Stabilization time for 'minor' changes. Experiments are performed on a type B catalyst at v=1.7 Nm/s and T=300-400^{o}C The gas contains 17-52 μg/Nm^3 $HgCl_2$, 0-4 ppm HCl, 0-310 ppm NH_3, 3.9%O_2 and 2.3%H_2O in N_2.

3.4.4.2 Control of repeatability

The repeatability of the experiments across different test days, catalyst and history on stream has been tested for experiments, where total mercury has not been measured. Two test schemes have been repeated on three different test days and two different catalyst samples: The conversion of Hg^0 is measured in the temperature interval 250-425^{o}C in figure 3.4, whereas figure 3.5 shows the effect of increasing HCl. The duration of the stabilization time for all these measurements is between 1-2 hours and the history-on-stream varied across test day and catalyst sample.
The standard deviation for the conversion for the reference measurement at T=350^{o}C and HCl=4.2 ppm, which is performed five times over four different test days, is σ=1.2%. The repeatability of the experimental tests is concluded to be good.

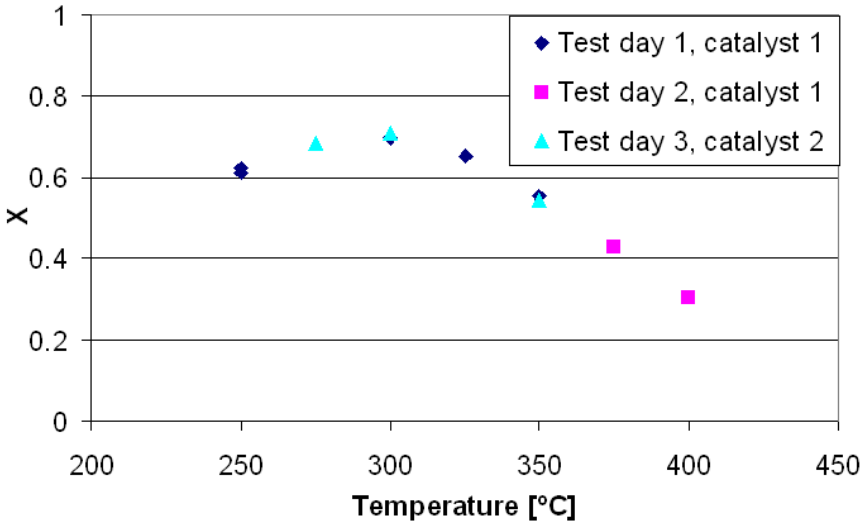

Figure 3.4: Measurements performed between 03.04.2011-17.04.2011 with a stabilization time between experiments of 1h<t<2h. Experiments are performed on a type B catalyst at v=10.8 Nm/s. The gas contains 8-12.5 μg/Nm^3 Hg^0, 4.2 ppm HCl, 100 ppm NO and NH_3, 3.8%O_2 and 5%H_2O in N_2.

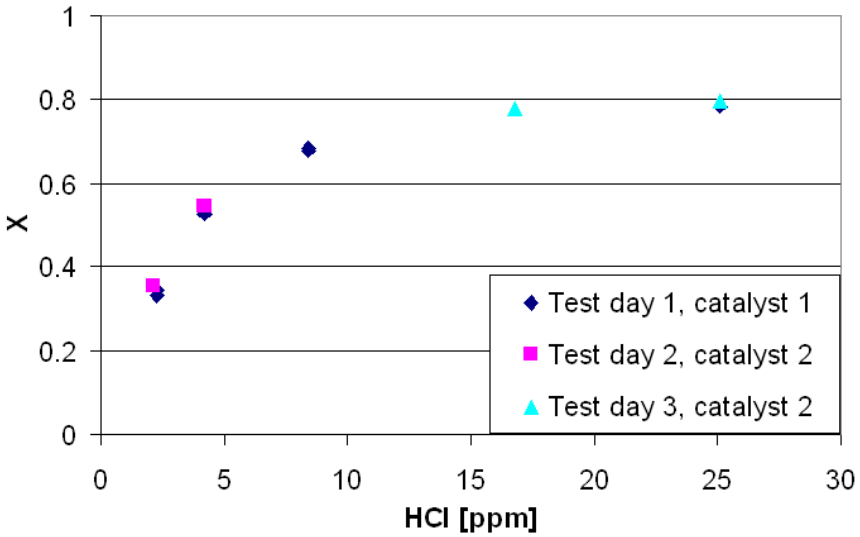

Figure 3.5: Measurements performed between 05.04.2011-18.04.2011 with a stabilization time between experiments of 1h<t<2h. Experiments are performed on a type B catalyst at v=10.8 Nm/s and T=350^{o}C. The gas contains 8-12.5 μg/Nm^3 Hg^0, 4.2 ppm HCl, 100 ppm NO and NH_3, 3.8%O_2 and 5%H_2O in N_2.

Chapter 4

Modelling methods

In this chapter the modelling methods are presented.

4.1 Form of model and assumptions

A kinetic model is set up for the concentration profiles of Hg^0, NH_3 and NO along the length of the SCR reactor at steady-state operation.

The model considers the following steps in the catalytic reactions:

- External mass transport of reactants from the bulk gas to the catalyst surface. Plug flow is assumed to take place in the monolithic channels and the rate of mass transport from the bulk gas to the external catalyst surface is described by a mass transfer coefficient k_g.
- Diffusion and reaction in the catalyst wall. The diffusion in the catalyst pores is described through an effective diffusion coefficient. Reactions will be taking place on the internal surface of the catalyst wall and are described by surface reaction rates $-r_s$.

Basic model assumptions are:

- Isothermal operation and negligible change in molar flow through reactions due to the low concentrations involved in the reactions
- Constant mass transfer coefficient k_g in the length of the catalyst channel
- The components and reactions involved in the Hg chemistry does not influence the DeNOx reaction.

4.2 Setting up equations

Steady-state mass balances are set up for component i=[NH_3,NO, Hg^0] in the catalyst wall and down through the monolith channel. The concentration of HCl is assumed constant in the reactor, since this component is present in a factor 1000 greater than mercury.

The equations will be set up with partial pressures as the dependent variable. The ideal gas law is applied, when going from concentrations to partial pressures $C_i = \frac{P_i}{R \cdot T}$.

The variables listed in table 4.1 are used in the equations. Appendix E gives a list of the symbols used.

Table 4.1: Definition of nomenclature for variables in equations

Dependent variables	Description	Unit
P_i	Partial pressure of component i: P_i: In the catalyst wall (f(x,z)) $P_{i,b}$: In the bulk gas (f(z)) $P_{i,0}$: In the bulk gas at the SCR inlet ($z = 0$) $P_{i,s}$: On the catalyst external surface ($x = h$)	atm
y_i	Dimensionless partial pressure in the catalyst wall $y_i = \frac{P_i}{P_{i0}}$	
Independent variables	**Description**	**Unit**
x	Distance in catalyst wall	m
z	Distance in monolith channel	m
x^*	Dimensionless distance in catalyst wall $x^* = \frac{x}{h}$	
u	Dimensionless distance in catalyst wall $u = (x^*)^2$	
z^*	Dimensionless distance in monolith channel $z^* = \frac{z}{L}$	

4.2.1 External mass transfer

The mass balance for component i over a differential length Δz along the monolith channel is set up for steady state operation

$$In - Out = 0$$

$$F_i(z) - \Big(F_i(z + \Delta z) + r_{g,i} \cdot a_c \cdot A_z \cdot \Delta z\Big) = 0 \quad \left[\frac{mol}{s}\right] \tag{4.1}$$

where F is the molar flow by convection in the channel and $r_{g,i} \cdot a_c \cdot A_z \cdot \Delta z$ is the flux of mass transfer from the bulk gas to the catalyst surface. a_c is the geometric surface area and A_z is the cross-sectional area of the monolith.
The molar flow can be rewritten as

$$F_i = U \cdot \frac{P_{i,b}}{R \cdot T} = v \cdot A_z \cdot \frac{P_{i,b}}{R \cdot T} \quad \left[\frac{mol}{s}\right] \tag{4.2}$$

where U is the volume gas flow and v is the linear gas flow (empty reactor).

The external mass transfer is given as the concentration driving force

$$r_{g,i} = k_{g,i} \cdot \frac{(P_{i,b} - P_{i,s})}{R \cdot T} \quad \left[\frac{mol}{m^2 \cdot s}\right] \tag{4.3}$$

Insertion of equations (4.2) and (4.3) in equation (4.1) and letting $\Delta z \rightarrow 0$ gives the differential mass balance for component i:

$$\frac{dP_{i,b}}{dz} + \frac{k_{g,i} \cdot a_c}{v} \cdot (P_{i,b} - P_{i,s}) = 0 \quad \left[\frac{atm}{m}\right] \tag{4.4}$$

where v is assumed constant. The initial condition for the equation is $P_{i,b}(z = 0) = P_{i,0}$.

4.2.2 Diffusion and reaction in the catalyst wall

The mass balance for component i over a differential distance Δx in the catalyst wall is set up for steady-state operation in plane geometry.
The catalyst wall thickness is given by $2h$, where $x = 0$ is the center of the wall as indicated on figure 4.1.

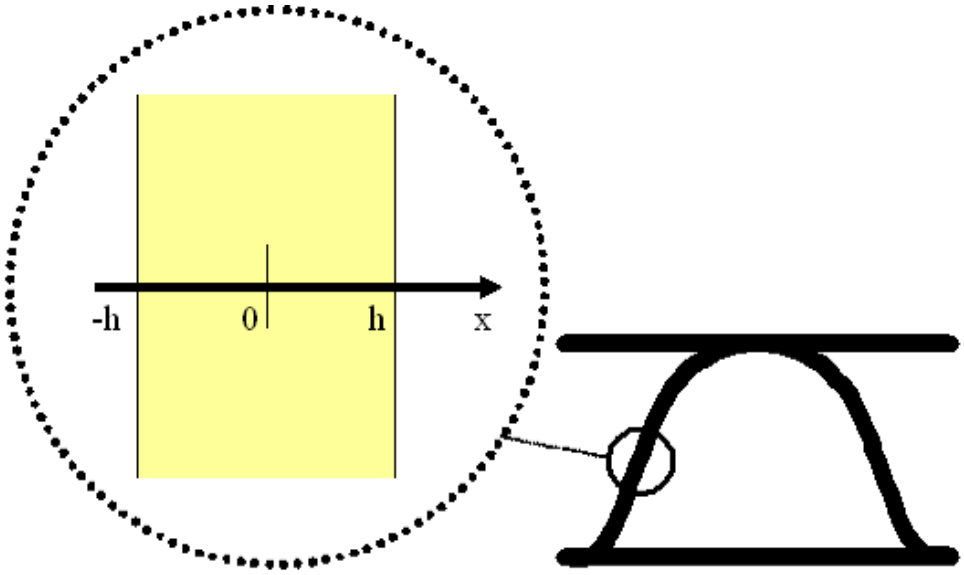

Figure 4.1: The mass balance in the catalyst wall is set up for plane geometry.

The mass balance takes the form

$$In - Out + Produced = 0$$
$$F_i(x) - \left(F_i(x + \Delta x) + r_i \cdot S \cdot \Delta x\right) = 0 \quad \left[\frac{mol}{s}\right] \tag{4.5}$$

where F is the molar flow by diffusion in the catalyst wall and $r_i \cdot S \cdot \Delta X$ is the production of component i in the volume element $S \cdot \Delta x$. S is the cross sectional area of catalyst in the x-direction.

The molar flow by diffusion in the catalyst pores is given by Ficks' law:

$$F_i = W_i \cdot S = -D_i^e \cdot \frac{d\left(\frac{P_i}{R \cdot T}\right)}{dx} \cdot S = -\frac{D_i^e}{R \cdot T} \cdot \frac{dP_i}{dx} \cdot S \quad \left[\frac{mol}{s}\right] \tag{4.6}$$

where W is the rate of diffusion in the x-direction in a unit area $\left[\frac{mol}{m^2 \cdot s}\right]$.

By insertion of equation (4.6) in equation (4.5), the differential mass balance becomes

$$\frac{dW_i}{dx} - r_{s,i} = 0 \Rightarrow$$
$$\frac{d^2 P_i}{dx^2} + \frac{R \cdot T}{D_i^e} \cdot r_i = 0 \quad \left[\frac{atm}{m^2}\right] \tag{4.7}$$

The boundary conditions are

1. Equal flux from the bulk gas to the catalyst surface ($x = h$) and from the surface into the catalyst wall:

$$W_{ext} = W_{int} \Rightarrow$$
$$k_{g,i} \cdot \frac{(P_{i,s} - P_{i,b})}{R \cdot T} = -\frac{D_i^e}{R \cdot T} \cdot \left.\frac{dP_i}{dx}\right|_{x=h} \Leftrightarrow$$
$$P_{i,s} = P_{i,b} - \frac{D_i^e}{k_{g,i}} \cdot \left.\frac{dP_i}{dx}\right|_{x=h} \tag{4.8}$$

2. Symmetry at the center of the catalyst wall: $\frac{dP_i}{dx}|_{x=0}$

4.3 Making the mass balances dimensionless

The following dimensionless variables are introduced

$$x^* = \frac{x}{h} \quad \Rightarrow \quad \frac{d^2}{dx^2} = \frac{d^2}{dx^{*2}} \cdot \frac{1}{h^2} \tag{4.9}$$

$$z^* = \frac{z}{L} \quad \Rightarrow \quad \frac{d}{dz} = \frac{d}{dz^*} \cdot \frac{1}{L} \tag{4.10}$$

$$y_i = \frac{P_i}{P_{i,0}} \tag{4.11}$$

The mass balance for component i in the monolith channel, eq. (4.4), becomes

$$\frac{dy_{i,b}}{dz^*} + \frac{k_{g,i} \cdot a_c \cdot L}{v} \cdot (y_{i,b} - y_{i,s}) = 0 \tag{4.12}$$

with the initial condition $y_{i,b}(z* = 0) = y_{i0}$.

The mass balance for component i in the catalyst wall, eq. (4.7), becomes

$$\begin{aligned} \frac{d^2 y_i}{dx^{*2}} + \frac{R \cdot T \cdot h^2}{D_i^e \cdot P_{i,0}} \cdot r_{s,i}(y_i \cdot P_{i,0}) = 0 \;\Leftrightarrow \\ \frac{d^2 y_i}{dx^{*2}} - \phi_i^2 \cdot \frac{-r_{s,i}(y_i \cdot P_{i,0})}{-r_{s,i}(P_{i,0})} = 0 \end{aligned} \tag{4.13}$$

where the Thiele modulus is given by

$$\phi_i^2 = \frac{R \cdot T \cdot h^2}{D_i^e \cdot P_{i,0}} \cdot (-r_{s,i}(P_{i,0})) \tag{4.14}$$

with the following boundary conditions

1. Equal flux from the bulk gas to the catalyst surface ($x^* = 1$) and into the catalyst wall:

$$y_{i,s} = y_i|_{x^*=1} = y_{i,b} - \frac{1}{Bi_i} \cdot \left.\frac{dy_i}{dx^*}\right|_{x^*=1}$$

2. $\left.\frac{dy_i}{dx^*}\right|_{x^*=0} = 0$

where $Bi_i = \frac{k_{g,i} \cdot h}{D_i^e}$.

These coupled differential equations can be solved numerically by discretization of the differential equations for the wall via orthogonal collocation and using an ODE-solver in the axial direction. This is illustrated in appendix C.

4.4 Mass transfer rates

4.4.1 External mass transfer

The mass transfer coefficient for the external gas diffusion can be found from

$$k_{g,i} = \frac{Sh_i \cdot D_i}{D_h} \tag{4.15}$$

where Sh_i is the dimensionless Sherwood number describing the rate of mass transfer for component i in a monolithic structure. D_i is the diffusion coefficient and D_h is the hydraulic diameter of the channel.
A correlation for the Sherwood number in the corrugated monolith channel has been developed based on measurements in the experimental setup described in section 3. The Hg^0 oxidation over high vanadia catalysts has been measured at different flow rates and temperatures for the two relevant hydraulic diameters. The reaction is assumed to be 100% external mass transfer limited over these high vanadia catalysts in a gas containing 17-105 $\mu g/Nm^3$ Hg^0, 50 ppm HCl, 4% O_2 and 2% H_2O in balance N_2, which is considered to produce a maximum surface reactivity. Comparison of the measurements with existing Sh correlations at Haldor Topsøe A/S suggests that this assumption is valid.
The developed correlation calculates an average Sherwood number in the entire channel length L and is on the form

$$Sh_i = f(Sc_i, Re, D_h, L) \tag{4.16}$$

This correlation will be applied in the model framework for estimating the mass transfer coefficients of Hg^0, NO and NH_3.

4.4.2 Bulk and pore diffusion

The bulk diffusion coefficients of Hg^0, NO and NH_3 are calculated as binary diffusion in N_2 based on the Chapman-Enskog kinetic theory for gases at low density according to Bird et al. (2002).

$$D_{AB} = 0.0018583\sqrt{T^3 \cdot \left(\frac{1}{M_A} + \frac{1}{M_B}\right)} \cdot \frac{1}{p \cdot \sigma_{AB}^2 \cdot \Omega_{D,AB}} \tag{4.17}$$

where D_{AB}[=]cm^2/s, σ_{AB}[=]Å,T[=]K and p[=]atm.

The collision integral $\Omega_{D,AB}$ is a function of the dimensionless temperature $T* = \frac{\kappa \cdot T}{\epsilon_{AB}}$:

$$\Omega_{D,AB} = \frac{1.06036}{T*^{0.15610}} + \frac{0.19300}{exp(0.47635 \cdot T*)} + \frac{1.03587}{exp(1.52996 \cdot T*)} + \frac{1.76474}{exp(3.89411 \cdot T*)} \tag{4.18}$$

The Lennard-Jones parameters for the gases are given in table 4.2.

Table 4.2: Lennard-Jones parameters (Reid et al., 1987).

Component	σ [Å]	$\frac{\epsilon}{\kappa}$ [K]
Hg^0	2.969	750
NO	3.492	116.7
NH_3	2.900	558.3

The effective diffusion coefficient D_i^e is determined by the pore-size distribution in the catalyst wall. The SCR catalyst from Haldor Topsøe has a trimodal pore structure with macro-, meso and micro-pores, which is illustrated in figure 4.2.

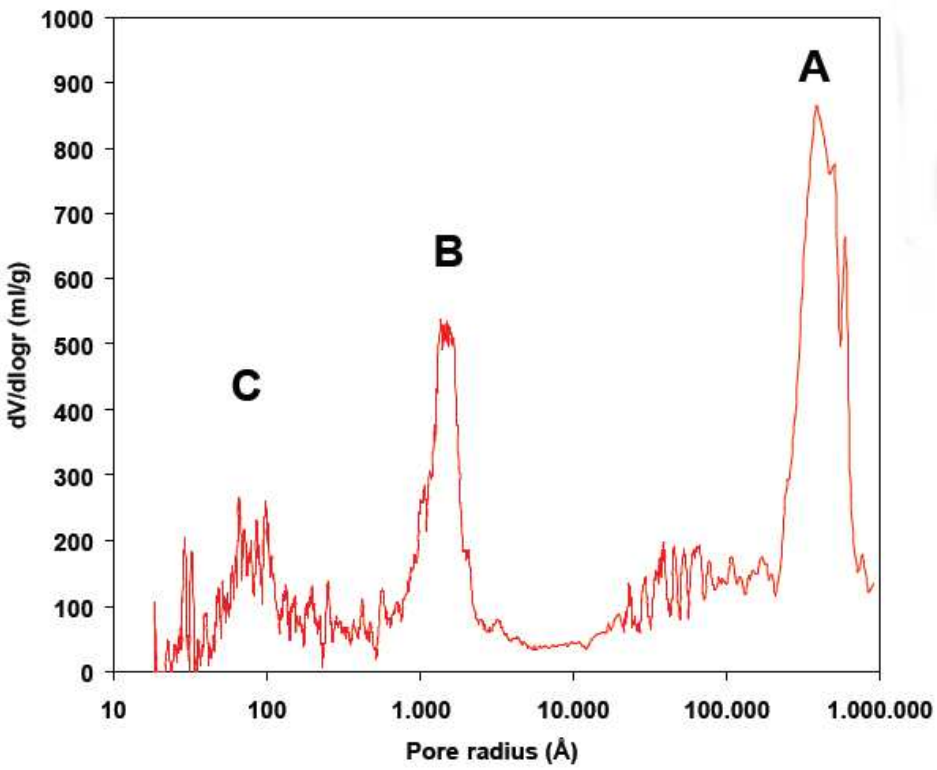

Figure 4.2: Three pore-size regimes exist in Haldor Topsøes SCR catalyst; A: Macro-pores, B: Meso-pores, C: Micro-pores.

The effective diffusion coefficient for the system of different pore sizes is calculated by subdividing the pore system into M regions, where an average pore radius (r_p) and porosity (ϵ) are calculated. The effective diffusion coefficient is then calculated in each of these regions and, finally, a value for the whole pore system is obtained by a simple summation of the individual values

$$D_i^e = \sum_{j=1}^{M_j} D_{i,j}^e \tag{4.19}$$

Calculation of the effective diffusion coefficient for component i in each pore-size region j is calculated based on the 'pore diffusion coefficient' as described in Evans et al. (1961):

$$D_{i,j}^{p} = \frac{1}{\frac{1}{D_{i,j}^{K}} + \frac{1}{D_{i}^{B}}} \tag{4.20}$$

where $D_{i,j}^{K}$ is the Knudsen diffusion given by

$$D_{i,j}^{K} = \frac{2}{3} \cdot r_{p,j} \cdot \sqrt{\frac{8 \cdot R \cdot T}{\pi \cdot MW_i}} \tag{4.21}$$

The effective diffusion coefficient is now given as:

$$D_{i,j}^{e} = \frac{D_{i,j}^{p} \cdot \epsilon}{\tau} \tag{4.22}$$

where τ is the turtuosity factor. In this model, the turtuosity is given the value 3, which corresponds to the theoretical diffusion through a randomly oriented system of cylindrical pores (Satterfield, 1980).

4.5 Surface reaction rates

The considered reactions are:

$$R1.\ \ 2\ HCl + Hg^0 + 1/2\ O_2 \ \leftrightarrow\ HgCl_2 + H_2O \tag{4.23}$$

$$R2.\ \ 2/3\ NH_3 + HgCl_2 \ \leftrightarrow\ 1/3\ N_2 + \ Hg^0 + 3\ HCl \tag{4.24}$$

$$R3.\ \ NO + NH_3 + 1/4\ O_2 \ \leftrightarrow\ \ N_2 + 3/2\ \ H_2O \tag{4.25}$$

The production rates of the individual component are dependent on rates of reaction 1-3 in the following way

$$-r_{Hg} = -r_{ox} + r_{red} \tag{4.26}$$

$$-r_{NH_3} = -r_{s,NO} = -r_3 \tag{4.27}$$

where r_{ox} and r_{red} represents the rate of the surface reactions R1 and R2, respectively.

The form of the reaction rate equations are introduced in chapter 8.

Chapter 5

A study of the mercury pseudo equilibrium after SCR catalysts

5.1 Introduction

The Hg^0 oxidation by HCl over SCR catalysts is inhibited by the concomitant DeNOx reaction (Hocquel, 2004; Machalek et al., 2003; Richardson et al., 2002; Sibley et al., 2008). No inhibition is observed for NO alone (Hong et al., 2010; Struckmann et al., 2008), so the the effect is presumably coming from NH_3.
Laboratory experiments have shown the following two effects on the mercury chemistry from the DeNOx reaction

1. The Hg^0 adsorption (without HCl) on SCR catalysts decreases in the presence of the DeNOx reaction (Eom et al., 2008; Hong et al., 2010)

2. The presence of NH_3 in the flue gas can result in a reduction of $HgCl_2$ to Hg^0 (Hocquel, 2004; Thorwarth, 2007)

The first effect may cause an inhibition of the kinetics of the catalytic Hg^0 reaction, since adsorption will be a step in the surface reaction. The second effect suggests that a reducing reaction is taking place concurrently to the Hg^0 oxidation, which will lower the overall oxidation of Hg^0 achieved over the SCR catalyst.
In an experiment by Struckmann et al. (2008), it is shown that the same mercury speciation (80 % $HgCl_2$) is achieved over three layers of SCR catalyst regardless of whether Hg^0 or $HgCl_2$ is present at the SCR inlet. This observation indicates that the mercury speciation is approaching equilibrium over the catalyst. However, the study strongly contradicts the general understanding in literature that Hg^0 oxidation is limited by kinetics (Senior et al., 2000). According to thermodynamic calculations, all mercury

should exist on the oxidized form $HgCl_2$ under typical SCR operating temperatures (Frandsen et al., 1994).

The objective of this study is to investigate the 'equilibrium speciation' of mercury that exists after long SCR reactors and, since this speciation is different from thermodynamic predictions, to quantify it for different gas compositions and operating temperatures. The study also serves to further elucidate the effect of NH_3 on the mercury chemistry.

5.2 Methods

The 'equilibrium speciation' for mercury over the SCR is achieved, when the contact time between the flue gas and the catalyst is so long that no changes in speciation is observed by further increasing the contact time.
Laboratory experiments will be carried out testing the effect of varying concentrations of NH_3 and HCl on the mercury speciation after the SCR in the temperature range 275-450^{o}C. No NO will be added, so the concentration of NH_3 will remain constant throughout the catalyst. The effect O_2 and H_2O will also be examined.

5.2.1 Experimental

A Topsøe DNX SCR catalyst (type B, see section 3.1) with a 'typical' vanadia-content is applied for these tests.
Initially, the fraction of oxidized mercury at the SCR outlet is measured for decreasing flow rates (and thus increasing contact times). The flow rate, where no further changes in mercury speciation are observed, is adopted for further tests. At this flow rate, the contact time between the flue gas and the catalyst is sufficient to achieve the 'equilibrium distribution' of Hg^0 and $HgCl_2$. Tests are performed for either Hg^0 or $HgCl_2$ at the SCR inlet.
The equilibrium speciation of mercury is subsequently measured for different concentrations of NH_3, HCl, O_2 and H_2O at the flow rate determined to give sufficient contact time between the flue gas and the SCR. Table 5.1 gives the specifications for the gas concentrations and flows for the experiments in this study.

Each experiment is allowed to stabilize for minimum 1 hour and total mercury measurements has been made for all tests with $HgCl_2$ verifying that the mass balance over the SCR closes within +/- 10%. All preliminary tests are performed at H_2O=2.5%, since Hg^T can only be measured at such low H_2O concentration.

5.2.2 Thermodynamic calculations

Global thermodynamic calculations have been performed via HSC Chemistry 6.1.

Table 5.1: Range of conditions tested

Catalyst	
Geometry	Type B
V_2O_5	'Typical'
Operating conditions	
Flow [NL/h]	82-244
Temperature [^oC]	275-450
Gas composition	
Hg^0	9-25 $\mu g/Nm^3$
$HgCl_2$	17-53 $\mu g/Nm^3$
O_2	0-7.1%
H_2O	2-6.4%
HCl	0-13 ppm
NH_3	0-405 ppm

5.3 Results

5.3.1 Preliminary tests

Plotted in figure 5.1 is the fraction of $HgCl_2$ at the SCR outlet at T=350^{o}C as function of flow rate for three different gas compositions: 1) 1.3 ppm HCl and no NH_3, 2) 1.3 ppm HCl and 80 ppm NH_3 and 3) no HCl and 80 ppm NH_3. The gas does not contain NO, which means that the NH_3 concentration will be constant over the SCR.

Data shows that in the absence of NH_3, all mercury leaving the SCR will approach 100% $HgCl_2$ for decreasing flows for even very low HCl=1.3 ppm.
In the absence of HCl, all mercury leaving the SCR will be Hg^0 in the entire range of flows tested regardless of Hg^0 or $HgCl_2$ is added. These preliminary results confirm that both oxidation of Hg^0 and reduction of $HgCl_2$ can take place over the SCR catalyst. The mercury speciation for the two latter gas compositions are both approaching the distribution predicted by thermodynamic calculations.
In the presence of HCl and NH_3, the mercury speciation will approach the same speciation ($\approx$ 53% $HgCl_2$) with either Hg^0 or $HgCl_2$ at the SCR inlet for decreasing flows. This observation is in accordance with the study by Struckmann et al. (2008) and shows that the mercury 'equilibrium speciation' at the SCR outlet changes in the presence of NH_3.

According to global thermodynamic calculations, there is no difference in the equilibrium speciation of mercury in the absence/presence of NH_3 for the given simulated flue gas. The measured mercury 'equilibrium speciation' after the SCR reactor does, therefore, not coincide with the thermodynamic equilibrium. In order not to confuse these two concepts, the SCR outlet speciation under equilibrium conditions will from now be referred to as the *stabilized* mercury speciation.

The *stabilized* mercury speciation is approached asymptotically for decreasing flows over

the SCR, but appears to have been reached +/- 5% at 82 NL/h. In order to further verify that this flow rate is sufficiently low to achieve a *stabilized* mercury speciation, duplicate measurements of mercury speciation have been performed at 82 NL/h to control that the speciation is independent of whether Hg^0 or $HgCl_2$ is added at the SCR inlet. Such control measurements have been performed for a number of different HCl and NH_3 concentrations in the temperature range T=300-400^{o}C. Examples of results are shown in figure 5.2, where it can be seen that the data coincides for Hg^0 and $HgCl_2$ at the inlet.
A flow rate of 82 NL/h will therefore be applied in the following studies and tests are only run with Hg^0.

Finally, it was confirmed that the $HgCl_2$ reduction with NH_3 is a catalytic reaction, since only minor reduction of $HgCl_2$ was measured over the SCR reactor in the absence of catalyst. For NH_3=100 ppm and HCl=4.3 ppm at 82 NL/h, the reduction of $HgCl_2$ was 2% at 350^{o}C and 8% at 400^{o}C over the empty reactor. The reduction of $HgCl_2$ is therefore considered to be a catalytic reaction.

5.3.2 Effects of NH_3 and HCl

Plotted in figure 5.3 is the *stabilized* mercury speciation after the SCR as function of temperature for different NH_3 concentrations at HCl=2.5 ppm. The experiment is run at this low HCl concentration in order to simulate 'worst-case' mercury speciation for low Cl-coals. The simulated flue gas otherwise contains 25 μg/Nm^3 Hg^0, 4% O_2 and 5% H_2O in balance N_2. Notice, the higher H_2O concentration compared to the preliminary experiments for which reason the measurements do not coincide.

The mercury speciation at temperatures below 300^{o}C is completely shifted towards $HgCl_2$ at all NH_3 concentrations. At T=325^{o}C and above, the speciation gradually shifts towards Hg^0. The *stabilized* mercury speciation in the absence of NH_3 is close to the calculated thermodynamic equilibrium, which supports the validity of the experimental measurements.
Data shows that the presence of NH_3 shifts the equilibrium towards Hg^0 at lower temperatures. At 425^{o}C, all mercury exist as Hg^0 in the presence of NH_3 down to 50 ppm. At low Cl-coals, this shows that no Hg^0 oxidation can be expected over an SCR operated at elevated temperature until most NH_3 has been consumed in the DeNOx reaction.

The effect of increasing NH_3 levels off after 50 ppm. Only a minor effect is seen by further increasing the concentration up to NH_3=400 ppm. NH_3 is known to adsorb on the catalyst. Possibly, the reason for the decreasing influence of NH_3 is due to saturation of the SCR with adsorbed NH_3 ($\theta_{NH_3} \rightarrow 1$).

Plotted in figure 5.4 is the *stabilized* mercury speciation after the SCR as function of temperature for different HCl concentrations at NH_3=100 ppm. Experimental results show that the *stabilized* mercury speciation is shifted towards $HgCl_2$, when the HCl concentration is increased - analogous to thermodynamic predictions. For HCl=13 ppm, the *stabilized* mercury speciation is around 60% $HgCl_2$ at 425^{o}C in contrast to 0% $HgCl_2$ for HCl=2.5 ppm.

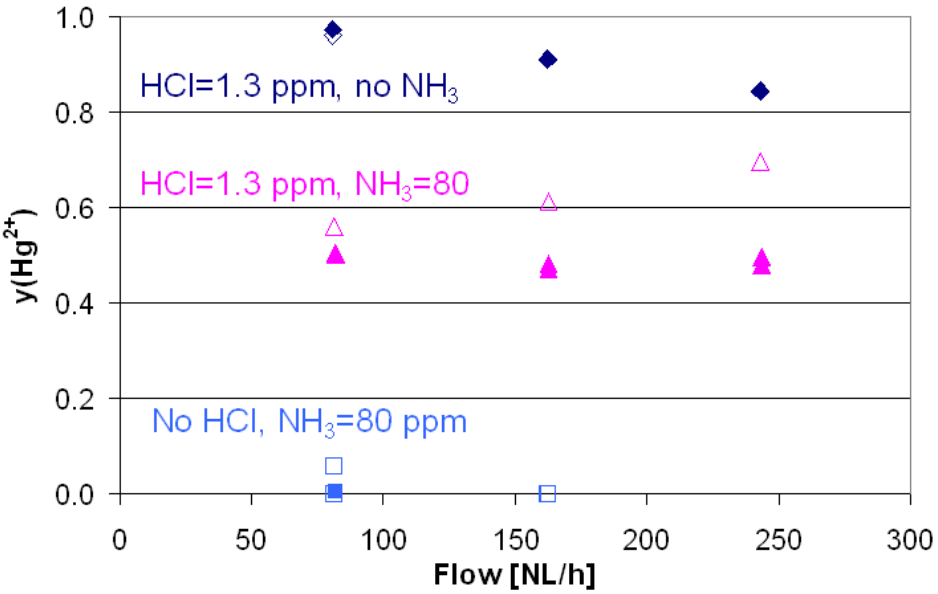

Figure 5.1: Fraction of $HgCl_2$ at SCR outlet as function of the flow rate (and thus the contact time). The gas contains Hg^0 or $HgCl_2$ in 4% O_2 and 2.5% H_2O in balance N_2 at T=350°C. Concentrations of HCl and NH_3 are as given in the figure. Closed brackets: Hg^0 at inlet, open brackets: $HgCl_2$ at inlet.

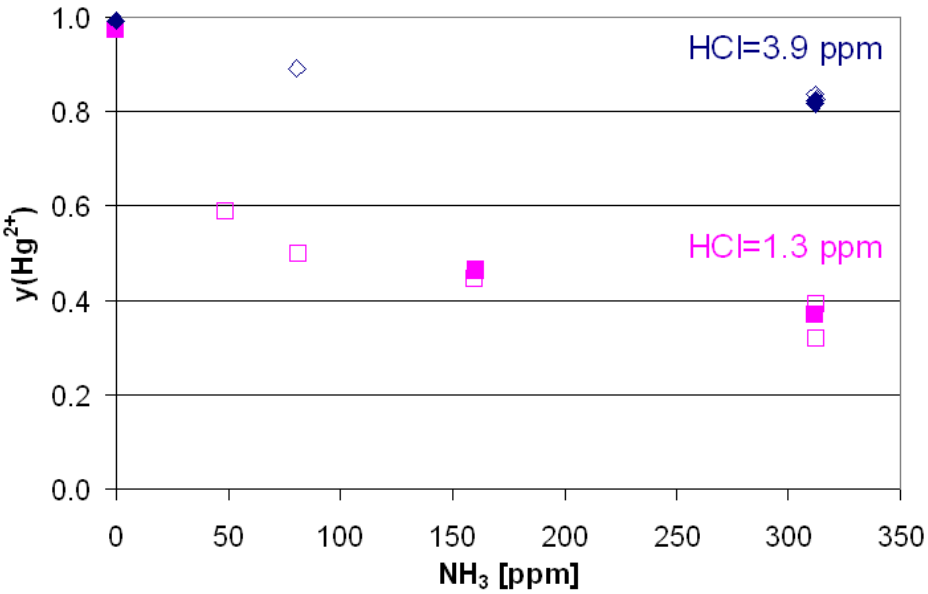

Figure 5.2: Fraction of $HgCl_2$ at SCR outlet as function of NH_3 and HCl at a flow rate of 82 NL/h. The gas contains Hg^0 or $HgCl_2$ in 4% O_2 and 2.5% H_2O in balance N_2 at T=350°C. Closed brackets: Hg^0 at inlet, open brackets: $HgCl_2$ at inlet.

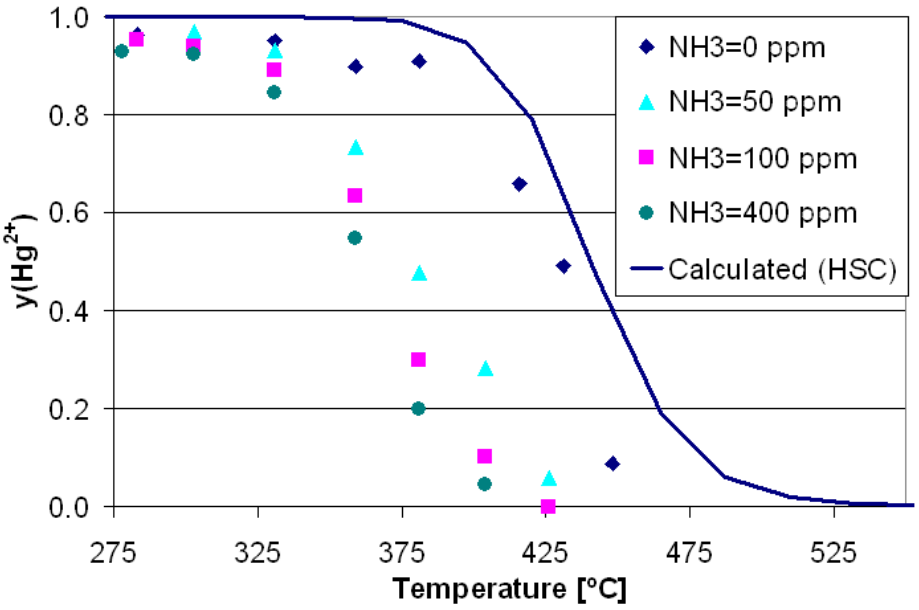

Figure 5.3: Fraction of $HgCl_2$ at SCR outlet as function of temperature for different NH_3 concentrations at a flow rate of 82 NL/h. The gas contains 25 $\mu g/Nm^3$ Hg^0, 2.5 ppm HCl, 4% O_2 and 5% H_2O in balance N_2.

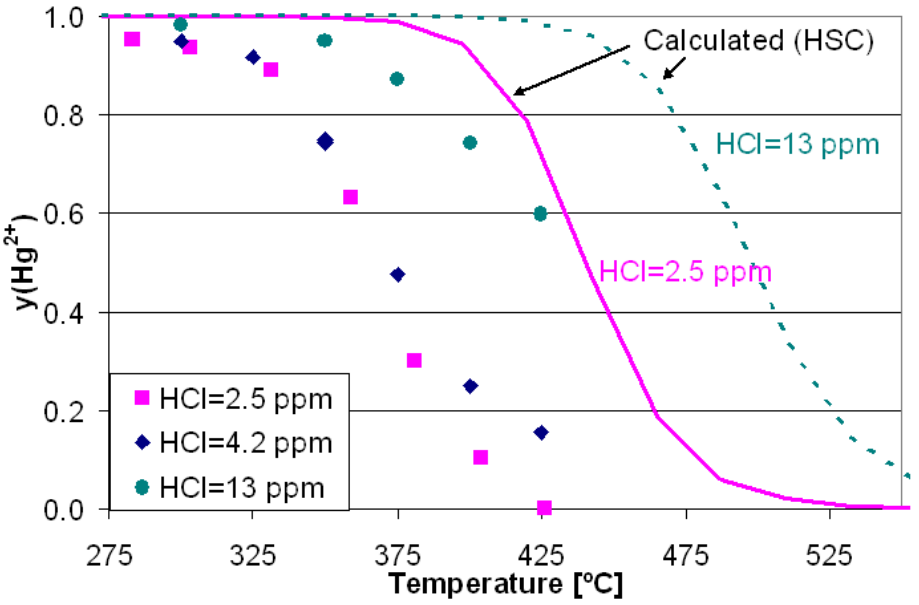

Figure 5.4: Fraction of $HgCl_2$ at SCR outlet as function of temperature for different HCl concentrations at a flow rate of 82 NL/h. The gas contains 25 $\mu g/Nm^3$ Hg^0, 100 ppm NH_3, 4% O_2 and 5% H_2O in balance N_2.

5.3.3 Effect of O_2 and H_2O

Plotted in figure 5.5 is the *stabilized* mercury speciation as function of the O_2 or H_2O concentration at T=350^{o}C with HCl=2.5 ppm and NH_3=100 ppm.
With increasing O_2 from 4-7%, a slight increase in $HgCl_2$ is seen. The effect of increasing H_2O in the range 2-6% is a slight decrease in the $HgCl_2$.

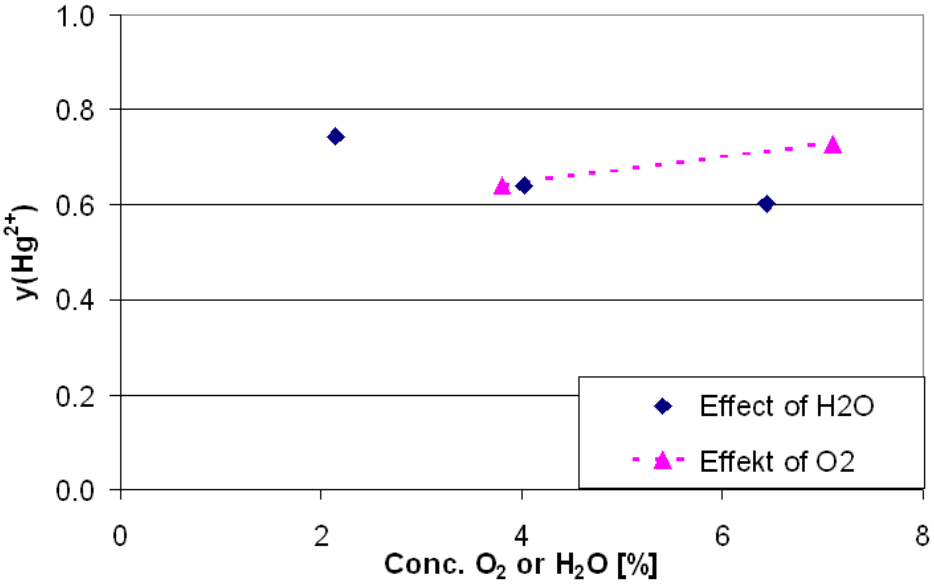

Figure 5.5: Fraction of $HgCl_2$ at SCR outlet as function of concentrations of O_2 and H_2O at a flow rate of 82 NL/h. The gas contains 25 μg/Nm^3 Hg^0, 2.5 ppm HCl, 100 ppm NH_3, 4% O_2 and 5% H_2O in balance N_2 at T=350^{o}C.

5.4 Discussion

Global thermodynamic equilibrium calculations suggest that the presence of NH_3 should not influence the equilibrium composition of mercury. However, results in this study demonstrate that the 'equilibrium' speciation of mercury after the SCR catalyst is indeed shifted towards Hg^0, when NH_3 is added to the gas.
The assumption of a global equilibrium in the flue gas presupposes that none of the reaction pathways of reactants to equilibrium products is limited by kinetics. This assumption clearly does not hold for mercury chemistry in flue gases. The realized mercury speciation will rather be a result of the number of reactions that are running at a considerable rate. The experiments in this study confirm that both $HgCl_2$ reduction and Hg^0 oxidation are taking place over the SCR.
It is here proposed that it is the relative rate of such oxidizing and reducing reactions that determine the *stabilized* mercury speciation over the SCR catalyst. The discussion is initiated by considering the potential net reactions involved.

5.4.1 $HgCl_2$ reduction

Thorwarth (2007) has proposed that a direct reduction of $HgCl_2$ by NH_3 can take place according to the net reaction

$$2\ NH_3 + 3\ HgCl_2 \ \leftrightarrow\ N_2 + 6\ HCl + 3\ Hg^0 \qquad (5.1)$$
$$\Delta G^f(T = 327; 427^oC) = (-181; -238)\ {}^{kJ}/_{mol}$$

The reaction has a negative ΔG^f at relevant temperatures with an increasingly negative value for increasing temperature.
An analogous reaction can be proposed including O_2 as a reactant with an even greater negative ΔG^f at relevant SCR operating temperatures:

$$6\ NH_3 + 3\ HgCl_2 + 3O_2 \ \leftrightarrow\ 3N_2 + 6\ HCl + 3\ Hg^0 + 6H_2O \qquad (5.2)$$
$$\Delta G^f(T = 327; 427^oC) = (-1529; -1600)\ {}^{kJ}/_{mol}$$

The thermodynamic equilibrium constants for both these reactions show that the equilibrium is shifted completely to the right. Both reactions offer plausible pathways for the observed reduction of $HgCl_2$.

An alternative hypothesis for the effect of NH_3 is the production of NH_4Cl via the reaction:

$$NH_3 + HCl \ \leftrightarrow\ NH_4Cl \qquad (5.3)$$
$$\Delta G^f(T = 327; 427^oC) = (-10.0; 15.4)\ {}^{kJ}/_{mol}$$

By production of NH_4Cl, HCl will be depleted from the gas phase, which effectively will push the thermodynamic equilibrium of mercury towards Hg^0. However for a large fraction of the temperature range for SCR operation, the reaction will not be spontaneous. Also, the increasing ΔG^f with temperature is in contrast to the observed increasing effect of NH_3 with temperature. The production of NH_4Cl is an unlikely explanation for the effect of NH_3 on the mercury chemistry over SCR catalysts.

5.4.2 Hg^0 oxidation

The net reaction for the Hg^0 oxidation is typically proposed to take the form

$$2\ HCl + Hg^0 + {}^1/_2\ O_2 \ \leftrightarrow\ HgCl_2 + H_2O \qquad (5.4)$$

since chlorine primarily is present at HCl in the flue gas and the reaction only takes place under oxidizing conditions.

The reaction is completely shifted to the right at relevant concentrations of HCl, O_2

and H_2O. The thermodynamic equilibrium constant takes the form

$$K_P = \frac{P_{HgCl_2} \cdot P_{H_2O}}{P_{Hg^0} \cdot P_{HCl}^2 \cdot P_{O_2}^{1/2}} \tag{5.5}$$

where it can seen that the equilibrium for this individual reaction is dependent on reactants/products in the following decreasing order of importance: HCl > H_2O > O_2.

5.4.3 Hypothesis of 'pseudo' equilibrium

In the absence of NO, it is now proposed that the following two net reactions[1] are taking place over the SCR catalyst

$$\begin{aligned} &R1.\ \ 6\ HCl + 3Hg^0 + 3/2\ O_2 \ \leftrightarrow\ 3\ HgCl_2 + 3H_2O \\ &R2.\ \ 2\ NH_3 + 3\ HgCl_2 \ \leftrightarrow\ N_2 + 3\ Hg^0 + 6\ HCl \\ &SUM\ \ 3/2\ O_2 + 2\ NH_3 \leftrightarrow\ 3\ H_2O + N_2 \end{aligned} \tag{5.6}$$

The hypothesis suggests that these two main reactions R1 and R2 determine the mercury speciation after the SCR, because these reactions are both running at a considerable rate.

Mercury is present in flue gases in a factor 1000 less than HCl, NH_3, O_2 and H_2O, so neither of these two reactions will impose changes in the concentration of these components. This means that both reaction R1 and R2 can be running simultaneously and only influence the mercury speciation. When the rates of reaction R1 and R1 are identical, the effect on the mercury speciation is cancelled out, which is seen by the sum of the two reactions.
Interestingly, this sum simply adds up to the oxidation of NH_3 with O_2, which is independent of both the mercury and HCl concentration.

By this hypothesis, the experimental observations can now be explained as follows:
For the case with only Hg^0 at the inlet, the reaction rate of R1 will dominate in the beginning of the catalyst, but as the concentration of $HgCl_2$ increases, so will the rate of R2. At a given mercury speciation achieved at some point along the length of the catalyst, the rates of the two reactions become identical. From this point, the mercury speciation will remain unchanged even though both reactions are continuously taking place. This is the *stabilized* mercury speciation that is measured in this study.
The *stabilized* mercury speciation is, hence, not a thermodynamic equilibrium, but can be considered as being in 'pseudo' equilibrium. This means that the relative rate of the two reactions determine the mercury speciation. The speciation will shift towards Hg^0 if R1 is the slower reaction and visa versa.
The experiments show that increasing HCl, increases the relative rate of R1 compared to R2. The effect of increasing NH_3 is a decrease in the relative rate of R1 compared to R2 pushing the pseudo equilibrium towards Hg^0.

[1] Reaction (5.2) is not included in this analysis, since the conclusions will be the same as for reaction (5.1).

The effect of O_2 and H_2O can be explained by studying reaction R1 alone. The promoting effect of O_2 is a result of reactant promotion on the overall rate of R1. The backwards reaction is completely dominating in the absence of O_2.
The inhibiting effect of H_2O is caused by an increase in the backwards reaction of R1.

5.4.4 Effect of catalyst composition

Finally, in order to further verify the hypothesis of pseudo equilibrium, the effect of changing the catalyst composition is tested. If two different surface reactions are taking place on the catalyst, the rates of the individual reactions will possibly not show the same dependency on the load of active material on the catalyst.
Plotted in figure 5.6 is the *stabilized* mercury speciation as function of temperature for three commercial type catalysts with a low, typical and high V_2O_5-loading. Results show that mercury speciation is indeed dependent on the catalyst composition, where an increasing fraction of $HgCl_2$ is seen for increasing V_2O_5. For the high V_2O_5 catalyst, the mercury speciation approaches the thermodynamic equilibrium.
The results demonstrate that the rate of reaction R1 relative to reaction R2 increases with the V_2O_5 load of the catalyst.

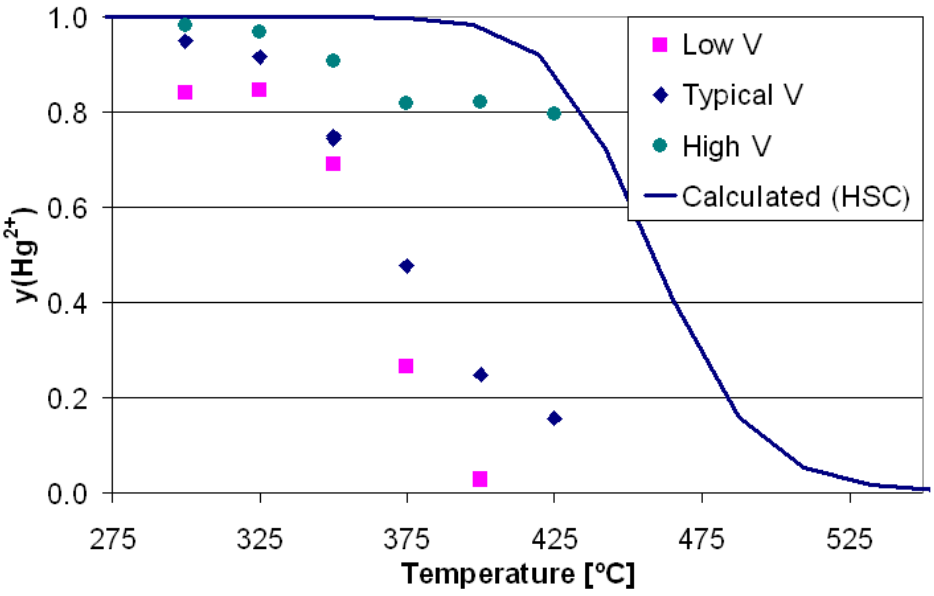

Figure 5.6: Fraction of $HgCl_2$ at SCR outlet as function of temperature over SCR catalysts with different V_2O_5-loads at a flow rate of 82 NL/h. The gas contains 25 $\mu g/Nm^3$ Hg^0, 4.2 ppm HCl, 100 ppm NH_3, 4% O_2 and 5% H_2O in balance N_2.

5.5 Conclusions

A $HgCl_2$ reduction by NH_3 is demonstrated to take place over SCR catalysts for T>325^{o}C. The following two mercury reactions are, thus, taking place over SCR catalysts:

$$R1.\ \ 6\ HCl + 3Hg^0 + {}^3\!/_2\ O_2 \ \leftrightarrow\ 3\ HgCl_2 + 3H_2O$$
$$R2.\ \ 2\ NH_3 + 3\ HgCl_2 \ \leftrightarrow\ N_2 + 3\ Hg^0 + 6\ HCl$$

An equilibrium speciation of mercury is shown to be achieved over SCR catalysts in the presence of NH_3 that does not coincide with the thermodynamic equilibrium. Rather, a pseudo equilibrium has been achieved for the given distribution of Hg^0 and $HgCl_2$, where the rates of the two above reactions are equal.

Measurements of the pseudo equilibrium have been performed for various gas compositions. The study, thus, quantifies the maximum fraction of $HgCl_2$ that can be achieved over an SCR catalyst for each given set of conditions. In the presence of NO, the NH_3 concentration will decrease down through the catalyst as the DeNOx reaction is taking place. This causes the pseudo equilibrium to gradually shift towards $HgCl_2$.

The effect of the $HgCl_2$ reduction can be dampened by increasing the V_2O_5 load of the catalyst, by decreasing operating temperature and by increasing the HCl concentration in the gas.

For low Cl-coals, the $HgCl_2$ reduction will be completely dominating for the mercury chemistry as long as NH_3 is present in the gas, when operating the SCR at elevated temperature T >350^{o}C. This effect can offer part of the explanation for the lower Hg^0 oxidation achieved over full-scale SCR reactors at low chlorine concentrations even though HCl is present in great excess compared to mercury.

Chapter 6

A kinetic study of the Hg^0 oxidation over SCR catalysts

6.1 Introduction

The Hg^0 oxidation over commercial SCR catalysts has across both lab-, pilot- and full-scale (e.g. (Hocquel, 2004; Senior, 2004b)) been observed to be

- Promoted by HCl
- Inhibited by the concomitant DeNOx reaction

Chapter 5 shows experimental evidence that a reduction of $HgCl_2$ takes place over SCR catalysts in the presence of NH_3 at temperatures above 325^{o}C. The following three net reactions are therefore proposed to be relevant for the catalytic oxidation of Hg^0:

$$R1.\ \ 2\ HCl + Hg^0 + {}^1/_2\ O_2 \ \leftrightarrow\ HgCl_2 + H_2O \tag{6.1}$$

$$R2.\ \ 2\ NH_3 + 3\ HgCl_2 \ \leftrightarrow\ N_2 + 3\ Hg^0 + 6\ HCl \tag{6.2}$$

$$R3.\ \ 2\ NO + 2\ NH_3 + {}^1/_2\ O_2 \ \leftrightarrow\ 2\ N_2 + 3\ H_2O \tag{6.3}$$

Reaction R1 is the oxidation of Hg^0 to $HgCl_2$ by HCl. Reaction R2 is the reduction of $HgCl_2$ by NH_3. Reaction R3 is the standard SCR reaction, where NO is reduced by NH_3.

The objective of this study is to investigate the steady-state Hg^0 oxidation over commercial SCR catalysts for different gas compositions and operating conditions. The

importance of the individual reactions R1-R3 on the observed Hg^0 oxidation will be quantified at different temperatures.

6.2 Methods

Laboratory experiments will be carried out in a simulated flue gas testing the effect of varying concentrations of HCl, NH_3, NO, O_2, H_2O and SO_2 on the kinetics of the steady-state Hg^0 oxidation over an SCR catalyst in the temperature range 250-425^{o}C.

6.2.1 Experimental

A Topsøe DNX SCR catalyst (type B, see section 3.1) with a 'typical' vanadia-content is applied for these tests.
The experiments are performed at a very high linear velocity of v=10.3 Nm/s and on a monolithic SCR catalyst with a very low hydraulic diameter. This will decrease the effect from external mass transfer and, thus, enhance the effect of the different test conditions on the surface reaction rate.

The steady-state oxidation of Hg^0 to $HgCl_2$ is recorded in each experiments (according to equation (3.1)). Each experiment is allowed to stabilize for minimum 1 hour, where steady-state presumably has been achieved (see section 3.4.4). All tests are performed with only Hg^0 at the SCR inlet, which means that the conversion equals the fraction of $HgCl_2$ at the SCR outlet: $X = y(Hg^{2+})$.

The conversions reported in this study do not represent what is expected over industrial

Table 6.1: Range of conditions tested. ($\frac{NO_2}{NOx} \approx 0.05$). The concentrations of the individual components at reference conditions are specified in parenthesis.

Catalyst	
Geometry	Type B
V_2O_5	'Typical'
Operating conditions	
Linear velocity v [Nm/s]	10.3
Temperature [^{o}C]	250-425 (350)
Gas composition	
Hg^0	4.2-13.5 $\mu g/Nm^3$
O_2	1.9-6.2% (4%)
H_2O	2-6.2% (5%)
HCl	2.5-55 ppm (4.2 ppm)
NH_3	0-350 ppm (100 ppm)
NOx	0-350 ppm (100 ppm)
SO_2	0-360 ppm (0 ppm)

SCR reactors. However, all tests within this study are performed on catalysts with identical dimensions and geometry at v=10.3 Nm/s, which makes the experimental data directly comparable.
The range of test conditions applied in this study are summarized in table 6.1. The reference gas composition is given in parenthesis; A low HCl concentration of 4.2 ppm is chosen as reference in order to enhance the variation in Hg^0 oxidation across different parameters.

6.2.2 Thermodynamic calculations

Global thermodynamic calculations have been performed via HSC Chemistry 6.1.

6.3 Results and discussion

6.3.1 Preliminary tests

Hg^0 is supplied to the simulated flue gas by a permeation tube maintained at constant temperature, see section 3.2.1. The rate of Hg^0 released from this tube is specified as being constant, but in practice that appears not to be the case. The experiments can therefore not be run at a constant concentration of Hg^0. For that reason, these preliminary experiments test the dependency of the Hg^0 oxidation on the total concentration of mercury.
Plotted in figure 6.1 is the Hg^0 oxidation over the SCR as function of the Hg^0 concentration at v=10.3 Nm/s and 350^0C. The gas is relevant to real flue gases containing Hg^0,O_2, H_2O, NO and NH_3 in N_2.

Results show that the observed Hg^0 oxidation over the SCR catalyst is independent of the total Hg^0 concentration in the range 2.4-12.5 $\mu g/Nm^3$. This means that the kinetics of the Hg^0 oxidation over SCR catalysts is 1^{st} order in the Hg^0 concentration.

6.3.2 Study of reaction 1 alone

Data for experiments run in the absence of NO and NH_3 are initially treated in order to consider the kinetics of reaction R1, separately.

Initially, it is confirmed that the Hg^0 oxidation with HCl is a catalytic reaction, since only negligible oxidation is measured over the SCR reactor in the absence of catalyst. The Hg^0 oxidation is only $\approx 2\%$ over the empty reactor in a gas containing 12.5 $\mu g/m^3$ Hg^0, 4.2 ppm HCl, 100 ppm NO, 3.9% O_2 and 5% H_2O in N_2.

6.3.2.1 Effect of HCl

Plotted in figure 6.2 is the oxidation of Hg^0 over the SCR catalyst for increasing HCl at 350^{o}C. For HCl=0 ppm, a continuous adsorption of Hg^0 will take place and no oxidized mercury is found in the gas phase (results not shown).
In the presence of 2.5 ppm of HCl, the Hg^0 oxidation is at a level of 82%. According to thermodynamic calculations, all mercury should exist as $HgCl_2$, which shows that the Hg^0 oxidation over the SCR is limited by kinetics under these conditions. The kinetics of the Hg^0 oxidation appear to be independent of the HCl concentration from 2.5 to 25 ppm.

The lack of dependency of the Hg^0 oxidation on HCl is not due to external mass transfer of Hg^0 limiting the reaction rate (when HCl>2.5 ppm). This is supported by a higher Hg^0 oxidation achieved over an SCR catalyst with higher V_2O_5-load in an experiment run at otherwise identical conditions. These results will be covered later in this chapter.

At ppm-levels, HCl is present in great excess compared to Hg^0 and can be considered to be at a constant concentration throughout the catalyst. Possibly, the rate of the surface reaction is independent of HCl, because the catalyst surface is saturated with adsorbed HCl even at HCl=2.5 ppm ($\theta_{HCl} \rightarrow 1$).

6.3.2.2 Effect of temperature

Plotted in figure 6.3 is the oxidation of Hg^0 over the SCR catalyst for increasing temperature in the range 250-425^{o}C for HCl=4.2 ppm and 46 ppm.
Firstly, the Hg^0 oxidation is constant at a level of 82% with increasing temperature in the range 250-350^{o}C. This indicates that adsorption phenomena must play a major role for the kinetics of the surface reaction. However, no effect of increasing HCl=4.2-46 ppm is observed in the temperature range 300-350^{o}C suggesting that adsorption of Hg^0 may be limiting the reaction rate and not adsorption of HCl.

For temperatures above 350^{o}C, the Hg^0 oxidation will decrease for HCl=4.2 ppm down to 69% at 425^{o}C, whereas the oxidation remains unchanged for HCl=46 ppm up to 400^{o}C. It appears that the reverse of reaction R1 is playing an increasing role for HCl=4.2 ppm, since the speciation approaches the thermodynamic equilibrium at these high temperatures.

6.3.2.3 Effect of O_2 and H_2O

Variations in the O_2=1.9-3.8% and H_2O=3.4-5% have been tested, which show a negligible influence on the catalyst activity at reference conditions (in the absence of NO and NH_3).

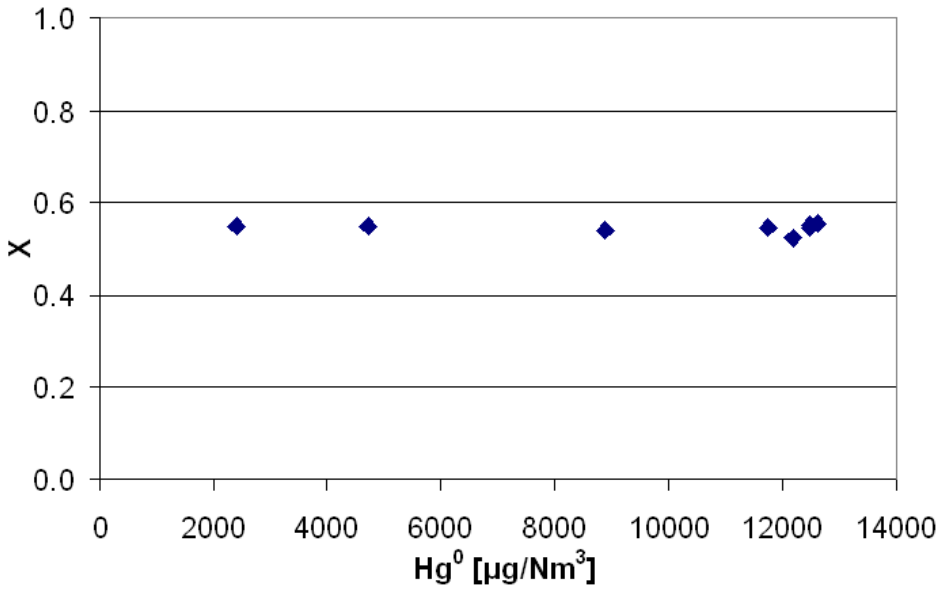

Figure 6.1: Steady-state oxidation of Hg^0 over the SCR as function of the Hg^0 concentration at v=10.3 Nm/s and T=350^{o}C. The gas contains 4.2 ppm HCl, 100 ppm NO and NH_3, 4% O_2 and 5% H_2O in balance N_2. The plot summarizes measurements from 7 different test days and 2 different catalysts.

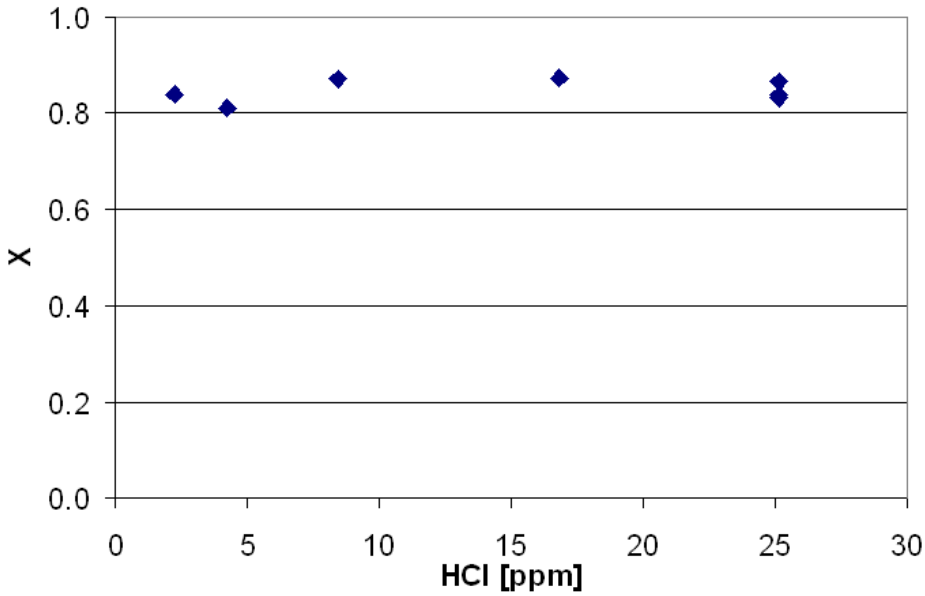

Figure 6.2: Steady-state oxidation of Hg^0 over the SCR as function of HCl at v=10.3 Nm/s and T=350^{o}C. The gas contains 7-12 $^{\mu g}/_{Nm^3}$ Hg^0, 4% O_2 and 5% H_2O in balance N_2.

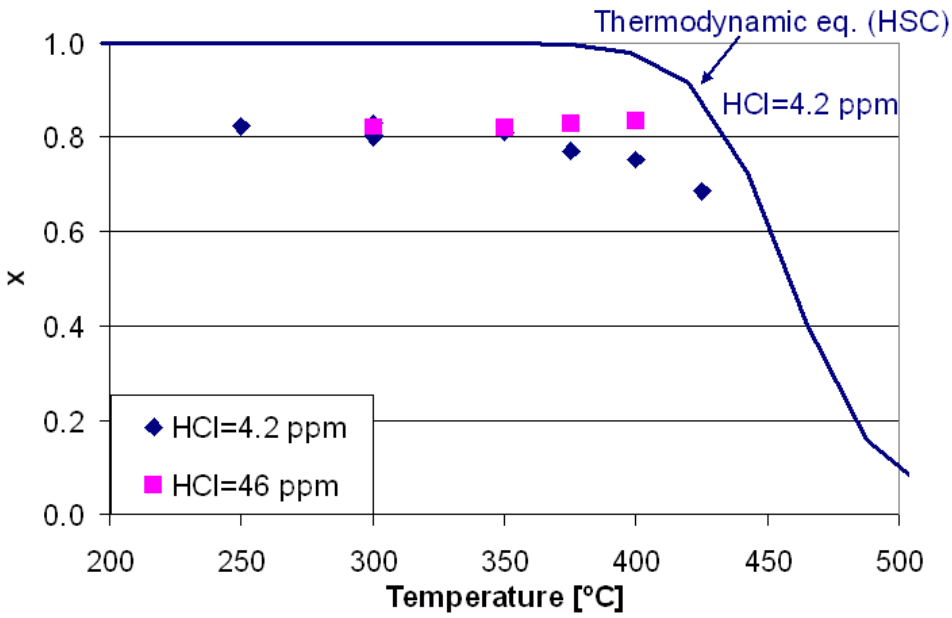

Figure 6.3: Steady-state oxidation of Hg^0 over the SCR as function of temperature for HCl=4.2 ppm and 46 ppm at v=10.3 Nm/s. The gas contains 6.1-9.1 $\mu g/Nm^3$ Hg^0, 4% O_2 and 5% H_2O in balance N_2.

6.3.2.4 Summary

Neither HCl (above 2.5 ppm), O_2 or H_2O appear to influence the rate of the Hg^0 oxidation via reaction R1 in the absence of NO and NH_3. Furthermore, an effect of temperature is only seen, when the thermodynamic equilibrium is approached.
It is likely that the kinetics of reaction R1 is governed by sorption phenomena of Hg^0.

6.3.3 Study of combined reaction 1, 2 and 3

When experiments are performed in the presence of both NO and NH_3, the DeNOx reaction will start taking place. Therefore, concentration profiles of both components will exist down through the catalyst channel and in the catalyst wall.

6.3.3.1 Effect of NO and NH_3

Plotted in figure 6.4 is the oxidation of Hg^0 over the SCR catalyst for increasing concentrations of NO, NH_3 or for a combination of the two. Experiments where both NO and NH_3 are present will be referred to as *under DeNOx conditions*.
The experiments are run at T=350^{o}C with 4.2 ppm HCl. The DeNOx degrees in these experiments are given in table 6.2.

Table 6.2: Measured DeNOx degrees at v=10.3 Nm/s and T=350^{o}C

Conc. NO=NH_3	100 ppm	350 ppm
DeNOx	72%	77%

Data shows that NO alone has no effect on the Hg^0 oxidation, whereas NH_3 alone causes a slight inhibition on the overall conversion of Hg^0 in accordance with reduction of $HgCl_2$ by reaction R2.
Interestingly, the results suggest that an synergistic inhibition between NO and NH_3 is taking place. No difference is seen in the measured Hg^0 oxidation at a given NH_3 concentration if the experiment is run with NO=NH_3 or with constant NO=350 ppm. This suggests that the synergistic inhibition is coupled to the DeNOx reaction R3 taking place.

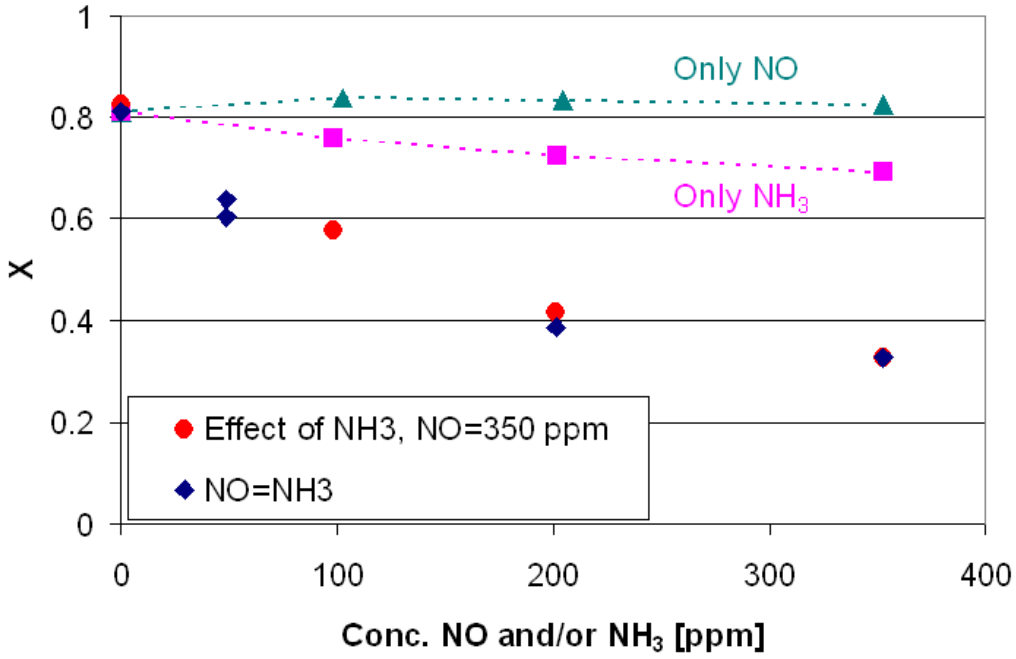

Figure 6.4: Steady-state oxidation of Hg^0 over the SCR as function of NO, NH_3 or a combinations of the two at v=10.3 Nm/s and T=350^{o}C. The gas contains 4.5-12.5 $^{\mu g}/_{Nm^3}$ Hg^0, 4.2 ppm HCl, 4% O_2 and 5% H_2O in balance N_2.

6.3.3.2 Effect of temperature

Plotted in figure 6.5 is the oxidation of Hg^0 over the SCR catalyst for increasing temperature in the range 250-425^{o}C for three different gas compositions: 1) 4.2 ppm HCl and no DeNOx, 2) 4.2 ppm HCl and 100 ppm NH_3 and 3) 4.2 ppm HCl and 100 ppm NH_3 and NO.

The DeNOx degree in these experiments are given in table 6.3.

Table 6.3: Measured DeNOx degrees at v=10.3 Nm/s and NO=NH_3=100 ppm.

Temp.	300^{o}C	350^{o}C	400^{o}C
DeNOx	68%	72%	74%

Generally, a lower Hg^0 oxidation is seen under DeNOx conditions. This proves that an inhibition from NH_3 with/without NO is taking place on the Hg^0 oxidation in the entire range of SCR operating temperatures. A maximum Hg^0 oxidation is seen around 300^{o}C under DeNOx conditions.

Two different mechanistic regimes appear to exist for the kinetics of the Hg^0-oxidation under DeNOx conditions: T<300^{o}C and T>350^{o}C. The temperature region T=300-350^{o}C represents a 'mixed regime'.

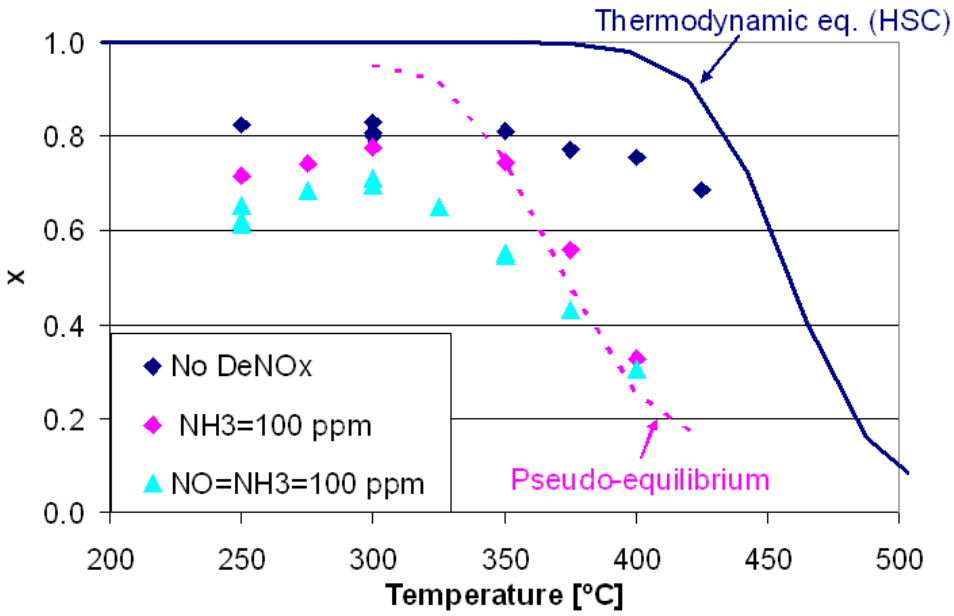

Figure 6.5: Steady-state oxidation of Hg^0 over the SCR as function of temperature at v=10.3 Nm/s. The gas contains 4.0-12.5 $\mu g/Nm^3$ Hg^0, 4.2 ppm HCl, 4% O_2 and 5% H_2O in balance N_2.

For temperatures above 350^{0}C, the mercury speciation is approaching the pseudo equilibrium, where the Hg^0 oxidation via reaction R1 is balanced out with the $HgCl_2$ reduction via reaction R2. The plotted pseudo equilibrium represents the upper level of $HgCl_2$ that can be achieved for HCl=4.2 ppm and NH_3=100 ppm. (This effect has been covered in chapter 5).
Results show that the pseudo equilibrium mercury speciation over the SCR is reached very fast for T>375°C. This means that the overall Hg^0 oxidation primarily depends on how the NH_3 concentration evolves in the reactor.

The synergistic inhibition by NO and NH_3 is evident in the entire temperature range 250-375^{o}C. At temperatures above 375^{o}C, the inhibition of the Hg^0 oxidation is obliterated due to the $HgCl_2$ reduction by NH_3 dominating the mercury chemistry.

For temperatures below 300^{o}C, the presence of NH_3 alone has an increasing inhibition on the Hg^0 oxidation with decreasing temperature. At this temperature, the $HgCl_2$ reduction via reaction R2 is unimportant and cannot explain the effect of NH_3.

6.3.3.3 Discussion on effects under DeNOx conditions

Vanadia has been shown to be the active specie for the Hg^0 oxidation over commercial SCR catalysts (Hocquel, 2004). It is now hypothesized that more specifically the vanadia Lewis sites (V^{5+}=0) are active in the catalytic Hg^0 oxidation in agreement with He et al. (2009).

Two possible explanations for the inhibiting effects under DeNOx conditions at low temperatures support the hypothesis:

- Effect of NH_3 alone below 300^{o}C: Nova et al. (2006) demonstrate an inhibiting effect of NH_3 on the DeNOx reaction at low temperatures up to 250^{o}C, since NH_3 in addition to adsorbing on Brønsted acid sites on the catalyst also adsorbs on Lewis-sites (V^{5+}=O) at low temperatures. This adsorption blocks the sites for other interactions and, thus, inhibits of the DeNOx reaction.

- Synergistic effect under DeNOx conditions: The mechanism for the DeNOx reaction involves the reduction of active Lewis sites (V^{5+}=O) on the SCR catalyst that need to be oxidized in order to regain activity (Topsoe, 1994):

$$2\ V^{4+} - OH + {}^1\!/_2\ O_2 \leftrightarrow\ 2\ V^{5+} = O + H_2O \tag{6.4}$$

  Lietti et al. (1996) report that the kinetics of the DeNOx reaction is limited by the reoxidation of Lewis sites at low temperatures.

Both these phenomena will analogously inhibit the catalytic Hg^0 oxidation if Lewis sites also are active sites for this reaction.

6.3.3.4 Effect of HCl

Plotted in figure 6.6 is the oxidation of Hg^0 over the SCR catalyst for increasing HCl at T=250^{o}C and 350^{o}C in two different gas compositions: 1) in the presence of 100 ppm NH_3 and 2) in the presence of 100 ppm NO and NH_3.
The level of Hg^0 oxidation achieved without NO and NH_3 is independent of HCl at these temperatures (as shown previously in figure 6.3) and is indicated by a full-line in the graph.

This experimental data support that two different mechanistic regimes exist across temperature:

- At 350^{o}C, a promoting effect of HCl on the Hg^0 oxidation is seen in the presence of NH_3 with/without NO. The synergistic inhibition is evident at this temperature. The Hg^0 oxidation increases with increasing HCl until reaches a maximum level. This maximum is slightly below the level of Hg^0 oxidation seen in the absence of NO and NH_3. At HCl=8 ppm, the effect of NH_3 alone is largely eliminated, whereas the effect of the DeNOx reaction is largely eliminated at HCl=25 ppm.
- At 250^{0}C, the effect of NH_3 alone appears to primarily be responsible for the inhibition of the Hg^0 oxidation. The synergistic inhibition of NO and NH_3 is minor. The Hg^0 oxidation is not promoted by increasing HCl and remains at a level of 70% compared to 82% in the absence of NH_3. Both these observations are in contrast to T=350^{o}C.

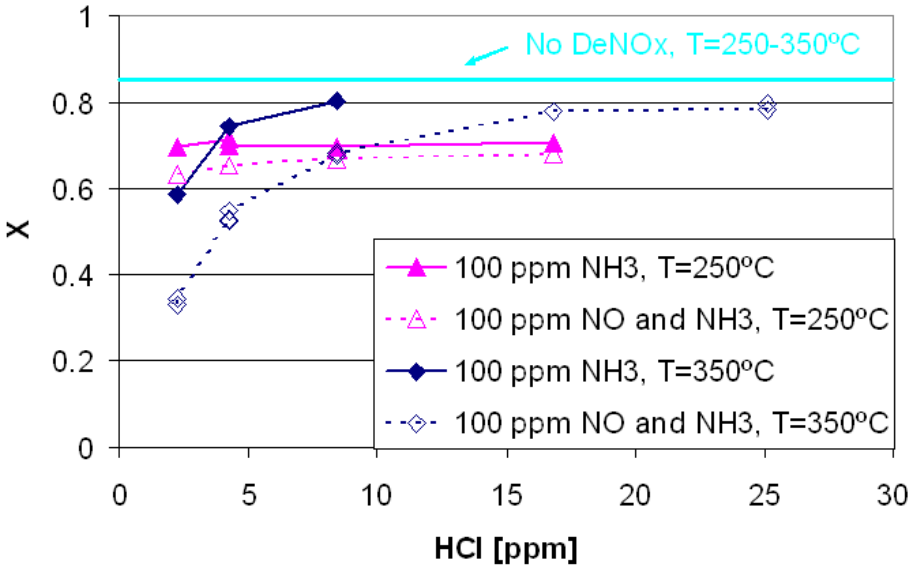

Figure 6.6: Steady-state oxidation of Hg^0 over the SCR as function of HCl at v=10.3 Nm/s. Experiments are performed at T=250 and 350^{o}C in the presence of NH_3 alone or under DeNOx conditions. The gas contains 4.2-12.2 $\mu g/Nm^3$ Hg^0, 4% O_2 and 5% H_2O in balance N_2. Indicated in the full line is the level of Hg^0 oxidation achieved in the absence of NO and NH_3 at both temperatures in the entire HCl-range.

6.3.3.5 Discussion on effects of HCl

The lack of promotion by HCl at T<300^{o}C shows that the availability of this component is not limiting the overall rate of Hg^0 oxidation. In section 6.3.2.2, it is proposed that

Hg^0 adsorption is limiting the rate of reaction R1. If NH_3 is inhibiting the Hg^0 oxidation by adsorption on Lewis sites, then the rate of Hg^0 oxidation is limited by Hg^0 adsorption on precisely Lewis sites.

Chapter 5 has demonstrated that increasing HCl enhances the relative importance of reaction R1 to reaction R2. The $HgCl_2$ reduction via reaction R2 influences mercury speciation for T>325^{o}C, which can explain that the effect of NH_3 alone at 350^{o}C is diminished by increasing HCl.
Surprisingly, the synergistic inhibition from NO and NH_3 is also reduced by increasing HCl. The cause of the promotion by HCl has been quite puzzling for me. Various (more or less realistic) explanations can be posed for the effect:

1. HCl is inhibiting the DeNOx reaction and less Lewis sites will therefore be consumed at elevated HCl. This effect has never been reported in literature for the DeNOx reaction, which is a quite 'mature' area of research. It is therefore considered to be unlikely.

2. In the reoxidation of vanadia-sites, some of the $HgCl_2$ is used as oxidant via the following reaction:

$$2\ V^{4+} - OH + \ HgCl_2 \leftrightarrow \ 2\ V^{5+} = O + 2\ HCl + Hg^0 \tag{6.5}$$

   Increasing HCl could inhibit this reaction by scavenging $HgCl_2$ from the catalyst surface or by shifting the equilibrium of the reaction to the left.

3. HCl also adsorbs on/interacts with Lewis sites. This implies that adsorption of HCl on Lewis sites is limiting the rate of the Hg^0 oxidation via reaction R1 under DeNOx conditions at 350^{o}C up to a level of HCl=25 ppm. After this HCl concentration, the Hg^0 adsorption is limiting for the overall rate of reaction R1. This appears to be the most likely explanation.

Nevertheless, the effect of HCl at T=350^{0}C is a promotion of Hg^0 oxidation up to the level seen in the absence of NH_3 and NO.

6.3.3.6 Effect of O_2 and H_2O

Plotted in figure 6.7 is the effect of O_2 and H_2O on the Hg^0 oxidation over the SCR catalyst at 350^{o}C with and without DeNOx.
Under DeNOx conditions, the effect of increasing H_2O is a slight inhibition of the Hg^0 oxidation, whereas increasing O_2 slightly promotes the oxidation. In contrast, variations in O_2=1.9-3.8% and H_2O=3.4-5% do not influence the kinetics of the Hg^0 oxidation in the absence of NO and NH_3.

At T=350^{o}C, the overall Hg^0 oxidation over the SCR under DeNOx conditions is approaching the pseudo equilibrium. The relative rate of the Hg^0 oxidation via reaction R1 to the $HgCl_2$ reduction via reaction R2 is governing the mercury speciation. Apparently, variations O_2 and H_2O influence the relative rate of reaction R1 and R2.

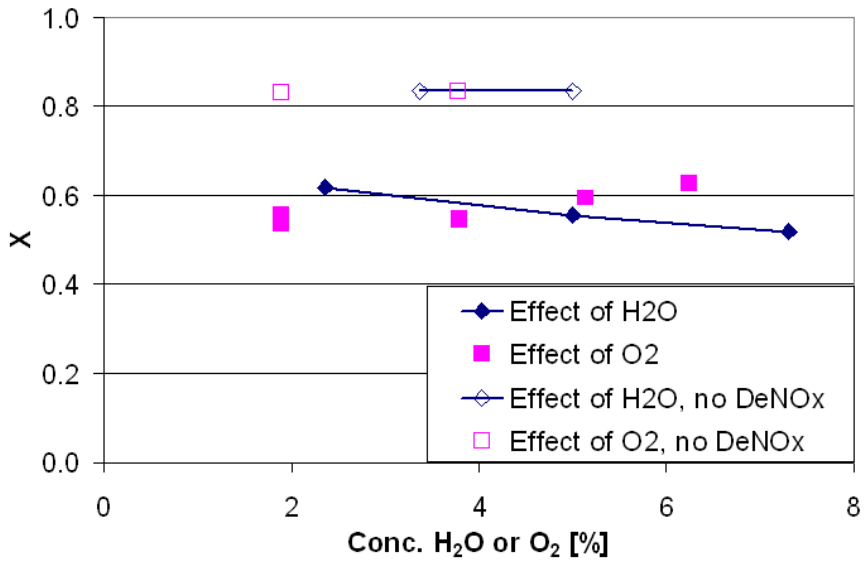

Figure 6.7: Steady-state oxidation of Hg^0 over the SCR as function of O_2 and H_2O at v=10.3 Nm/s and 350^{o}C with and without 100 ppm NO and NH_3. The gas contains 6.4-12.6 $\mu g/Nm^3$ Hg^0, 4% O_2 and 5% H_2O in balance N_2.

6.3.3.7 Effect of SO_2

SO_2 will be present in real combustion gases. Experiments in the presence of 350 ppm SO_2 have been carried out in order to verify that the observed effects on the Hg^0 oxidation are still relevant in the presence of this component.
The oxidation of Hg^0 oxidation for increasing HCl at T=350^{o}C under DeNOx conditions is again tested - at conditions otherwise identical to section 6.3.3.4. No change on Hg^0 oxidation compared to the previous experiment is observed.

6.3.3.8 Effect of catalyst composition

Plotted in figure 6.8 is the Hg^0 oxidation over the SCR catalyst at 350^{o}C as function of HCl under DeNOx conditions for three different catalyst compositions: Low, typical and high V_2O_5.

The DeNOx degree in these experiments are given in table 6.4.

Table 6.4: Measured DeNOx degrees at v=10.3 Nm/s, T=350^{o}C and NO=NH_3=100 ppm.

V_2O_5	Low	Typical	High
DeNOx	69%	72%	89%

Results show that increasing V_2O_5 load both promotes the DeNOx reaction and the

overall Hg^0 oxidation over the SCR. Different levels of Hg^0 oxidation is seen for the three V_2O_5 loads. For all V_2O_5 loads, the effect of increasing HCl under DeNOx conditions is a promotion of the Hg^0 oxidation until a maximum level is reached around HCl=17 ppm.
In chapter 5, it is established that increasing V_2O_5 dampens the relative rate of reaction R2 compared to R1 (see figure 5.6). This can explain the different levels of Hg^0 oxidation for low HCl concentrations for the three V_2O_5 loads.

The Hg^0 oxidation has also been measured in the absence of NO and NH_3 for typical and high V_2O_5 loads. Little/no effect is seen for increasing HCl under these conditions (as shown in section 6.3.2.1) and the levels of Hg^0 oxidation are simply indicated as full lines in the graph. Only reaction R1 is in play in these experiments, so the experimental results show that increasing V_2O_5 specifically increase the rate of reaction R1. This suggests that more Hg^0 adsorption sites, possibly vanadia Lewis sites, have been created by the increase in V_2O_5 load.

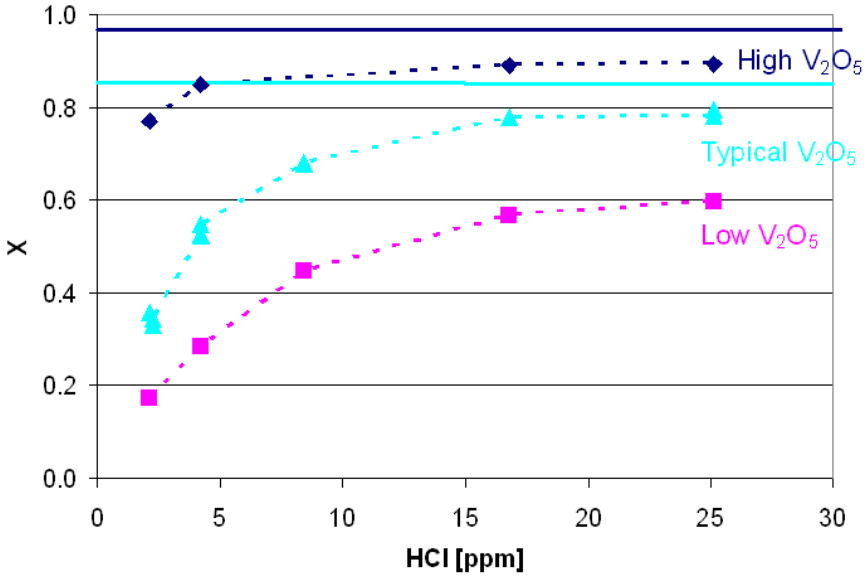

Figure 6.8: Steady-state oxidation of Hg^0 over the SCR as function of HCl for low, typical and high V_2O_5-load of the catalyst at v=10.3 Nm/s and 350^{o}C. The gas contains 8.8-12.7 $^{\mu g}/_{Nm^3}$ Hg^0, 100 ppm NO and NH_3, 4% O_2 and 5% H_2O in balance N_2. The full lines indicate the level of Hg^0 oxidation achieved for typical and high V_2O_5 in the absence of NO and NH_3 for otherwise identical experiments.

6.4 Conclusions

This study demonstrates that the following three reactions influence the kinetics of the Hg^0 oxidation over SCR catalysts:

$$R1.\ \ 2\ HCl + Hg^0 + 1/2\ O_2 \ \leftrightarrow\ HgCl_2 + H_2O$$
$$R2.\ \ 2\ NH_3 + 3\ HgCl_2 \ \leftrightarrow\ N_2 + 3\ Hg^0 + 6\ HCl$$
$$R3.\ \ 2\ NO + 2\ NH_3 + 1/2\ O_2 \ \leftrightarrow\ 2\ N_2 + 3\ H_2O$$

Different effects by NO and NH_3 on the overall Hg^0 oxidation have been shown to be of importance in the range of SCR operating temperatures.

- At T>325°C, $HgCl_2$ reduction by NH_3 via reaction R2 will take place. The observed Hg^0 oxidation will reflect the relative rate of the Hg^0 oxidation (R1) to the $HgCl_2$ reduction (R2).
- At T<300°C, NH_3 will adsorb on Lewis sites on the catalyst making them less available for Hg^0 oxidation (R1).
- The combination of NO and NH_3 serves a synergistic inhibition on the Hg^0 oxidation in the temperature range 250-375^{0}C. Above this temperature, the synergistic effect is obliterated due to reaction R2 being dominating. The synergistic effect is proposed to be caused by the consumption of Lewis sites in the DeNOx reaction (R3), which must be oxidized to regain activity. This reduces the number of active sites available for the Hg^0 oxidation (R1).

Results indicate that the rate of Hg^0 oxidation (R1) in the absence of NO and NH_3 is limited by adsorption of Hg^0 on vanadia Lewis sites. Since the Hg^0 oxidation increases with increasing the V_2O_5 load, it appears that more Hg^0 adsorption sites have been produced.

The effect of reaction R2 can be dampened by increasing HCl or by increasing the V_2O_5 load. Furthermore, the synergistic inhibition by NO and NH_3 is reduced by increasing HCl. Increasing V_2O_5 or HCl (at T>300°C) are, therefore, means for optimizing the overall Hg^0 oxidation over SCR catalysts.

Finally, the study has demonstrated that different kinetic regimes exist within relevant SCR operating temperatures. The effect of various parameters can thus be different, when operating in each of these regimes.

Chapter 7

A mechanistic study of mercury reactions over SCR catalysts

7.1 Introduction

Reactions in heterogeneous catalysis are always a series of steps, including adsorption on the surface, reaction and desorption back into the gas phase.

The following two mercury reactions have been proposed in chapter 6 to take place over SCR catalysts:

$$R1.\ \ 2\ HCl + Hg^0 + {}^1\!/_2\ O_2 \ \leftrightarrow\ HgCl_2 + H_2O$$
$$R2.\ \ 2\ NH_3 + 3\ HgCl_2 \ \leftrightarrow\ N_2 + 3\ Hg^0 + 6\ HCl$$

The $HgCl_2$ reduction via reaction R2 has not been studied previously.
The mechanism for the Hg^0 oxidation via reaction R1 is poorly understood. He et al. (2009) speculate that the catalytic reaction takes place by a Langmuir-Hinshelwood mechanism, where both Hg^0 and HCl are adsorbing on the catalyst. Reaction then takes place between the adsorbed species forming $HgCl_2$ that is readily released from the catalyst.

Chapter 6 studies the kinetics of the overall Hg^0 oxidation over SCR catalysts. The experimental data suggest that reaction R1 is limited by the adsorption of Hg^0 on vanadia Lewis sites on the catalyst. This means that a study of precisely this phenomenon can give valuable information on the overall rate of the reaction R1.

The adsorption of Hg^0 over commercial SCR catalysts has been studied by e.g. (Eom et al., 2008; Hocquel, 2004; Hong et al., 2010; Thorwarth, 2007). It is found that

- The Hg^0 adsorption increases with increasing V_2O_5 (Hocquel, 2004). XPS data

indicate that the adsorption takes place on vanadia Lewis sites (Eom et al., 2008)

- The Hg^0 adsorption greatly increases in the presence of O_2 compared to a pure N_2-atmosphere (Eom et al., 2008), since mercury most likely is adsorbing as HgO(ads) on the SCR.
- The presence of HCl in the gas decreases/eliminates Hg^0 adsorption, while gaseous $HgCl_2$ is produced (Hocquel, 2004).
- The Hg^0 adsorption on SCR catalysts decreases in the presence of the DeNOx reaction (Eom et al., 2008; Hong et al., 2010). A step increase in NH_3 causes a desorption of Hg^0 from the SCR (Thorwarth, 2007). The desorption is possibly occurring by NH_3 reducing the HgO(ads) to Hg^0, which is released from the catalyst.

No experimental data has been found that directly investigate the adsorption of HCl and $HgCl_2$, which may be first steps in the catalytic reactions R1 and R2, respectively.

The objective of this study is to further elucidate the mechanisms for the two catalytic reactions R1 and R2 and to derive overall rate expressions for the reactions over the SCR.
The study will start by experimentally investigating the adsorption of the reactants Hg^0, $HgCl_2$ and HCl on the SCR catalyst in different testing conditions as a means to gain information on the first steps in the catalytic reactions R1 and R2. Based on experimental evidence and principles from microkinetic modelling, elementary steps for the catalytic reactions R1 and R2 will be proposed and overall rate expressions will be derived.

7.2 Methods

Laboratory experiments will be carried out in a simulated flue gas testing the adsorption of Hg^0 on SCR catalysts in different gas compositions, operating temperature and catalyst compositions. The adsorption of Hg^0 is only studied in the absence of HCl, because then no gaseous oxidized mercury is formed and the adsorption can be studied separately from the catalytic oxidation. Each adsorption experiment is terminated by a step increase in HCl from 0 to 8 ppm and the transient sorption phenomena is recorded for each set of conditions.

$HgCl_2$ is only studied under a set of reference conditions. HCl adsorption is also only studied under reference conditions, but for three different catalyst compositions.

7.2.1 Experimental

A Topsøe DNX SCR catalyst (type A, see section 3.1) with a 'typical' vanadia-content is applied for these tests. The TiO_2 carrier (without V_2O_5 and WO_3) for the type A catalyst is also tested.

Adsorption is studied by passing a gas with Hg^0, $HgCl_2$ or HCl over a fresh SCR catalyst and then record the removal of the given component over the reactor relative to the inlet level. All experiments within this study are performed on catalysts with identical dimensions and geometry and at the same gas flow, which makes the experimental data directly comparable.

Table 7.1 gives the specifications for the concentrations and flows for the experiments in this study. Experiments are run at a low H_2O concentration in order to be able to measure total mercury via the reduction unit.

Table 7.1: Range of conditions tested. The numbers in parentheses specify the reference conditions.

Catalyst	
Geometry	Type A
V_2O_5	'Typical', absent
Operating conditions	
Flow [NL/h]	160-163 (163)
Temperature [^{o}C]	350-400 (350)
Gas composition	
Hg^0	0-22 $\mu g/Nm^3$
$HgCl_2$	0-41 $\mu g/Nm^3$
O_2	0-4% (4)
H_2O	2% (2)
HCl	0-100 ppm

7.3 Experimental results

7.3.1 Hg^0 adsorption

The preliminary tests provide experimental support for the basic presumptions on the Hg^0 adsorption over SCR catalysts. In this way, arguments used to support that Hg^0 adsorption is limiting the rate of the Hg^0 oxidation are underpinned. The transient mercury behavior by a step increase in HCl gives valuable information on the mechanism for the catalytic Hg^0 oxidation.

7.3.1.1 Preliminary

Plotted in figure 7.1 is the transient Hg^0 adsorption on fresh SCR catalysts for five different test conditions. The reference gas contains 12 $\mu g/Nm^3$ Hg^0, 4% O_2 and 2% H_2O in N_2.
The different test conditions entail: 1) Reference gas at T=350^{o}C over SCR, 2) Reference gas at T=400^{o}C over SCR, 3) Reference gas with 37 ppm NH_3 at T=350^{o}C, 4) Reference gas at T=350^{o}C over TiO_2 carrier and 5) Hg^0 in N_2 atmosphere at T=350^{o}C over SCR.

No oxidized mercury is measured at the SCR outlet for either of these experiments.

The effects are summarized here:

1. The reference experiment shows a continuous adsorption of Hg^0 on a fresh SCR catalyst in the presence of O_2 in the gas. 30% of the inlet Hg^0 is being adsorbed after 25 minutes of exposure.

2. The Hg^0 adsorption decreases with increasing temperature T=350-400^{o}C. In section 6.3.2.2, a low temperature dependency for the rate of reaction R1 is observed. This is suggested to be due to adsorption of Hg^0 limiting the overall rate of reaction, since adsorption typically decreases with temperature. This experiment simply proves that Hg^0 adsorption in fact decreases with temperature.

3. 37 ppm NH_3 (in the absence of NO) is confirmed to cause a decrease in Hg^0 adsorption. The difference in Hg^0 adsorption compared to the reference experiment increases over the time, which coincides with the SCR catalyst concomitantly being saturated with adsorbed NH_3. This could indicate that primarily adsorbed NH_3 serve to destabilize adsorbed mercury, probably by reducing HgO(ads).

4. No adsorption of Hg^0 is observed on the TiO_2 carrier. This proves that the adsorption of mercury is linked to the metal oxides V_2O_5 and/or WO_3.

5. A very low capacity for Hg^0 adsorption is observed in a N_2-atmosphere, where no further adsorption is observed after only 5 minutes of exposure. This supports that the adsorption primarily takes place as HgO(ads).

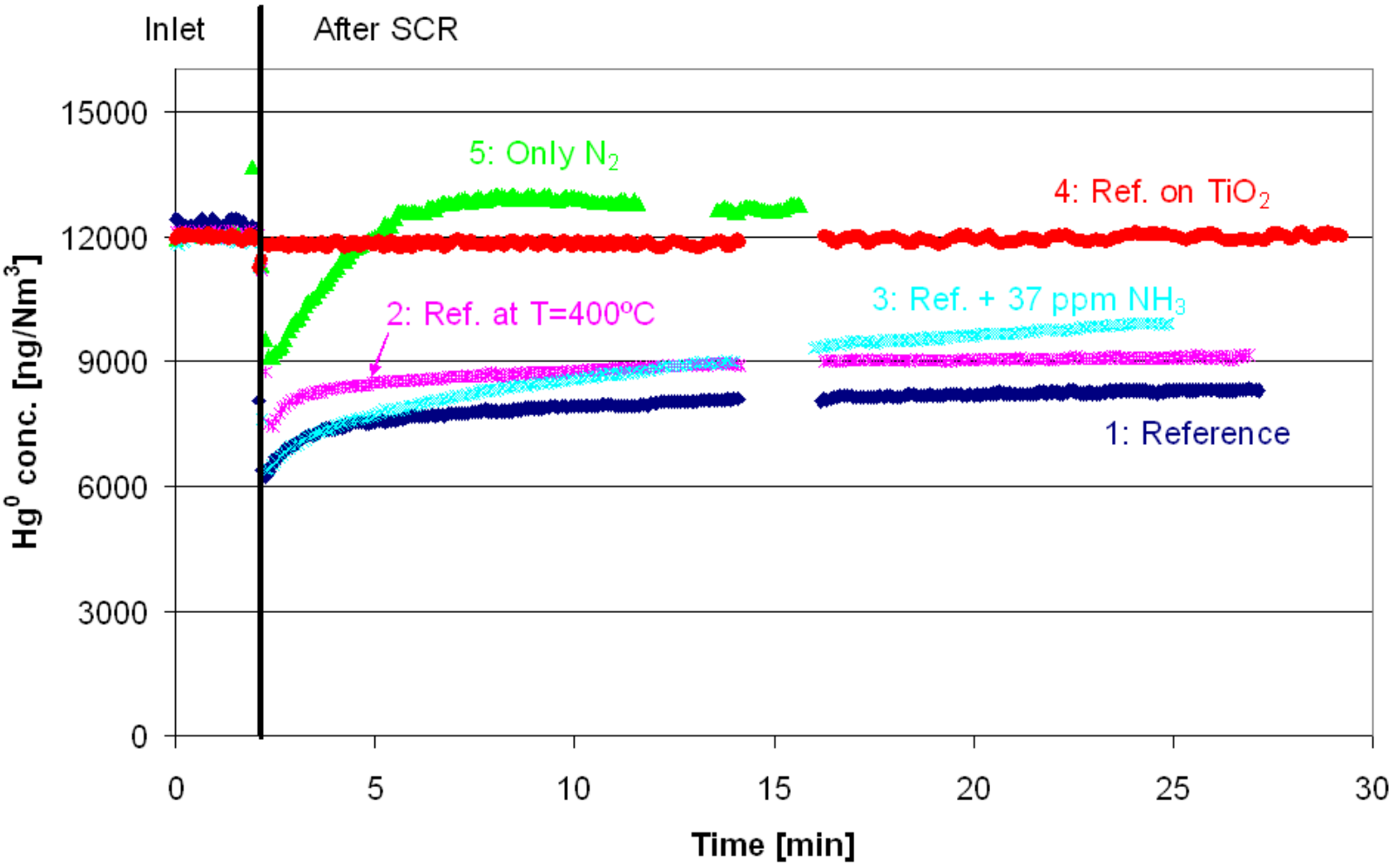

Figure 7.1: Transient Hg^0 adsorption over fresh SCR catalysts with time for T=350^{o}C and U=163 NL/h (160 NL/h for the N_2 atmosphere) for five different test conditions. The gas contains 12 $\mu g/Nm^3$ Hg^0, 4% O_2 and 2% H_2O in balance N_2 (unless otherwise stated). The bypass Hg^0 concentration is measured for t=0-2 minutes. At time t=2 minutes, the gas is passed over the SCR.

7.3.1.2 *Effect of Hg^0 concentration*

Plotted in figure 7.2 is the transient Hg^0 adsorption on fresh SCR catalyst for two different Hg^0 concentrations. The experiments show that the relative Hg^0 adsorption is independent of the Hg^0 concentration for 12-22 $\mu g/Nm^3$ Hg^0. The kinetics of the adsorption is thus 1st order in Hg^0.
This coincides with the rate of the Hg^0 oxidation being 1st order in Hg^0, which has been demonstrated in section 6.3.1.

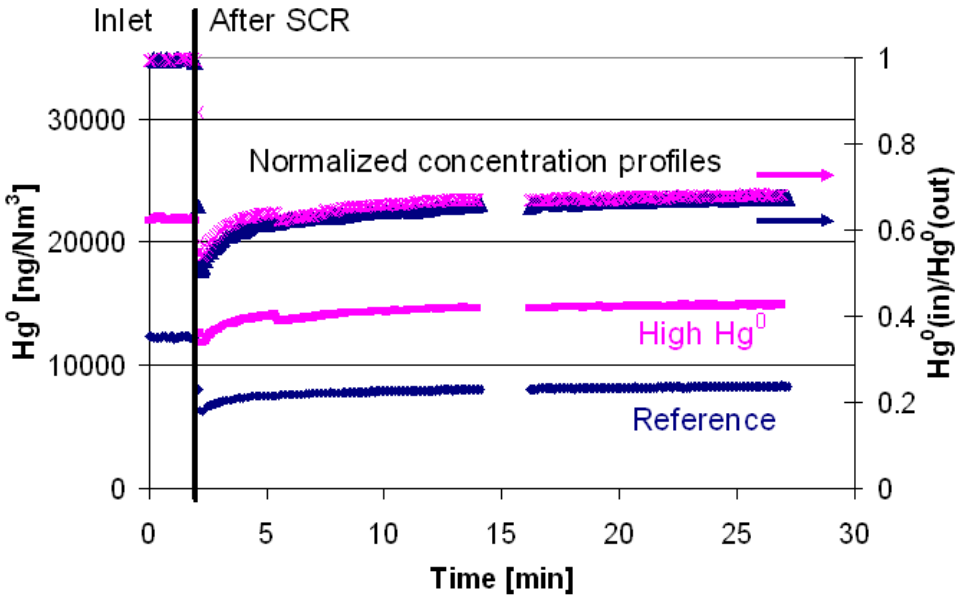

Figure 7.2: The transient Hg^0 adsorption over fresh SCR catalysts with time for T=350^{o}C and U=163 NL/h. The gas contains either 12 or 22 $\mu g/Nm^3$ Hg^0, 4% O_2 and 2% H_2O in balance N_2. The normalized concentration profiles are given by $\frac{Hg^0}{Hg^0(in)}$. At t=2 minutes, the gas is passed over the fresh SCR.

7.3.1.3 *Transient sorption phenomena*

A step increase from 0-8 ppm HCl is imposed on all the latter tests after the initial Hg^0 adsorption.

In all experiments with O_2 in the gas over SCR catalysts, a major desorption of $HgCl_2$ occurs by the addition of HCl and a continuous oxidation of Hg^0 then takes place. This is in line with observations by Hocquel (2004). The SCR catalyst has a large capacity for mercury adsorption, probably as HgO(ads). Since no oxidized mercury is found in the gas phase, HgO is not expected to be volatile. By addition of HCl, the adsorbed mercury will preferentially bind to chlorine and $HgCl_2$ is produced. Due to the volatility of this specie, $HgCl_2$ is readily desorbed from the surface.

In the experiment over the TiO_2 carrier, there is no noticeable effect by adding 8 ppm

HCl. The TiO_2 is both inactive in terms of Hg^0 adsorption and oxidation.

For the experiment with Hg^0 in a N_2 atmosphere, the whole transient experiments including both the Hg^0 adsorption and the step increase in HCl=0-8 ppm is shown in figure 7.3.
Two interesting observations are made from the experiment: Firstly, the step increase from 0-8 ppm HCl causes a further adsorption of Hg^0 for a short time period (from t=13-20 minutes). Some Hg^0 is apparently adsorbing in connection with HCl on the SCR if oxygen is not available. This suggests that HCl is adsorbing on the SCR catalyst and that adsorbed chlorine interacts with mercury.
Secondly, a continuous oxidation of Hg^0 takes place with HCl even in the absence of O_2 in the gas. That shows that lattice oxygen can react with Hg^0 and, due to the low concentration of mercury, supply enough oxygen for the Hg^0 oxidation reaction for a very long time.
Neither Hg^0 adsorption or oxidation takes place before the addition of HCl. The experiment suggests that the catalytic Hg^0 oxidation involves HCl in an adsorbed form.

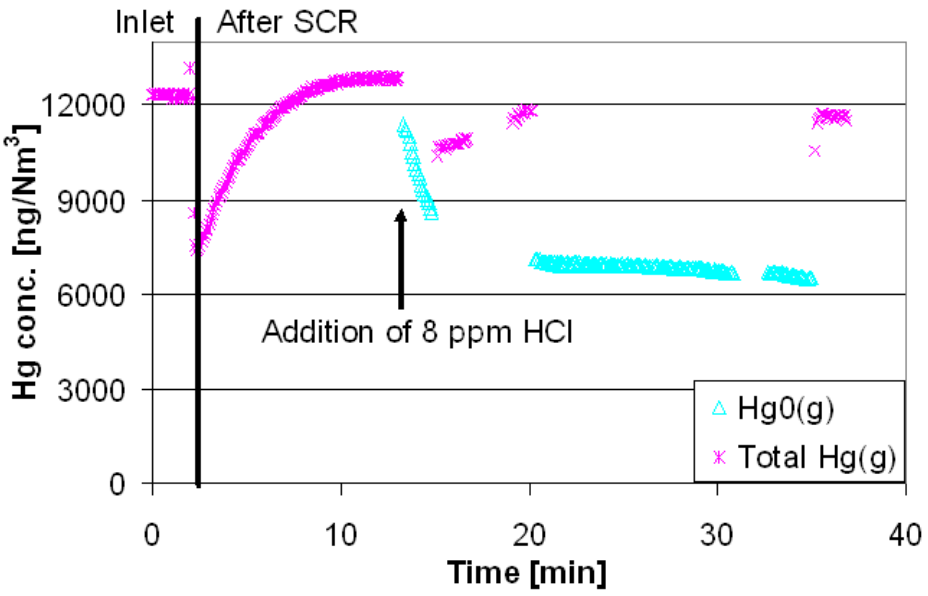

Figure 7.3: The transient Hg^0 adsorption over a fresh SCR catalyst with time for T=350^{o}C and U=160 NL/h in a N_2-atmosphere. At t=2 minutes, the gas is passed over the fresh SCR. At t=13 minutes, an addition of 8 ppm HCl is made. Adsorption of Hg^0 takes place until t=20 minutes, which can be seen by a decrease in total Hg at the SCR outlet. The step increase in HCl is also followed by a continuous Hg^0 oxidation.

7.3.2 $HgCl_2$ adsorption

Plotted in figure 7.4 is the transient $HgCl_2$ adsorption on a fresh SCR catalyst at 350^{o}C. The gas contains 41 $\mu g/Nm^3$ $HgCl_2$, 4% O_2 and 2% H_2O in balance N_2.

Both adsorption and reduction of $HgCl_2$ is demonstrated to take place over SCR catalyst. HCl is absent from the gas, so all mercury should exist as Hg^0 according to thermodynamic calculations. The net $HgCl_2$ reduction is taking place via the reverse of reaction R1, since no NH_3 is present.

In the experiment by Thorwarth (2007), no continuous adsorption or reduction of $HgCl_2$ takes place over the SCR catalyst in the presence of $\approx$ 13 ppm HCl. Section 7.3.1.3 has just demonstrated that $HgCl_2$ readily desorbs from the SCR by a step increase in HCl. This must be due to HCl effectively scavenging $HgCl_2$ from the catalyst surface.
The current experiment now indicates that $HgCl_2$ in the absence of HCl is being separated from chlorine over the SCR catalyst. The result is both an adsorption of mercury, probably as HgO(ads), and a release of Hg^0 from the catalyst.

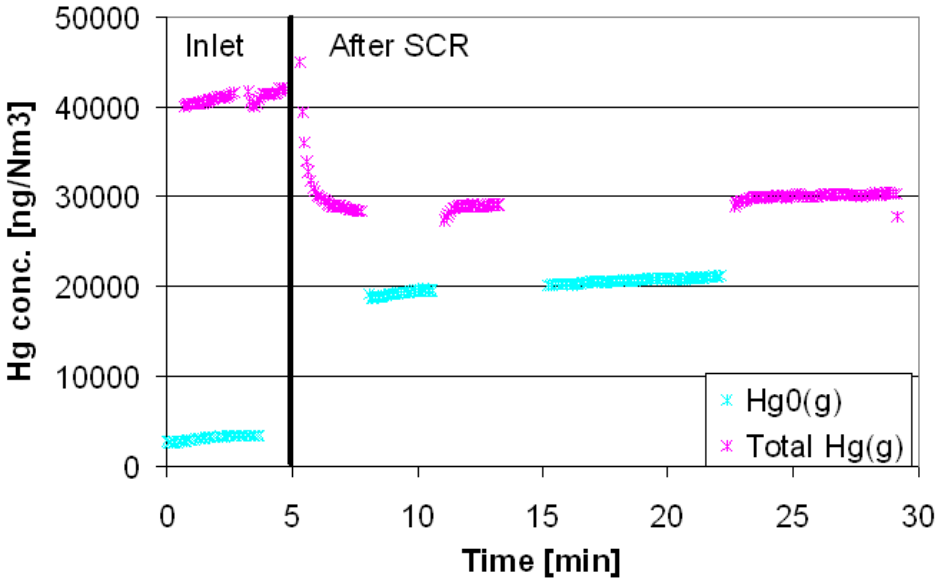

Figure 7.4: The transient $HgCl_2$ adsorption over the SCR with time for T=350^{o}C and U=163 NL/h. The gas contains 41 $\mu g/Nm^3$ $HgCl_2$, 4% O_2 and 2% H_2O in balance N_2. At t=5 minutes, the gas is passed over the fresh SCR catalyst.

7.3.3 HCl adsorption

Plotted in figure 7.5 is the capacity of fresh SCR catalysts for HCl adsorption at 350^{o}C for three different catalyst types: 1) a fresh SCR catalyst, 2) a TiO_2 carrier, and 3) an SCR catalyst that has been pretreated with NH_3. The gas contains 100 ppm HCl, 4% O_2 and 2% H_2O in balance N_2 for all three experiments. The capacities are reported here, because the duration of the HCl adsorption is so short.

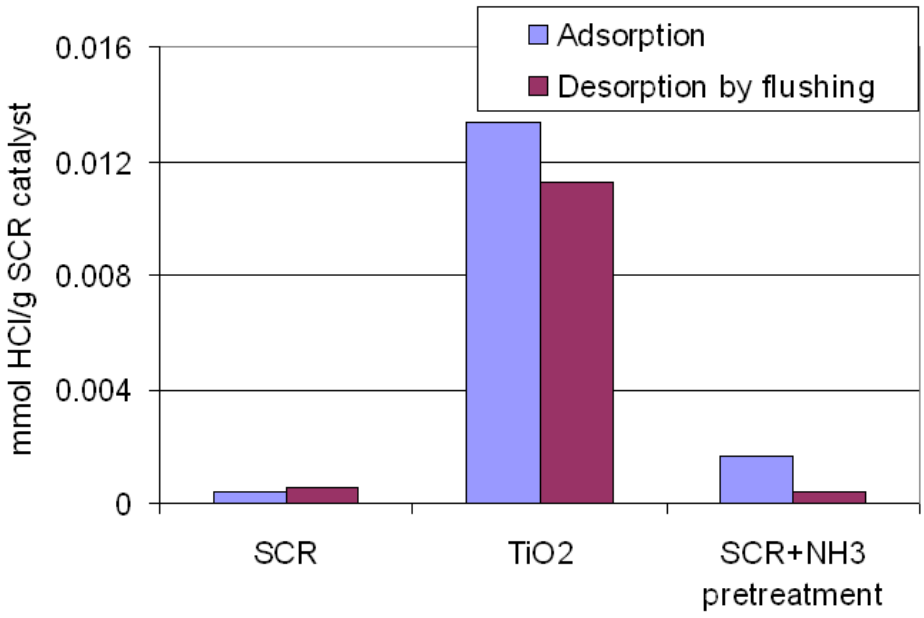

Figure 7.5: Capacity of fresh SCR catalysts for HCl adsorption at T=350^{o}C. The gas contains 100 ppm HCl, 4% O_2 and 2% H_2O in balance N_2. Three different catalysts have been tested: 1) a fresh SCR catalyst, 2) a TiO_2 carrier and 3) an SCR catalyst that has been pretreated with NH_3. The HCl adsorption over an empty reactor is negligible compared to the reported capacities.

1. When exposing the fresh SCR catalyst to 100 ppm HCl, the catalyst is saturated with adsorbed HCl within 1 min, which demonstrates a low capacity of SCR catalysts for HCl-adsorption. The adsorption appears to also be very weak in nature, since all adsorbed HCl will be released within 3 minutes, when the catalyst subsequently is flushed in 4% O_2 and 2% H_2O in balance N_2.

2. The HCl adsorption on TiO_2 carrier is greatly increased (factor 33) compared to the V_2O_5/WO_3 impregnated catalyst. The acidity of the catalyst surface increases by the impregnation with these metal-oxides, which can explain the greater affinity of HCl for unimpregnated TiO_2.
   85% of the adsorbed HCl will desorb by flushing the catalyst. The desorption from TiO_2 is slower than for the SCR catalyst and takes approximately 30 minutes, which suggests a stronger binding of HCl on TiO_2.
   Hocquel (2004) has demonstrated the ability of TiO_2 to reduce $HgCl_2$. It has been shown in section 7.3.1.1 that no Hg^0 will adsorb on TiO_2, whereas the current experiment shows that HCl does adsorb on TiO_2. A possible explanation for the $HgCl_2$ reduction over SCR catalyst can therefore be the binding of chlorine on TiO_2 releasing Hg^0.

3. The effect of NH_3 on the Hg^0 adsorption has previously been tested in literature, but the effect of NH_3 on the HCl adsorption has never been tested. If such an interaction is taking place, it can also be part of the explanation for the inhibition

of NH_3/DeNOx on the Hg^0 oxidation.
The fresh SCR catalyst is pretreated in 200 ppm NH_3 in 4% O_2 and 2% H_2O in balance N_2 at 350^oC until the catalyst is saturated with adsorbed NH_3. The catalyst is then flushed in 4% O_2 and 2% H_2O in balance N_2 for 15 minutes until very little desorption of NH_3 is observed from the catalyst.
The NH_3 pretreated catalyst now shows a four times greater adsorption capacity for HCl, which proves that an interaction between NH_3 and HCl does indeed take place. The additional HCl adsorption may have different properties and be stronger in nature, since the subsequent flushing only release 25% of the adsorbed HCl.
An increased HCl adsorption corresponds to less acidic properties of the catalyst surface. Possibly, a co-adsorption of HCl on the adsorbed alkaline NH_3 is taking place. Such an interaction can render both NH_3 and HCl unavailable for other reactions.

7.4 Discussion

The adsorption of Hg^0 on the SCR catalyst appears to be an important step in the catalytic Hg^0 oxidation. Hg^0 oxidation has only been observed in these experiments under conditions, where Hg^0 adsorption is observed as well.

The rate of the Hg^0 oxidation is 1st order in the Hg^0 concentration. The same dependency on Hg^0 is seen for the rate of the Hg^0 adsorption. This supports that Hg^0 adsorption is a rate limiting step in the Hg^0 oxidation.

Hg^0 oxidation over the SCR is demonstrated to take place via adsorbed HCl in a N_2 atmosphere. It is therefore likely that the Hg^0 oxidation under oxidative conditions also involve adsorbed HCl.

HCl has a very low affinity for adsorption on SCR catalysts, but the reported capacity will still provide HCl(ads) concentrations in great excess to mercury. The HCl adsorption may primarily take place on uncovered TiO_2 sites, but that does not rule out that some HCl is adsorbing in connection with V_2O_5.

Hg^0 is observed to adsorb in connection with chlorine on the SCR catalyst (with V_2O_5 and WO_3) and a production of $HgCl_2$ immediately follows. In contrast, no Hg^0 adsorption/oxidation is seen in connection with chlorine on the TiO_2 carrier.

- It is proposed that the Hg^0 oxidation is coupled to HCl adsorbed on V_2O_5, whereas the $HgCl_2$ reduction is coupled to the binding of chlorine from $HgCl_2$ on TiO_2.

The presence of NH_3 inhibits the adsorption of Hg^0 by reducing adsorbed HgO.

- It is proposed that that NH_3 causes the $HgCl_2$ reduction via reaction R2 because NH_3 is continuously reducing adsorbed $HgO/HgCl_2$ to Hg^o that is released from the catalyst.

Finally, NH_3 is demonstrated to influence the HCl adsorption. The increased adsorption of HCl in the presence of NH_3 opens for the possibility that a co-adsorption of HCl and NH_3 is taking place over SCR catalysts. Such binding could render the co-adsorbed components unavailable for other reactions and, therefore, influence both the DeNOx reaction, the Hg^0 oxidation and the $HgCl_2$ reduction.

7.5 Microkinetic modelling of the Hg^0 oxidation via reaction R1

Experimental data from the current adsorption study and from chapter 6 form the basis for the following proposed properties of the Hg^0 oxidation via reaction R1.

7.5.1 Properties of overall reaction rate

The rate of the Hg^0 oxidation over the SCR should fulfill the following criteria:

- 1st order in P_{Hg} (see section 6.3.1)
- Independent of HCl in the absence of NO and NH_3 (see section 6.3.2)
- Dependent on the NH_3 adsorption on oxidized Lewis sites at T<300^{o}C (see section 6.3.3.2)
- Dependent on the fraction of oxidized Lewis sites available, when the DeNOx reaction is consuming them (see section 6.3.3.2)

7.5.2 Steps in the surface reaction

The following steps in the catalytic Hg^0 oxidation are taking place:

- Both Hg^0 and HCl are adsorbing on the SCR. Reaction takes place between the adsorbed species on vanadia.
- The Hg^0 adsorption on V_2O_5 is the rate determining step (RDS) for the surface reaction.
- $HgCl_2$ readily desorbs from the surface

7.5.3 Elementary reactions

The surface reaction is modelled as having one active site, where both Hg^0 and HCl are adsorbing. The binding is not competitive, since Hg^0 still can bind if HCl is already present. Lewis sites (V^{5+}=O) are hypothesized to be active sites for the Hg^0-oxidation.

1/2 O_2 is consumed in the net Hg^0 oxidation via reaction R1. This means that two V^{5+}=O sites must be reduced in the Hg^0-oxidation for the consumption of 1/2 O_2 in the reoxidation of these sites:

$$2\ V^{4+} - OH + 1/2\ O_2 \leftrightarrow\ 2\ V^{5+} = O + H_2O \tag{7.1}$$

In the following, the notation 'L*' represent an oxidized Lewis site V^{5+}=O on the catalyst, whereas Lred* represent the reduced site V^{4+}-OH.

1. $Hg^0(g) + L* \leftrightarrow\ Hg*$ (RDS)
2. $HCl(g) + L* \leftrightarrow\ HCl*$
3. $Hg* + HCl* \leftrightarrow\ HgCl* + Lred*$
4. $HgCl* + HCl* \leftrightarrow\ HgCl_2* + Lred*$
5. $HgCl_2* \leftrightarrow\ HgCl_2(g) + L*$
6. $Lred* + 1/4 O_2(g) \leftrightarrow\ L* + 1/2 H_2O(g)$

Step 2-5 are assumed to be fast reactions, since a step addition of HCl in the gas causes an immediate release of oxidized $HgCl_2$ and since only very little mercury remains adsorbed on the catalyst in the presence of HCl.

Step 6 is the reoxidation of vanadia Lewis sites. The indicated reaction is clearly not elementary, but will simply be considered as given.

It is assumed that the Hg^0 adsorption (step 1) is the single rate determining step for the catalytic Hg^0 oxidation. In the absence of the DeNOx reaction, this assumption should be valid. Under DeNOx conditions, this may not hold true, since the rate of the reoxidation of Lewis sites can become limiting for the DeNOx reaction at low temperatures (Lietti et al., 1996). Under such conditions, the rate of the reoxidation will also limit the Hg^0 oxidation.

7.5.4 Derivation of rate expression

For simplicity, the rate of the Hg^0 oxidation via reaction R1 is initially derived in the absence of NO and NH_3.

7.5.4.1 Without NO and NH_3

In the absence of the DeNOx reactions, the rate of the overall surface reaction is approximated by the Quasi-equilibrium approximation, where adsorption of Hg^0 on the surface (step 1) is the single rate determining step. The other steps are assumed to be in equilibrium. The rate of the reaction is therefore given as follows:

$$-r_1 = k_1^+ \cdot P_{Hg^0} \cdot C_L - k_1^- \cdot C_{Hg} \quad [mol/m^3 \cdot s] \tag{7.2}$$

$$-r_2 = k_2^+ \cdot P_{HCl} \cdot C_L - k_2^- \cdot C_{HCl} = 0 \Rightarrow K_2 = \frac{C_{HCl}}{P_{HCl} \cdot C_L} \tag{7.3}$$

$$-r_3 = k_3^+ \cdot C_{Hg} \cdot C_{HCl} - k_3^- \cdot C_{HgCl} \cdot C_{Lred} = 0 \Rightarrow K_3 = \frac{C_{HgCl} \cdot C_{Lred}}{C_{Hg} \cdot C_{HCl}} \tag{7.4}$$

$$-r_4 = k_4^+ \cdot C_{HgCl} \cdot C_{HCl} - k_4^- \cdot C_{HgCl_2} \cdot C_{Lred} = 0 \Rightarrow K_4 = \frac{C_{HgCl_2} \cdot C_{Lred}}{C_{HgCl} \cdot C_{HCl}} \tag{7.5}$$

$$-r_5 = k_5^+ \cdot C_{HgCl2} - k_5^- \cdot P_{HgCl_2} \cdot C_L = 0 \Rightarrow K_5 = \frac{P_{HgCl_2} \cdot C_L}{C_{HgCl_2}} \tag{7.6}$$

$$-r_6 = k_6^+ \cdot C_{Lred} \cdot P_{O_2}^{1/4} - k_6^- \cdot P_{H_2O}^{1/2} \cdot C_L = 0 \Rightarrow K_6 = \frac{P_{H_2O}^{1/2}}{P_{O_2}^{1/4}} \cdot \frac{C_L}{C_{Lred}} \tag{7.7}$$

C_i indicates the concentration of the adsorbed specie i.

By multiplication of the individual equilibrium constants, the following expression for C_{Hg} appears:

$$K_2^2 \cdot K_3 \cdot K_4 \cdot K_5 \cdot K_6^2 = \frac{C_L}{C_{Hg}} \cdot \frac{P_{HgCl_2}}{P_{HCl}^2} \cdot \frac{P_{H_2O}}{\sqrt{P_{O_2}}} \tag{7.8}$$

$$C_{Hg} = \frac{C_L}{K_2^2 \cdot K_3 \cdot K_4 \cdot K_5 \cdot K_6^2} \cdot \frac{P_{HgCl_2}}{P_{HCl}^2} \cdot \frac{P_{H_2O}}{\sqrt{P_{O_2}}} \tag{7.9}$$

This is inserted in the rate of step 1:

$$-r_1 = k_1^+ \cdot P_{Hg^0} \cdot C_L - k_1^- \cdot \frac{C_L}{K_2^2 \cdot K_3 \cdot K_4 \cdot K_5 \cdot K_6^2} \cdot \frac{P_{HgCl_2}}{P_{HCl}^2} \cdot \frac{P_{H_2O}}{\sqrt{P_{O_2}}} \Leftrightarrow$$

$$-r_1 = k_1^+ \cdot P_{Hg^0} \cdot C_L \left(1 - \frac{1}{K_1 \cdot K_2^2 \cdot K_3 \cdot K_4 \cdot K_5 \cdot K_6^2} \cdot \frac{P_{HgCl_2}}{P_{HCl}^2 \cdot P_{Hg}} \cdot \frac{P_{H_2O}}{\sqrt{P_{O_2}}}\right) \tag{7.10}$$

The equilibrium constant for the net oxidation reaction equals: $K_P = K_1 \cdot K_2^2 \cdot K_3 \cdot K_4 \cdot K_5 \cdot K_6^2$. The rate equation becomes:

$$-r_1 = k_1^+ \cdot C_L \cdot P_{Hg^0} \left(1 - \frac{1}{K_p} \cdot \frac{P_{HgCl_2}}{P_{HCl}^2 \cdot P_{Hg}} \cdot \frac{P_{H_2O}}{\sqrt{P_{O_2}}}\right) \quad [mol/m^3 \cdot s] \tag{7.11}$$

The concentrations of oxidized Lewis sites in the absence of NO and NH_3 will be given by

$$C_{TL} = C_L + C_{Lred} + C_{Hg} + C_{HCl} \approx C_L \tag{7.12}$$

where C_{TL} is the total number of Lewis sites. $C_{Hg} << C_L$ due to the low concentration of Hg. The consumption of oxidized Lewis sites in the Hg^0 oxidation is negligible, because of the low concentrations involved, so $C_{Lred} << C_L$. C_{HCl} has been eliminated

from the equation, since the presence of HCl on the Lewis site does not hinder Hg^0 adsorption on the same site.

7.5.4.2 With DeNOx reaction

NH_3 adsorption on Lewis sites

It is hypothesized in chapter 6 that NH_3 is adsorbing on Lewis sites at temperatures below 300^{o}C. The adsorption is assumed to take place via the following reaction and to be in equilibrium:

$$\begin{aligned} &7.\ NH_3(g) + L* \leftrightarrow\ NH_3* \\ &-r_7 = k_7^+ \cdot P_{NH_3} \cdot C_L - k_7^- \cdot C_{NH_3} = 0\ \Rightarrow\ K_7 = \frac{C_{NH_3}}{P_{NH_3} \cdot C_L} \end{aligned} \tag{7.13}$$

For simplicity, it is assumed that a fixed fraction of the total adsorbed NH_3 will adsorb on Lewis sites: $K_7 = f_L \cdot K_{NH_3}$.

Consumption of oxidized Lewis sites in the DeNOx reaction

The DeNOx reaction is consuming oxidized Lewis sites. If the reoxidation of Lewis sites is limiting the DeNOx reaction rate, then only a fraction of oxidized Lewis sites are available for the Hg^0 oxidation.
Redistribution between reduced and oxidized Lewis sites will have several implications on the steps in the catalytic Hg^0 oxidation:

- Fewer oxidized Lewis sites are available for adsorption of Hg^0 and HCl via step 1 and 2.
- The equilibrium of step 3 and 4 can be pushed to the left due to a higher concentration of $Lred*$

This means that the overall reaction rate will become a complex function of more steps in the surface reaction.

Experimental results in section 6.3.3.4 show that increasing HCl concentration can decrease the inhibiting effect of the DeNOx reaction on the Hg^0 oxidation at 350^{o}C. This suggests that the overall Hg^0 oxidation rate is also limited by 1) the adsorption of HCl on Lewis sites, and/or 2) the rates of steps 3 and 4. In conclusion, there is experimental evidence that the Hg^0 adsorption (step 1) is not the only rate determining step under DeNOx conditions.

In order to get a rate expression that is mathematically tractable, the Hg^0 adsorption is assumed to remain the rate limiting step under all conditions. The consumption of oxidized Lewis sites is taken into account by a lower concentration of oxidized Lewis sites C_L being available under DeNOx conditions.

7.5.5 Mass balance for Lewis sites

The mass balance for Lewis sites under DeNOx condition becomes

$$C_{TL} = C_L + C_{Lred} + C_{NH_3} \Leftrightarrow \quad C_L = \frac{C_{TL}}{1 + \frac{C_{Lred}}{C_L} + f_L \cdot K_{NH_3} \cdot P_{NH3}} \tag{7.14}$$

An estimate of the fraction $\frac{C_{Lred}}{C_L}$ is derived as follows; The rate equation for the DeNOx reaction is of the form

$$-r_{NO} = k_{NO} \cdot P_{NO} \cdot \frac{K_{NH_3} \cdot P_{NH_3}}{1 + K_{NH_3} \cdot P_{NH_3}} \tag{7.15}$$

The rate of the reoxidation is given by

$$-r_6 = k_6^+ P_{O_2}^{1/4} \cdot C_{Lred} - k_6^- P_{H_2O}^{1/2} \cdot C_L \tag{7.16}$$

At steady state, the concentration of C_L will be constant in time:

$$\frac{dC_L}{dt} = r_{NO} - r_6 = 0 \;\Rightarrow\; r_{NO} = r_6 \tag{7.17}$$

where one C_L-site is consumed in the DeNOx reaction and one C_L-site is produced in the reoxidation.
If only the forward reaction of step 6 is considered, the following correlation arises:

$$r_{NO} = r_6 \;\Leftrightarrow$$
$$k_{NO} \cdot P_{NO} \cdot \frac{K_{NH_3} \cdot P_{NH_3}}{1 + K_{NH_3} \cdot P_{NH_3}} = k_6^+ P_{O_2}^{1/4} \cdot C_{Lred} \tag{7.18}$$

By deriving the rate expression for the DeNOx reaction (not performed here), it can be shown that the rate constant k_{NO} is proportional to C_L. An estimate of $\frac{C_{Lred}}{C_L}$ is now derived by inserting $k_{NO} = k'_{NO} \cdot C_L$

$$\frac{C_{Lred}}{C_L} = \frac{k'_{NO} \cdot P_{NO} \cdot \frac{K_{NH_3} \cdot P_{NH_3}}{1 + K_{NH_3} \cdot P_{NH_3}}}{k_6^+ P_{O_2}^{1/4}} \tag{7.19}$$

The constant k_{reox} is given by $k_{reox} = \frac{k_6^+}{k'_{NO}}$.

This mass balance for Lewis sites finally becomes:

$$C_L = \frac{C_{TL}}{1 + \frac{P_{NO} \cdot \frac{K_{NH_3} \cdot P_{NH_3}}{1 + K_{NH_3} \cdot P_{NH_3}}}{k_{reox} \cdot P_{O_2}^{1/4}} + f_L \cdot K_{NH_3} \cdot P_{NH3}} \tag{7.20}$$

7.5.6 Summary

The rate equation for the Hg^0-oxidation in reaction R1 (referred to $-r_{ox}$) now becomes

$$-r_{ox} = \frac{k_1 \cdot P_{Hg^0}}{1 + \frac{P_{NO} \cdot \frac{K_{NH_3} \cdot P_{NH_3}}{1+K_{NH_3} \cdot P_{NH_3}}}{k_{reox} \cdot P_{O_2}^{1/4}} + f_L \cdot K_{NH_3} \cdot P_{NH3}} \left(1 - \frac{1}{K_p} \cdot \frac{P_{HgCl_2}}{P_{HCl}^2 \cdot P_{Hg^0}} \cdot \frac{P_{H_2O}}{\sqrt{P_{O_2}}}\right) \quad [mol/m^3 \cdot s] \tag{7.21}$$

where $k_1 = k_1^+ \cdot C_{TL}$.

This rate expression does not mechanistically account for the promoting effect of HCl on the Hg^0 oxidation under DeNOx conditions. In this model, the components HCl, O_2, H_2O will only influence the reverse of reaction R1, when approaching the thermodynamic equilibrium.

7.6 Microkinetic modelling of the $HgCl_2$ reduction via reaction R2

Experimental data from the current adsorption study and from chapters 5 and 6 form the basis for the following proposed properties of the $HgCl_2$ reduction via reaction R2.

The reaction rate of R2 cannot be studied separately from reaction R1, so the experimental studies have only established the effects of various test conditions on the relative rate of the two reaction rates.

7.6.1 Properties of overall reaction rate

The overall rate of the $HgCl_2$ reduction over the SCR should fulfill the following criteria:

- 1st order in P_{HgCl_2}. The overall Hg^0 oxidation over the SCR at T=350^{o}C, where both reaction R1 and R2 are taking place, is 1st order in the Hg^0 concentration (see section 6.3.1). The pseudo equilibrium mercury speciation, where the rate of R1=R2, is independent of the total concentration of mercury Hg^T=9-53 $\mu g/Nm^3$ (see chapter 5). This suggests that reaction R2 is 1st order in $HgCl_2$.
- Inhibited by HCl (see section 5.3.2). The relative rate of reaction R2 to R1 decreases with increasing HCl. Since there is no promotion by HCl on reaction R1 under DeNOx conditions, then HCl must inhibit reaction R2.
- Promoted by NH_3 (see section 5.3.2). The effect of NH_3 levels off after 100 ppm, which could correlate with the surface being saturated with adsorbed NH_3 after this concentration. It is therefore likely that adsorbed NH_3 reacts with mercury.

7.6.2 Steps in the surface reaction

The following steps in the catalytic $HgCl_2$ reduction are taking place:

- Adsorption of $HgCl_2$ on TiO_2
- Adsorption of NH_3 on vanadia Brønsted sites.
- Reduction of adsorbed $HgCl_2$ by adsorbed NH_3.
- Desorption of Hg^0 from the surface.

7.6.3 Elementary reactions

Two active sites are proposed. The B*-sites represent Brønsted sites, where NH_3 is known to adsorb. The Ti*-sites represent TiO_2 sites, where $HgCl_2$ is proposed to bind via Cl (see discussion in section 7.4).
The following steps in the surface reaction are proposed.

1. $NH_3(g) + B* \leftrightarrow \ NH_3*$

2. $HgCl_2(g) + Ti* \leftrightarrow \ HgCl_2*$

3. $^2/_3NH_3* + HgCl_2* \leftrightarrow \ Hg^0(g) + 2HCl(g) + {}^1/_3N_2 + Ti* + B*$ (RDS)

4. $HCl + NH_3* \leftrightarrow NH_4Cl*$

5. $HCl + Ti* \leftrightarrow HCl*$

The adsorption of reactants takes place in steps 1 and 2. The proposed step 3 is the reaction between adsorbed species and is clearly a lumped step. This step is assumed to be the rate determining step, since this will result in a dependency on both HCl and NH_3 in the overall reaction rate in accordance with the experimental observations.

Step 5 is adsorption of HCl on the TiO_2, which blocks the sites for $HgCl_2$ adsorption.

An additional effect of HCl is included in step 4, where co-adsorption of NH_3 and HCl is taking place. It is hypothesized that co-adsorbed NH_3 is unavailable for the $HgCl_2$ reduction.

7.6.4 Derivation of rate expression

The rate of the overall surface reaction is approximated by the Quasi-equilibrium approximation, where the surface reaction between adsorbed $HgCl_2$ and NH_3 (step 3) is the single rate determining step. The other steps are assumed to be in equilibrium. The rate of the reaction is therefore given as follows:

$$-r_1 = k_1^+ \cdot P_{NH_3} \cdot C_B - k_1^- \cdot C_{NH_3} \;\Rightarrow\; K_{NH_3} = \frac{C_{NH_3}}{P_{NH_3} \cdot C_B} \tag{7.22}$$

$$-r_2 = k_2^+ \cdot P_{HgCl_2} \cdot C_{Ti} - k_2^- \cdot C_{HgCl_2} \;\Rightarrow\; K_{HgCl_2} = \frac{C_{HgCl_2}}{P_{HgCl_2} \cdot C_{Ti}} \tag{7.23}$$

$$-r_3 = k_3^+ \cdot C_{NH_3}^{2/3} \cdot C_{HgCl_2} \quad [mol/m^3 \cdot s] \tag{7.24}$$

$$-r_4 = k_4^+ \cdot P_{HCl} \cdot C_{NH_3} - k_4^- \cdot C_{NH_4Cl} \;\Rightarrow\; K_{NH_4Cl} = \frac{C_{NH_4Cl}}{P_{HCl} \cdot C_{NH_3}} \tag{7.25}$$

$$-r_5 = k_5^+ \cdot P_{HCl} \cdot C_{Ti} - k_5^- \cdot C_{HCl} \;\Rightarrow\; K_{HCl} = \frac{C_{HCl}}{P_{HCl} \cdot C_{Ti}} \tag{7.26}$$

Only the forward reaction of step 3 is considered, since all the products are desorbed gaseous species. The rate becomes

$$\begin{aligned} -r_3 &= k_3^+ \cdot C_{NH_3}^{2/3} \cdot C_{HgCl_2} \\ &= k_3^+ \cdot (K_{NH_3} \cdot P_{NH_3} \cdot C_B)^{2/3} \cdot (K_{HgCl_2} \cdot P_{HgCl_2} \cdot C_{Ti}) \end{aligned} \tag{7.27}$$

The total number of Brønsted (C_{TB}) and titania (C_{TT}) sites on the catalyst, respectively, can be described as

$$C_{TB} = C_B + C_{NH_3} + C_{NH_4Cl} \;\Rightarrow\; C_B = \frac{C_{TB}}{1 + K_{NH_3} \cdot P_{NH_3} \cdot (1 + K_{NH_4Cl} \cdot P_{HCl})} \tag{7.28}$$

$$C_{TT} = C_{Ti} + C_{HCl} + C_{HgCl_2} \;\Rightarrow\; C_{Ti} = \frac{C_{TT}}{1 + K_{HCl} \cdot P_{HCl}} \tag{7.29}$$

where $C_{HgCl_2} << C_{Ti}$.

7.6.5 Summary

The rate equation for the $HgCl_2$-reduction in reaction R2 (referred to $-r_{red}$) becomes:

$$-r_{red} = k_3 \cdot \left(\frac{K_{NH_3} \cdot P_{NH_3}}{1 + K_{NH_3} \cdot P_{NH_3} \cdot (1 + K_{NH_4Cl} \cdot P_{HCl})} \right)^{2/3} \cdot \frac{P_{HgCl_2}}{1 + K_{HCl} \cdot P_{HCl}} \quad [mol/m^3 \cdot s] \tag{7.30}$$

where $k_3 = k_3^+ \cdot C_{TB}^{2/3} \cdot C_{TT} \cdot K_{HgCl_2}$.

This rate expression will not account for the enhanced effects of O_2 and H_2O, when both reaction R1 and R2 are taking place (see section 6.3.3.6).

7.7 Conclusions

The adsorption of the three reactants Hg^0, HCl and $HgCl_2$ in reaction R1 and R2 over SCR catalysts has been studied as a means to further elucidate the steps in the catalytic reactions. Based on the experimental data and microkinetic principles, two overall reaction rates have been proposed for the mercury surface reactions R1 and R2.

The rate limiting step in the Hg^0 oxidation via reaction R1 is the adsorption of Hg^0 on oxidized Lewis sites. Under DeNOx conditions, the availability of Hg^0 adsorption sites decreases due to 1) adsorption of NH_3 on Lewis sites for T<300^{o}C and 2) the consumption of oxidized Lewis sites in the DeNOx reaction. Both these effects are incorporated in the reaction rate expression.

The $HgCl_2$ reduction is proposed to take place via adsorbed $HgCl_2$ on TiO_2 with adsorbed NH_3 on vanadia Brønsted sites.

Chapter 8

Modelling of the Hg^0 oxidation over SCR reactors

8.1 Introduction

The Hg^0 oxidation over monolithic SCR reactors will both be governed by the rates of mass transfer and by the rates of relevant surface reactions.
Reactor models for the Hg^0 oxidation exist (e.g. Niksa and Fujiwara (2005); Senior (2006)), where both the effects of external mass transfer, diffusion and reaction in the catalyst wall are taken into account. In these models, the overall Hg^0 oxidation is incorporated as a single oxidation reaction taking place by an Eley-Rideal mechanism over the catalyst. The inhibition of the DeNOx reaction on the Hg^0 oxidation is accounted for by assuming that a competitive adsorption between NH_3 and Hg^0/HCl is taking place on the catalyst. Based on the experimental evidence presented in this thesis, the existing models do not incorporate the correct reaction mechanism.

The objective of this study is to build a kinetic model for the steady-state Hg^0 oxidation over monolithic SCR catalysts incorporating the relevant mercury chemistry that has been identified and quantified in chapters 5-7.
The concentration profiles of Hg^0, NO and NH_3 will therefore be modelled over the SCR catalyst as the following three net reactions are taking place:

$$R1.\ \ 2\ HCl + Hg^0 + 1/2\ O_2 \ \leftrightarrow\ HgCl_2 + H_2O$$
$$R2.\ \ 2\ NH_3 + 3\ HgCl_2 \ \leftrightarrow\ N_2 + 3\ Hg^0 + 6\ HCl$$
$$R3.\ \ 2\ NO + 2\ NH_3 + 1/2\ O_2 \ \leftrightarrow\ 2\ N_2 + 3\ H_2O$$

where R1 is the Hg^0 oxidation by HCl, R2 is the $HgCl_2$ reduction by NH_3 and R3 is the standard DeNOx reaction.

This more mechanistically based model can give insight into the effects dominating the overall kinetics of the Hg^0 oxidation over SCR reactors for different gas composition and operating conditions.

8.2 Methods

The modelling framework takes both external mass transfer, diffusion and reaction in the catalyst wall into account, when modelling the steady-state Hg^0 oxidation over monolithic SCR reactors.

Model parameters in the mercury reactions rates R1 and R2 will be fitted to experimental data from laboratory tests on catalysts with a 'typical' V_2O_5 load.
Model validation will take place by comparing model predictions to another set of laboratory experiments run at typical operating conditions for high dust SCR applications.

8.2.1 Modelling

The model methodology is described in chapter 4

8.2.2 Experimental

Experimental data used for the parameter estimation has been described previously in chapters 5-6. These tests are run at a high linear velocity on Type B catalysts with a 'typical' vanadia-content.

Table 8.1: Range of conditions tested. ($\frac{NO_2}{NOx} \approx 0.05$). The concentrations of the individual components at reference conditions are specified in parenthesis.

Catalyst	
Geometry	Type A
V_2O_5	'Typical'
Operating conditions	
Linear velocity v [Nm/s]	2.2
Temperature [^{o}C]	275-425 (350)
Gas composition	
Hg^0	12-24 $\mu g/Nm^3$
O_2	4%
H_2O	5%
HCl	3.4-25 ppm (4.5 ppm)
NH_3	0-150 ppm (100 ppm)
NOx	0-150 ppm (100 ppm)
SO_2	0 ppm

A Topsøe DNX SCR catalyst (type A, see section 3.1) with a 'typical' vanadia-content is applied for tests run at industrially relevant conditions. The experiments are performed at a linear velocity v=1.6-3.2 Nm/s and on a monolithic SCR catalyst with a hydraulic diameter corresponding to a 'typical' high dust application. The range of test conditions applied in this study are summarized in table 8.1.
Notice that the Hg^0 oxidation reported from these laboratory experiments does not represent those from full-scale installations, since the tested monoliths are shorter than for full-scale SCR reactors.

8.3 Rate expressions for the surface reactions

8.3.1 Reaction R1

A rate expression for the Hg^0 oxidation via reaction R1 has been derived from micro-kinetic modelling in chapter 7 and is given in equation (7.21). It takes the form

$$-r_{ox} = \frac{k_1 \cdot P_{Hg^0}}{1 + \frac{P_{NO} \cdot \frac{K_{NH_3} \cdot P_{NH_3}}{1+K_{NH_3} \cdot P_{NH_3}}}{k_{reox} \cdot P_{O_2}^{1/4}} + f_L \cdot K_{NH_3} \cdot P_{NH3}} \left(1 - \frac{1}{K_p} \cdot \frac{P_{HgCl_2}}{P_{HCl}^2 \cdot P_{Hg^0}} \cdot \frac{P_{H_2O}}{\sqrt{P_{O_2}}}\right) \left[{}^{mol}/_{m^3 \cdot s}\right] \tag{8.1}$$

where the model parameters are $k_1[=]{}^{mol}/_{m^3 \cdot s \cdot atm}$, $k_{reox}[=]atm^{3/4}$ and f_L. A rate constant $k_{ox} = \frac{k_1 \cdot R \cdot T}{a_c}$ in units [m/s] replaces k_1 in the rate equation.

The temperature dependency of both rate parameters k_{ox} and k_{reox} will be described via Arrhenius expressions.

8.3.2 Reaction R2

A rate expression for the $HgCl_2$ reduction via reaction R2 has been derived from micro-kinetic modelling in chapter 7 and is given in equation (7.30). It takes the form

$$-r_{red} = -r_3 = k_3 \cdot \left(\frac{K_{NH_3} \cdot P_{NH_3}}{1 + K_{NH_3} \cdot P_{NH_3} \cdot (1 + K_{NH_4Cl} \cdot P_{HCl})}\right)^{2/3} \cdot \frac{P_{HgCl_2}}{1 + K_{HCl} \cdot P_{HCl}} \left[{}^{mol}/_{m^3 \cdot s}\right] \tag{8.2}$$

where the model parameters are the adsorption coefficients K_{NH_4Cl} (HCl adsorption on adsorbed NH_3) and K_{HCl} (HCl adsorption on TiO_2) and the reaction rate constant $k_3[=]{}^{mol}/_{m^3 \cdot s \cdot atm}$. This form of the rate expression will not be applied in the modelling framework for two reasons:

1. The reaction rate of R2 is overdetermined from this rate expression based on the

available experimental data. 6 fitting parameters arise from the rate expression, since the temperature dependency of each physical parameter will be described via Arrhenius expressions.

2. It has not been possible to correctly describe the trend in the Hg^0 oxidation as function on HCl. This means that the dependency of R1 and/or R2 on HCl is incorrect. The HCl dependency of R2 is in the order of $n \approx$ -1. For R1, only the reverse reaction is dependent of HCl.

Since reaction R1 is more well-described (and not overdetermined) from the experimental data, it is decided to let the rate expression for R1 remain unchanged. Instead, the rate expression for R2 is altered to the following empirical form:

$$-r_{red} = k_3 \cdot P_{HgCl_2} \left(\frac{K_{NH_3} \cdot P_{NH_3}}{1 + K_{NH_3} \cdot P_{NH_3}} \right)^{2/3} \cdot \left(\frac{1}{1 + K_{HCl} \cdot P_{HCl}} \right)^{n_{HCl}} \quad [mol/m^3 \cdot s] \quad (8.3)$$

The model parameters now consist of $k_3[=]mol/m^3 \cdot s \cdot atm$, $K_{HCl}[=]1/atm$ and n_{HCl}, where the latter determines the order of HCl dependency. K_{HCl} is simply assigned the constant value of 10^6 $1/atm$ and no longer represents a physical parameter.
A rate constant $k_{red} = \frac{k_3 \cdot R \cdot T}{a_c}$ in units [m/s] replaces k_3 in the rate equation.

8.3.3 Reaction R3

In the operating window of 300-400^{o}C, a simple Eley-Rideal mechanism is often adopted for describing the kinetics of the reaction (Beeckman and Hegedus, 1991; Beretta et al., 1998). Via this mechanism, it is assumed that NH_3 adsorbs on the surface and reacts with gaseous or weakly bound NO.
The rate expression takes the form

$$-r_{NO} = k_{NO} \cdot P_{NO} \cdot \frac{K_{NH_3} \cdot P_{NH_3}}{1 + K_{NH_3} \cdot P_{NH_3}} \quad [mol/m^3 \cdot s] \quad (8.4)$$

where $k_{NO}[=]mol/m^3 \cdot s \cdot atm$ and $K_{NH_3}[=]1/atm$.
The values of the reaction rate constant k_{NO} and the adsorption coefficient K_{NH_3} for commercial SCR catalysts have been estimated at Haldor Topsøe A/S. These estimates are directly applied in the modelling work for the Hg^0 oxidation.

8.4 Parameter estimation

Estimation of model parameters in the rates for R1 and R2 is based on the experimental data presented in chapters 5 and 6. In these experiments, the Hg^0 oxidation is measured over monolithic SCR catalysts, which means that the overall rate of Hg^0 oxidation is governed by mass transport limitations. To reduce the effect of external mass transport, these experiments have been carried out at a high linear velocity (v=10.3 Nm/s) and on a Type B catalyst with a low hydraulic diameter. This enhances the influence of the

surface reaction rates on the overall rate of Hg^0 oxidation. In this way, the uncertainty in the measured surface reaction rate is reduced and the data provide a better foundation for parameter estimation.

The parameter fitting is performed, so the best 'visual' fit to experimental data is achieved. Table 8.2 shows the form of each fitting parameter and briefly describes the estimation of each value.

Table 8.2: Model parameters. The fitting of parameters is performed in the order as listed.

Step 1: Fitting across data in the absence of NO and NH_3	
$k_{ox} = A_{ox} \cdot exp\left(\frac{-E_{ox}}{R \cdot T}\right)$	k_{ox} is fitted to match the data in figure 6.5 at each temperature in the range $250^oC < T < 350^oC$. The temperature interval is chosen, so the thermodynamic limitation is unimportant. An Arrhenius plot is made for the estimated value of k_{ox} from which A_{ox} and E_{ox} are calculated.
Step 2: Fitting across data with NH_3 in the absence of NO	
f_L=0.008	f_L is fitted to visually best match the data in figure 6.5 across T for $250^oC < T < 300^oC$. The fitted value of k_{ox} from the previous step is applied. Reaction R2 is unimportant at this low temperature.
$K_{HCl} = 10^6\ {}^1/_{atm}$	Assumed
$k_{red} = A_{red} \cdot exp\left(\frac{-E_{red}}{R \cdot T}\right)$	For the pseudo equilibrium data in figure 5.3, the following relation holds: $r_{ox} = r_{red} \Rightarrow$ $k_{term} = \frac{k_{ox}}{k_{red}} \cdot (1 + K_{HCl} \cdot P_{HCl})^n = \frac{y_{HgCl_2,eq}}{1-y_{HgCl_2,eq}} \left(\frac{K_{NH_3} \cdot P_{NH_3}}{1+K_{NH_3} \cdot P_{NH_3}}\right)^{2/3} \cdot \frac{1+f_L \cdot K_{NH_3} \cdot P_{NH3}}{1-\frac{1}{K_p} \cdot \frac{y_{HgCl_2,eq}}{(1-y_{HgCl_2,eq})} \cdot \frac{P_{H_2O}}{P_{HCl}^2 \cdot \sqrt{P_{O_2}}}}$ k_{term} is calculated via the right hand side from the experimental data at each $350^oC < T < 425^oC$. Both k_{ox} and k_{red} are described via Arrhenius expressions, so the same applies for k_{term}. A_{term} and E_{term} are found (via an Arrhenius plot) from which A_{red} and E_{red} can be isolated.
n_{HCl}=3	Fitted to data in figure 6.6 at $T = 350^oC$ for HCl=2.5-25 ppm for NH3=100 ppm.
Step 3: Fitting across data with a full gas matrix	
$k_{reox} = A_{reox} \cdot exp\left(\frac{-E_{reox}}{R \cdot T}\right)$	k_{reox} is fitted to match the data in figure 6.5 at each temperature in the range $250^oC \leq T \leq 350^oC$. Reaction R2 is not completely controlling below T=375^{o}C, so only data T$\leq$ 350^{o}C is used. An Arrhenius plot is made for the estimated value of k_{reox} from which A_{reox} and E_{reox} are calculated.

8.5 Model evaluation

The models ability to describe the experimental trends in different gas compositions and operating conditions is initially evaluated against the same data used for the parameter estimation.

8.5.1 Effect of temperature

The predictions across temperature illustrate that the model successfully accounts for the different mechanistic regimes that exist under DeNOx conditions.
Plotted in figure 8.1 are model predictions of Hg^0 oxidation over the SCR catalyst compared to experimental data across temperature for three different gas compositions: 1) 4.2 ppm HCl and no DeNOx, 2) 4.2 ppm HCl and 100 ppm NH_3 and 3) 4.2 ppm HCl and 100 ppm NH_3 and NO.

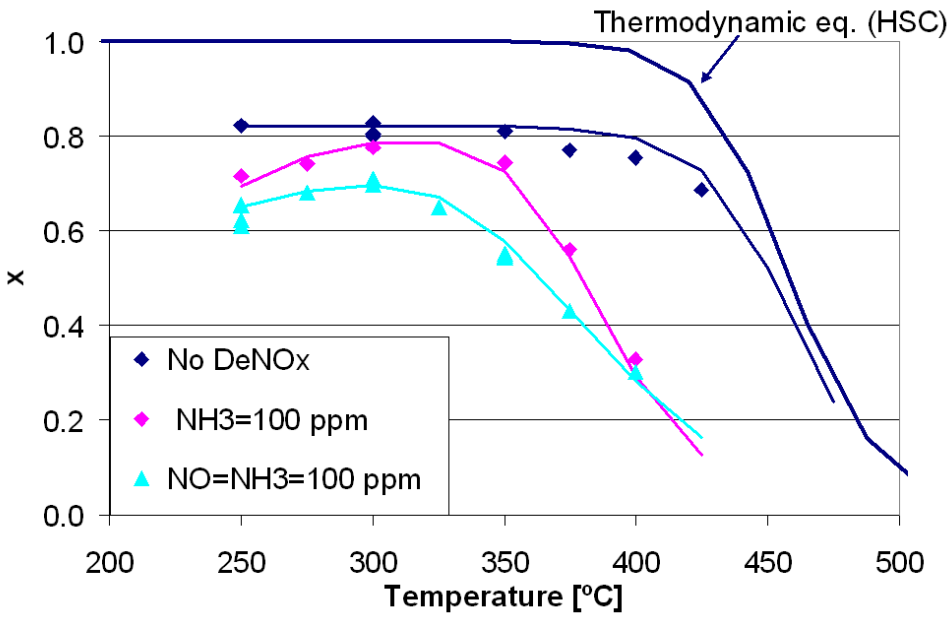

Figure 8.1: Steady-state oxidation of Hg^0 over the SCR as function of temperature at v=10.3 Nm/s. The gas contains 4.0-12.5 $^{\mu g}/_{Nm^3}$ Hg^0, 4.2 ppm HCl, 4% O_2 and 5% H_2O in balance N_2. Model estimates are given in full lines.

The reaction rate constant k_{ox} for reaction R1 decreases with temperature, because Hg^0 adsorption decreases with increasing temperature. Correspondingly, a very flat temperature dependency of the Hg^0 oxidation is present in the absence of DeNOx, since the increasing rates of mass transfer with temperature compensate for the decreasing surface reaction rate.
At T>400^{o}C, the reverse of reaction R1 becomes increasingly important, since the

thermodynamic equilibrium is approached. The activation energy for reaction R1 is given by E_{ox}=-28.2 kJ/mol. This parameter can be viewed upon as the adsorption enthalpy of Hg^0: $E_{ox} = -\Delta H_{ads}$.

In the presence of NH_3, the model accounts for the decreasing Hg^0 oxidation at T<300^{o}C via adsorption of NH_3 on Lewis sites, where Hg^0 also adsorbs. The model describes the adsorption coefficient for NH_3 on Lewis acid sites as a fixed fraction (0.8%) of the overall adsorption coefficient for NH_3 on SCR catalysts.
At the higher temperatures T>350^{o}C, the decreasing Hg^0 oxidation is described by reaction R2 becoming increasingly important. The activation energy for reaction R2 is estimated to be E_{red}= 179.1 kJ/mol.

In the presence of both NO and NH_3, the synergistic inhibition of the two components for 250^{o}C<T<375^{o}C is modelled as a consumption of oxidized Lewis sites that must be reoxidized to regain activity. The parameter k_{reox} increases with temperature, which corresponds to an increasing rate of reoxidation with increasing temperature.

8.5.2 Effect of HCl

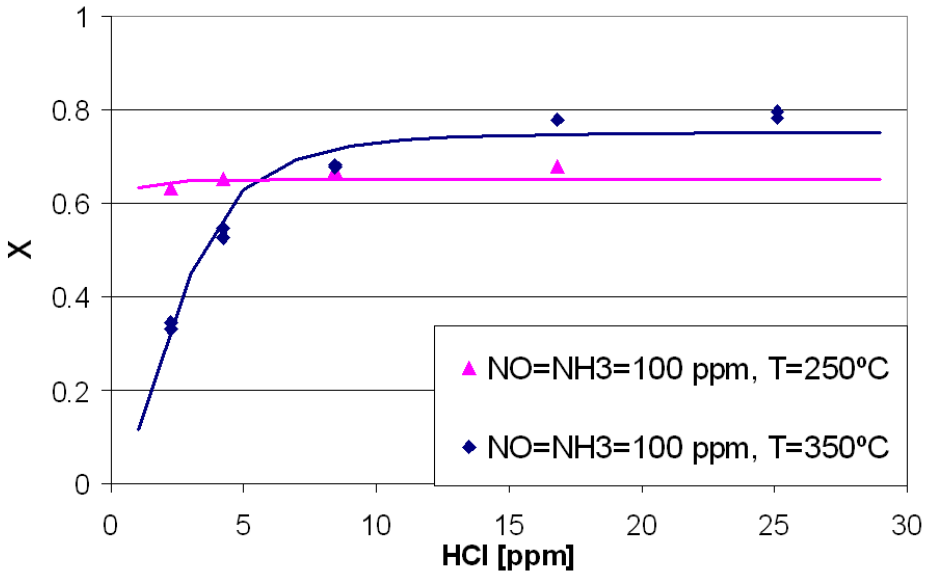

Figure 8.2: Steady-state oxidation of Hg^0 over the SCR as function of HCl for T=250-350^{o}C at v=10.3 Nm/s. The gas contains 4.2-12.5 $^{\mu g}/_{Nm^3}$ Hg^0, 100 ppm NH_3 and NO, 4% O_2 and 5% H_2O in balance N_2. Model estimates are given in full lines.

Plotted in figure 8.2 are model predictions of the Hg^0 oxidation over the SCR catalyst compared to the experimental data across HCl for T=250 and 350^{o}C with and without 100 ppm NH_3 and NO.
The model accounts for the different effects of HCl that takes place at different temperatures. At T=250^{o}C, there is no effect from increasing HCl, since the adsorption of

Hg^0 on Lewis sites is limiting the overall Hg^0 oxidation. At T=350^{o}C, an increased Hg^0 conversion is achieved by increasing HCl, since this decreases the rate of reaction R2.

HCl is experimentally seen also to diminish the synergistic inhibition by NO and NH_3 (see section 6.3.3.4), which is not accounted for in the model. Therefore, the dependency of R2 on HCl effectively accounts for both effects with an overall HCl dependency given by $\left(\frac{1}{1+10^6 \cdot P_{HCl}}\right)^3$. The high value of $n_{HCl} = 3$ stresses the need to get a better mechanistic understanding of the effect of HCl on the catalytic Hg^0 oxidation.

8.5.3 Effect of NO and NH_3

Plotted in figure 8.3 are model predictions of the Hg^0 oxidation over the SCR catalyst compared to the experimental data for increasing NH_3 with/without NO at T=350^{o}C.

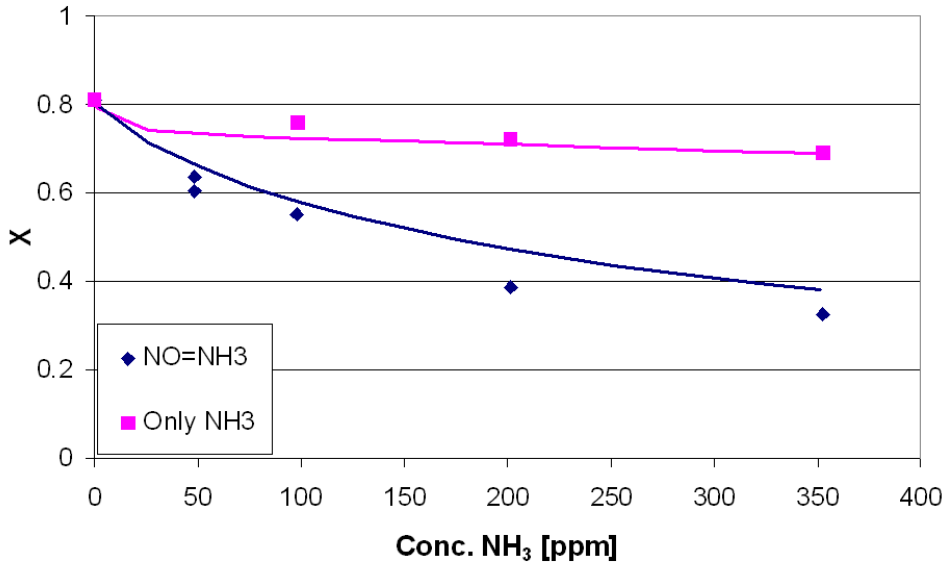

Figure 8.3: Steady-state oxidation of Hg^0 over the SCR as function of NH_3 with and without NO for T=350^{o}C at v=10.3 Nm/s. The gas contains 4.5-12.5 $^{\mu g}/_{Nm^3}$ Hg^0, 4.2 ppm HCl, 4% O_2 and 5% H_2O in balance N_2. Model estimates are given in full lines.

In the presence of NH_3 alone, the Hg^0 oxidation will decrease with increasing NH_3 due to reaction R2 simultaneously taking place. The model accurately accounts for this at 350^{o}C.
Under DeNOx conditions, the model predicts decreasing Hg^0 oxidation with increasing NO and NH_3 corresponding to an increased number of Lewis sites being consumed. The model slightly overestimates the Hg^0 oxidation at elevated NO and NH_3 concentrations. A simplified dependency of reaction R1 on the DeNOx reaction has been applied in the derivation of the rate expression (see section 7.5.4.2), which may explain the discrepancy.

8.5.4 Summary

The model is able to describe the experimental trends in the overall Hg^0 oxidation over the SCR for different gas compositions and operating temperatures. This supports that the model framework accurately accounts for most of the relevant mercury chemistry taking place over SCR catalysts in the given simulated flue gas.

8.6 Model validation

Experiments have been performed measuring the Hg^0 oxidation over a monolithic SCR catalyst with a larger hydraulic diameter (type A) at a linear velocity of v=2.2 Nm/s. The operating conditions, catalyst composition and geometry can be classified as typical to high dust SCR applications. The purpose of these experiments has been to produce industrially relevant data against which the model can be validated.

The catalyst composition is identical to the previous experiment, which means that the fitted model parameters for the surface reaction rates should remain unchanged, when modelling these experiments. Only the external mass transfer coefficient should be influenced by the change in catalyst geometry and linear velocity. Unfortunately, the data produced in these experiments appears to be inconsistent with previous data. This issue must be considered before model validation can be performed.

8.6.1 Experimental inconsistencies

Plotted in figure 8.4 are model predictions of the Hg^0 oxidation over the SCR for increasing HCl with/without 100 ppm NO and NH_3 at v=2.2 Nm/s and T=350^{o}C.
The model accurately predicts the experimental data in the absence of NO and NH_3, but fails to predict the extent of Hg^0 oxidation under DeNOx conditions. The failure is because the model underestimates the inhibition from the DeNOx reaction at low HCl.

A comparison between the experimental data in chapter 6 and in the current section is therefore performed and inconsistent data between the two experimental schemes have been identified:
Figure 8.5 shows the observed catalyst activity for increasing NH_3=NO at T=350^{c}C. A greater inhibition from the DeNOx reaction is observed for the experiments at v=2.2 Nm/s compared to v=10.3 Nm/s. Changes in the surface reaction rate should intuitively be manifested in the observed catalyst activity more evidently when operating at v=10.3 Nm/s, since mass transfer is less important at this linear velocity. Yet, the contrary is seen for these experiments.

The difference between the experiments is still not understood. Nevertheless, the current experiments (v=2.2 Nm/s, type A) have reproduced all experimental trends in the Hg^0 oxidation that is found for the previous experiments (v=10.3 Nm/s, type B). It is therefore concluded that:

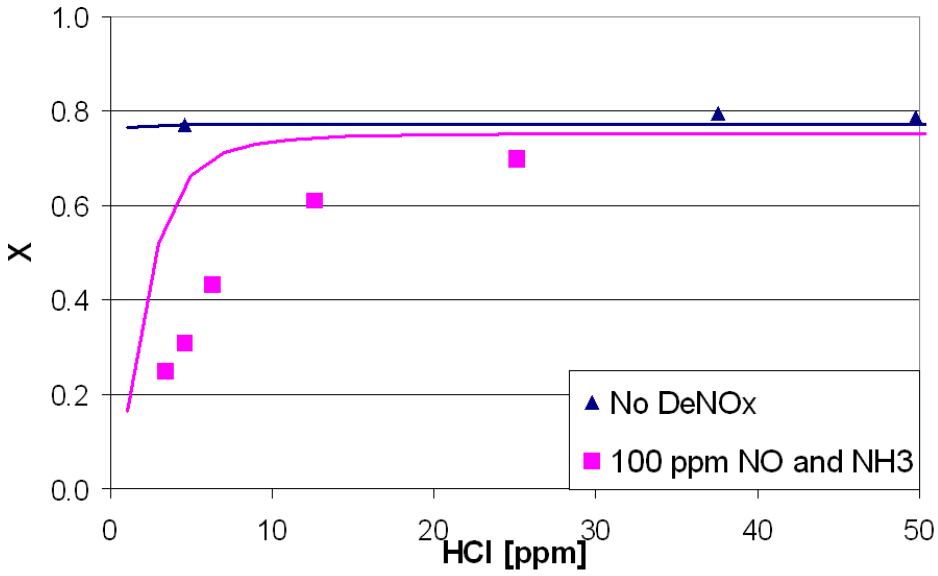

Figure 8.4: Steady-state oxidation of Hg^0 over the SCR across HCl at v=2.2 Nm/s and T=350^{o}C with and without 100 ppm NO and NH_3. The gas contains 17.6-18.2 $^{\mu g}/_{Nm^3}$ Hg^0, 4% O_2 and 5% H_2O in balance N_2. Model estimates are given in full lines.

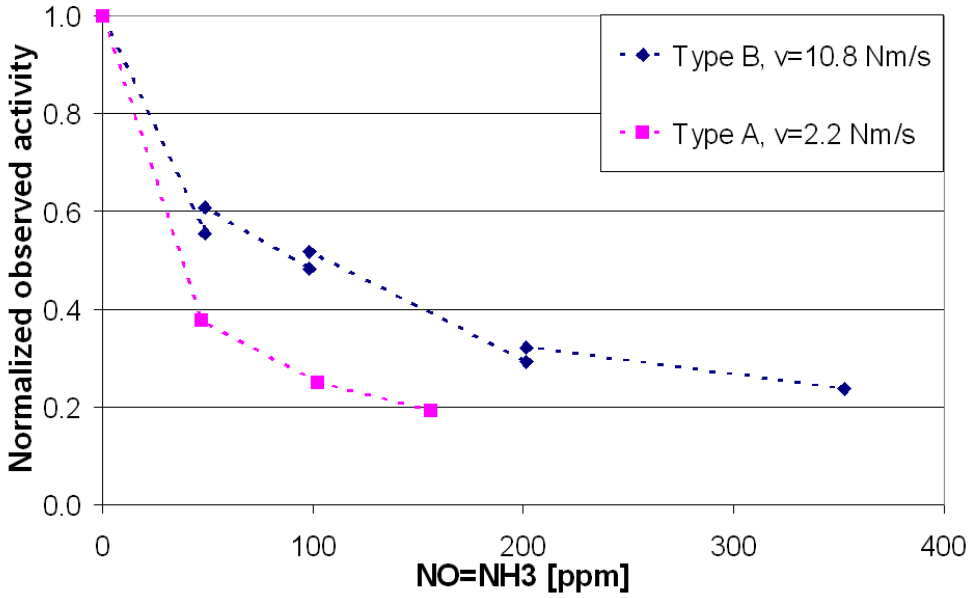

Figure 8.5: Observed catalyst activity for Hg^0 oxidation over the SCR for increasing NO=NH_3 at T=350^{o}C for the two different test schemes: 1) type A catalyst at v=2.2 Nm/s and 2) type B catalyst at v=10.3 Nm/s. The gas contains 4.5-17.6 $^{\mu g}/_{Nm^3}$ Hg^0, 4.2 ppm HCl, 4% O_2 and 5% H_2O in balance N_2. The normalized observed catalyst activities are given by $\frac{k_{obs}}{k_{obs}(NO=NH_3=0)}$.

- The same mercury chemistry is taking place for the two experimental schemes. Accordingly, the model framework does account for the relevant mercury chemistry over the SCR.
- The size order of the inhibition by DeNOx is very uncertain from these experiments and should be further elucidated in future experiments.

The experimental results will later be shown alongside model predictions in figures 8.6 and 8.7.

8.6.2 Model performance at industrially relevant conditions

The model framework is now applied for describing the current experimental data. The effect of the DeNOx reaction on the rate of Hg^0 oxidation (R1) is taken into account via the model parameter k_{reox} that describes the rate of reoxidation of Lewis sites. The parameter k_{reox} is re-fitted to match the current experimental data. The value of k_{reox} is reduced by a factor 16 in the new fit.

Plotted in figures 8.6 and 8.7 are the model predictions of the Hg^0 oxidation over the SCR across a) temperature, b) HCl, c) NO=NH_3 and d) the linear gas velocity.
The figures illustrate that the model accurately predicts the trends in Hg^0 oxidation across these four variables. Using the new value of k_{reox}, the model framework is therefore considered to be valid under testing conditions typical to high dust SCR applications.

All remaining model predictions in this study will be applying this value of k_{reox}.

8.7 Model predictions for high dust SCR conditions

The validated model is now applied to understand the mechanisms determining the overall Hg^0 oxidation over SCR catalysts at industrially relevant conditions.

8.7.1 Effect of inlet Hg speciation

Plotted in figure 8.8 is the model prediction of the $HgCl_2$ fraction after the SCR catalyst in the temperature range T=250-450^{o}C for both 100% and 50% Hg^0 at the SCR inlet. Since the rates of reaction R1 and R2 are dependent on both the concentrations of Hg^0 and $HgCl_2$, it is not straightforward predicting the outlet speciation of mercury. Predictions are shown for HCl=4.2-13 ppm in the presence of 100 ppm NO and NH_3.

At low temperatures, only mercury reaction R1 is taking place. This reaction is 1^{st} order dependent on the Hg^0 concentration and independent of the $HgCl_2$ concentration, which means that a fixed conversion **X** of the inlet Hg^0 will be achieved over the SCR.

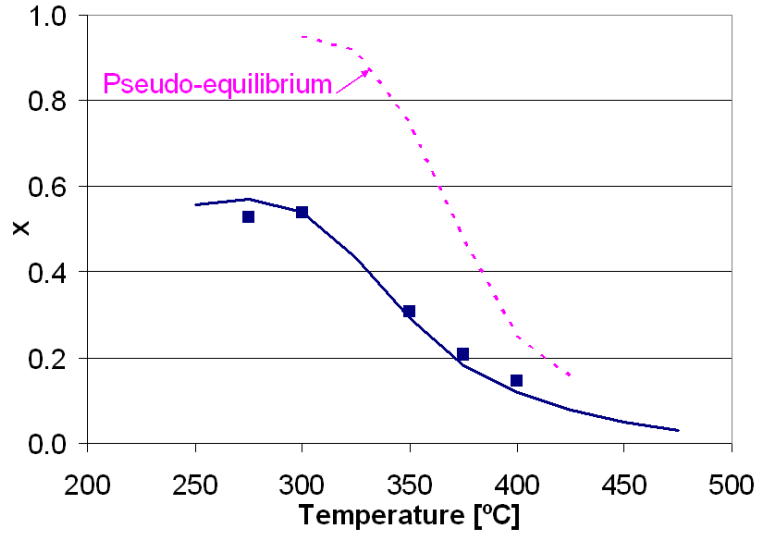

(a) Effect of temperature.

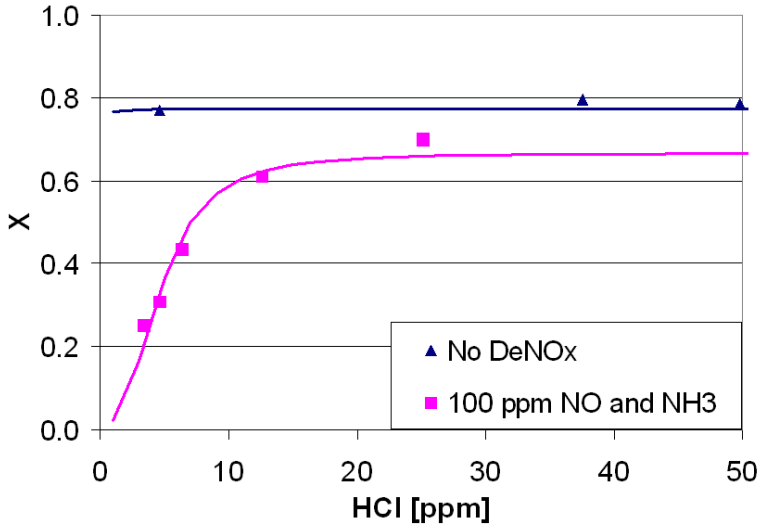

(b) Effect of HCl.

Figure 8.6: Steady-state oxidation of Hg^0 over the SCR at v=2.2 Nm/s and T=350^{o}C. The gas contains 17.6-18.2 $\mu g/Nm^3$ Hg^0, 4.2 ppm HCl, 100 ppm NO and NH_3, 4% O_2 and 5% H_2O in balance N_2. Model estimates are given in full lines.

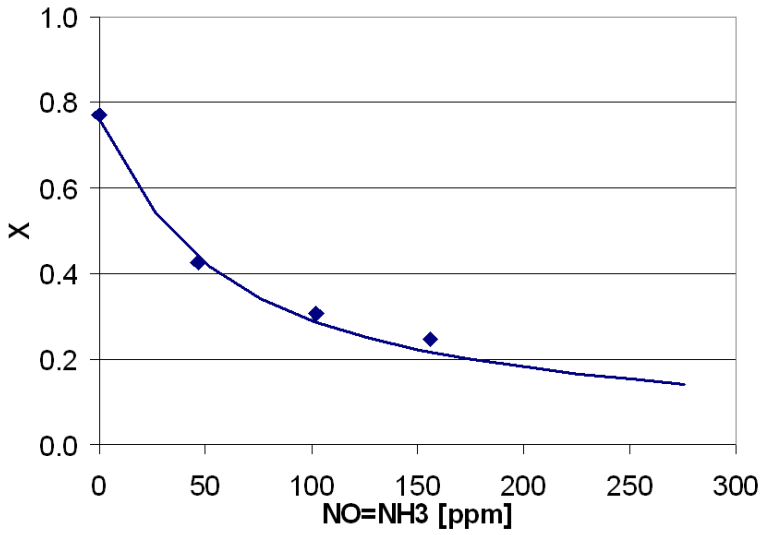

(a) Effect of $NO{=}NH_3$.

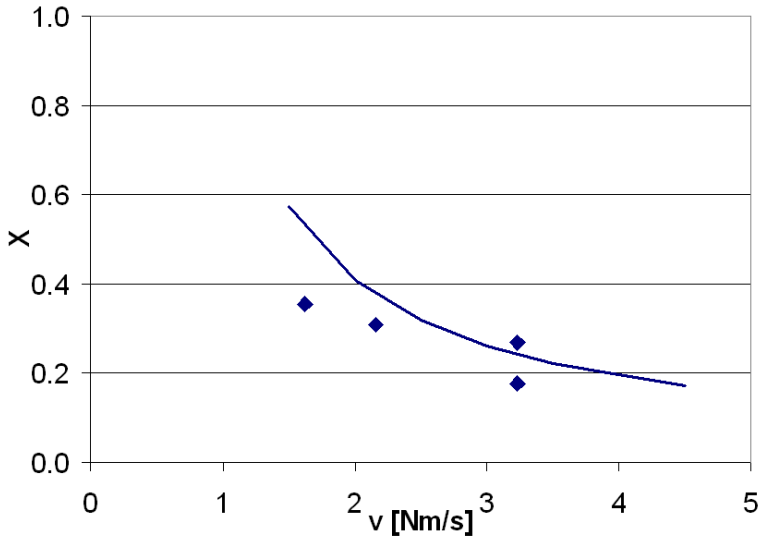

(b) Effect of linear gas velocity.

Figure 8.7: Steady-state oxidation of Hg^0 over the SCR at v=2.2 Nm/s and T=350°C. The gas contains 17.6-18.2 $\mu g/Nm^3$ Hg^0, 4.2 ppm HCl, 100 ppm NO and NH_3, 4% O_2 and 5% H_2O in balance N_2. Model estimates are given in full lines.

The fraction of $HgCl_2$ at the SCR outlet is therefore given as:

$$y_{HgCl_2} = y_{HgCl_2}(in) + X \cdot (1 - y_{HgCl_2}(in)) \tag{8.5}$$

At T>325^{o}C, reaction R2 comes into play. The reaction rate of R2 increases with increasing $HgCl_2$, which means that the Hg^0 oxidation over the SCR **is** dependent on the mercury speciation at the SCR inlet. The result is that the $HgCl_2$ fraction at the SCR outlet is less dependent on the inlet speciation compared to T=250^{o}C.

Note that the fraction of $HgCl_2$ at the SCR outlet is only dependent on the HCl concentration at the higher temperatures, where reaction R2 is important.

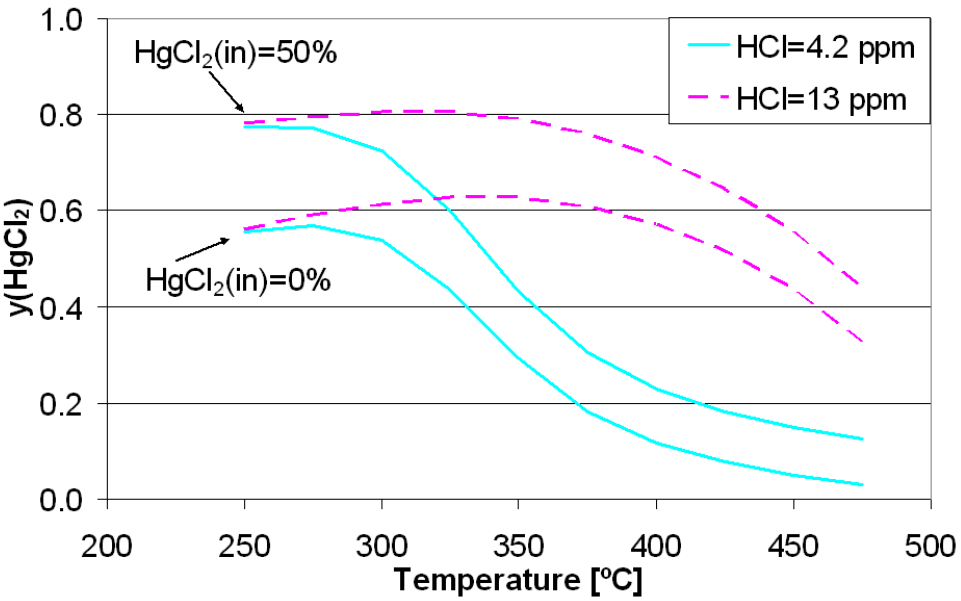

Figure 8.8: Model predictions of the steady-state Hg^0 oxidation over the SCR across temperature for different inlet speciations of mercury at v=2.2 Nm/s. In addition to Hg^0 and $HgCl_2$, the model gas contains 4.2-13 ppm HCl, 100 ppm NO and NH_3, 4% O_2 and 5% H_2O in balance N_2.

8.7.2 Kinetic regimes

The concentration profile of Hg^0 in the catalyst wall is studied in order to identify the kinetic regimes that are dominating the overall Hg^0 oxidation over the SCR at different conditions.

Plotted in figures 8.9 and 8.10 are the wall concentrations of Hg^0 at the SCR inlet and outlet at T=250 and 400^{o}C. The predictions are shown for 100% and 50% Hg^0 at the SCR inlet in figure 8.9 and 8.10, respectively. The model gas contains 4-13 ppm HCl, 100 ppm NO and NH_3, 4% O_2 and 5% H_2O in N_2.

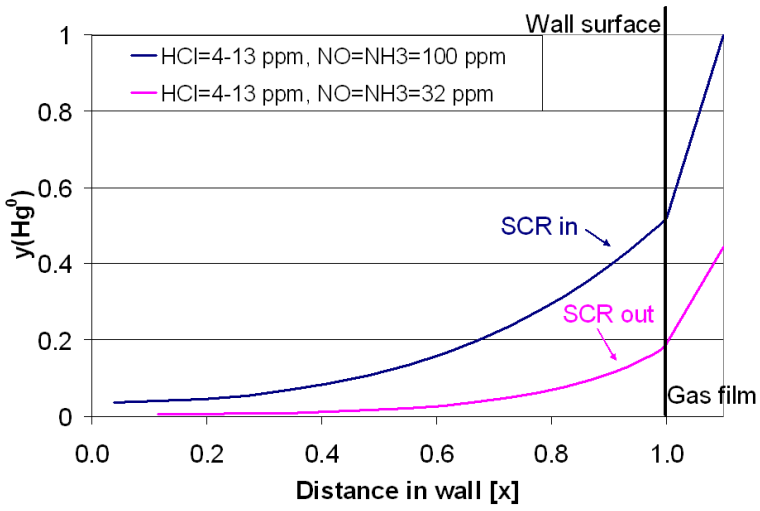

(a) T=250°C, HCl=4.2/13 ppm and y_{Hg^0}(in)=1.

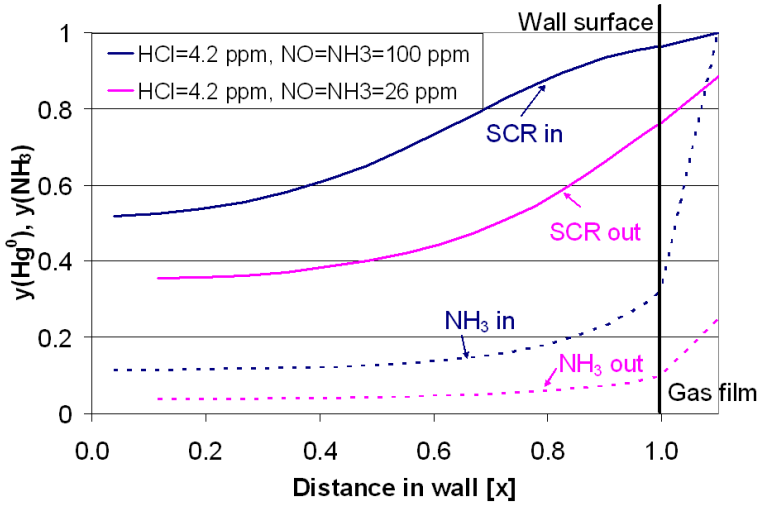

(b) T=400°C, HCl=4.2 ppm and y_{Hg^0}(in)=1.

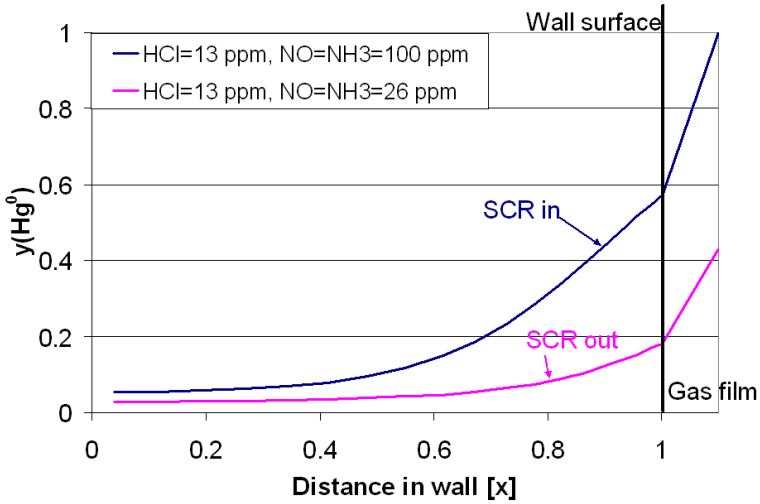

(c) T=400°C, HCl=13 ppm and y_{Hg^0}(in)=1.

Figure 8.9: Model predictions of the concentration profile of Hg^0 in the catalyst wall at v=2.2 Nm/s with 100% Hg^0 at the SCR inlet. x=0 represents the center of the catalyst wall and x=1 represents the surface. The model gas contains 100 ppm NO and NH_3, 4% O_2 and 5% H_2O in N_2. A DeNOx degree of 68-74% is achieved over the SCR corresponding to 26-32 ppm NO and NH_3 at the SCR outlet.

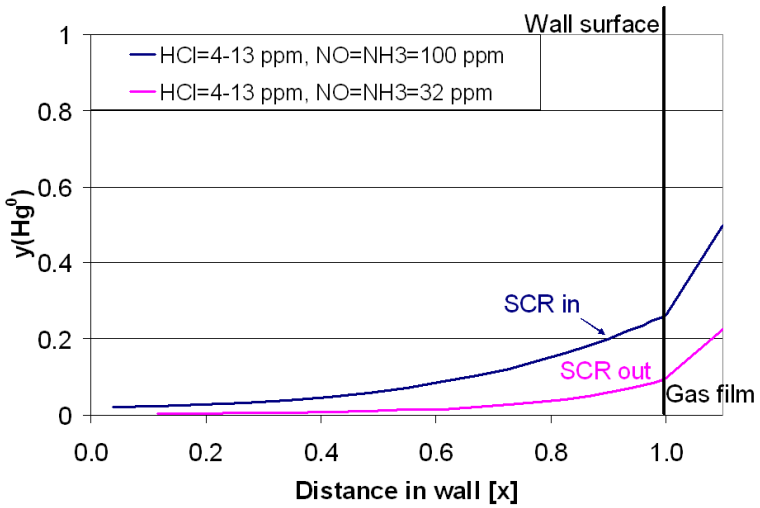

(a) T=250^{o}C, HCl=4.2/13 ppm and y_{Hg^0}(in)=0.5.

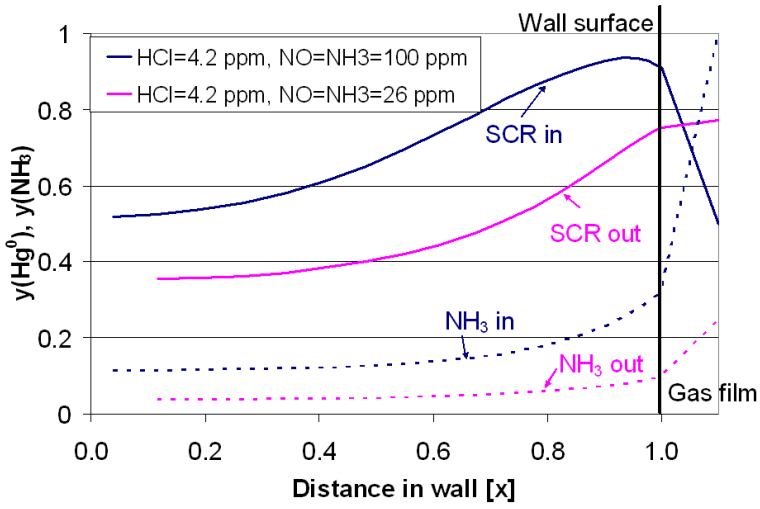

(b) T=400^{o}C, HCl=4.2 ppm and y_{Hg^0}(in)=0.5.

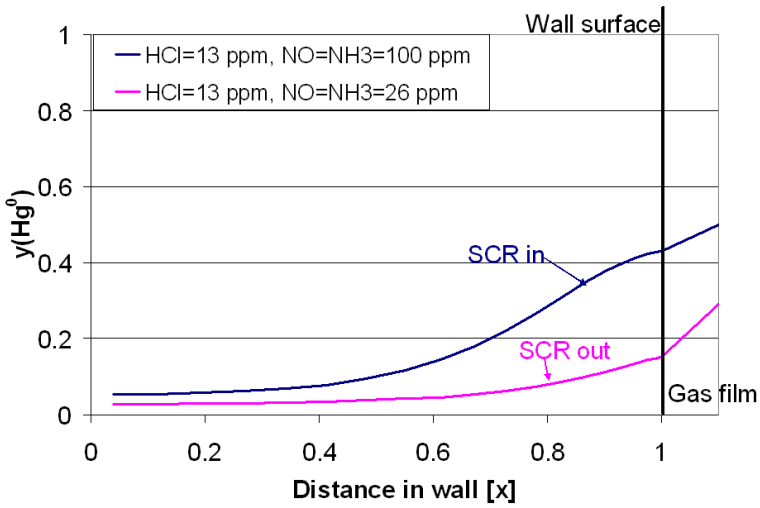

(c) T=400^{o}C, HCl=13 ppm and y_{Hg^0}(in)=0.5.

Figure 8.10: Model predictions of the concentration profile of Hg^0 in the catalyst wall at v=2.2 Nm/s with 50% Hg^0 at the SCR inlet. x=0 represents the center of the catalyst wall and x=1 represents the surface. The model gas contains 100 ppm NO and NH_3, 4% O_2 and 5% H_2O in N_2. A DeNOx degree of 68-74% is achieved over the SCR corresponding to 26-32 ppm NO and NH_3 at the SCR outlet.

At T=250^{o}C, the Hg^0 concentration profile is independent of the HCl concentration (4.2-13 ppm). External mass transfer is greatly limiting the overall rate of the Hg^0 oxidation. It can be seen in figure 8.9(a) that only 50% Hg^0 is present at the catalyst surface, when 100% Hg^0 is present in the bulk gas. The rate of external mass transfer is not fast enough to level out this concentration gradient as Hg^0 is oxidized via reaction R1 in the catalyst wall. Also, a concentration gradient exists in the catalyst wall, which shows the concurrent importance of pore diffusion.
At this low temperature, the reaction rate is independent of the inlet mercury speciation, so the conclusions are unchanged for the inlet mercury speciation of 50% Hg^0 (figure 8.10(a)).

The Hg^0 concentration profile is dependent of the HCl concentration at 400^{o}C. For 4.2 ppm HCl, the $HgCl_2$ reduction is fast in the presence of NH_3. The relative rate of surface reactions R1 and R2 is determining the overall rate of Hg^0 oxidation. Figure 8.9(b) shows that for 100% Hg^0 in the bulk gas, there is virtually no oxidation of Hg^0 taking place near the surface in the catalyst wall, where the concentration of NH_3 is highest. Figure 8.10(b) even shows that for 50% Hg^0 in the bulk gas, there is an effective production of Hg^0 in the catalyst wall, because the $HgCl_2$ reduction is faster than the Hg^0 oxidation.
At the SCR outlet, the bulk NH_3 concentration has dropped to 26 ppm and an overall Hg^0 oxidation has started to take place. Mass transfer remains unimportant throughout the length of the SCR under these conditions.

For HCl=13 ppm, the rate of reaction R2 has been somewhat dampened. This means that for 100% Hg^0 at the SCR inlet both external mass transfer and pore diffusion are primarily limiting the rate of the overall Hg^0 oxidation (see figure 8.9(c)). Figure 8.10(c) shows that both surface reactivity and mass transfer are important with 50% Hg^0 at the SCR inlet.

In conclusion, the model predictions suggest that the following kinetic regimes exist under typical high dust SCR conditions:

- At low temperature T<300^{o}C: Rates of mass transfer (both external and pore diffusion) will govern the overall Hg^0 oxidation over the SCR.
  The conversion (X) of inlet Hg^0 over the SCR is independent of the inlet mercury speciation, but the total $HgCl_2$ fraction at the SCR outlet will directly reflect the seperat contributions (as given in eq.(8.5)).

- At T≥350^{o}C and low HCl (≤ 4 ppm): The $HgCl_2$ reduction with NH_3 (R2) is important and the mercury surface reaction rates are governing the overall Hg^0 oxidation over the SCR even at low NO=NH_3=26 ppm.
  The mercury speciation after the SCR is largely determined by the pseudo equilibrium between reaction R1 and R2 at the SCR outlet conditions. The inlet mercury speciation will be of little importance for the total fraction of $HgCl_2$ leaving the SCR.

- At T≥350^{o}C and high HCl (≥ 13 ppm): Rates of mass transfer (both external and pore diffusion) will govern the overall Hg^0 oxidation over the SCR. Only a minor

influence of the inlet mercury speciation on the total fraction of $HgCl_2$ leaving the SCR is present, since the reaction R2 is in play.

8.8 Conclusions

A mechanistically based model framework has been set up describing the Hg^0 oxidation over SCR catalysts. The resulting model successfully reproduce the trends in Hg^0 oxidation over monolithic SCR reactors that have been observed in a simulated flue gases across two different experimental schemes. This verifies that the relevant mercury chemistry has been incorporated in the model for describing the Hg^0 oxidation.

The synergistic inhibition by NO and NH_3 on the Hg^0 oxidation is a matter of uncertainty, since a great difference in the magnitude of the effect is seen across experiments. The synergistic inhibition is modelled as a consumption of active Lewis sites in the DeNOx reaction, which need to be reoxidized in order to regain activity for the Hg^0 oxidation. Further experiments should be performed in order to further understand and properly quantify the effect.

Future work entails evaluating the model against full-scale SCR data in order to elucidate if the proposed mercury chemistry over the SCR reactor is still relevant in real flue gases.

Chapter 9

Guidelines for maximizing Hg^0 oxidation over SCR reactors

Based on the experimental study and the modeling work in this PhD-work, the following guidelines are set up for maximizing Hg^0 oxidation over high dust SCR reactors across different applications.

For operating temperatures T $\geq$ 325^{o}C
The overall Hg^0 oxidation will be governed by a $HgCl_2$ reduction by NH_3 at low HCl concentrations. Means for maximizing the Hg^0 oxidation over the SCR reactor are:

- Increasing the vanadia concentration of the catalyst will increase the relative rate of the Hg^0 oxidation to the $HgCl_2$ reduction.
- Increasing the HCl concentration in the flue gas, which will increase the relative rate of the Hg^0 oxidation to the $HgCl_2$ reduction.
- Decreasing the SCR operating temperature will decrease the rate of $HgCl_2$ reduction.
- The addition of an extra catalyst layer will provide a catalyst volume in the reactor, where the NH_3 concentration is low and the $HgCl_2$ reduction is unimportant.

The Hg^0 oxidation will greatly be limited by external mass transport for HCl$\geq$ 13 ppm up to T=425^{o}C. (See suggestions in next paragraph).

For low operating temperatures T <325^{o}C
The overall Hg^0 oxidation will greatly be limited by external mass transport for HCl$\geq$ 4 ppm.

Means for increasing the rate of external mass transport (and thus maximize the Hg^0 oxidation over the SCR reactor) include:

- Decreasing the hydraulic diameter of the SCR catalyst.
- Increasing the linear gas velocity.

Notice that changing the catalyst composition or adding halogen to the gas under external mass transport limitation will only have a minor influence on the catalytic Hg^0 oxidation over the SCR reactor.

Chapter 10

Conclusions and future work

This PhD-study has worked towards quantifying the Hg^0 oxidation over commercial SCR catalysts for different gas compositions and operating conditions. For the purpose, an extensive experimental study of the Hg^0 oxidation over SCR catalysts has been carried out in a laboratory setup under different well-controlled conditions.
Analysis of the experimental data has provided a greater mechanistic understanding of the mercury chemistry over SCR catalysts and has pinpointed the relevant mechanisms taking place under different operating conditions. Based on this understanding, reaction rate expressions for mercury reactions has been derived and a kinetic model for the Hg^0 oxidation over SCR monolithic catalysts has been built.

10.1 Mechanistic understanding

It was chosen to study the influence of the DeNOx reaction and HCl on the mercury chemistry, since these were shown to have crucial importance for the catalytic Hg^0 oxidation.
Via the experimental work in this study, the presence of the DeNOx reaction has been identified to inhibit the Hg^0 oxidation via three different mechanisms:

1. By adsorption of NH_3 on active Lewis sites on the SCR catalyst for temperatures T<300^{o}C, the adsorption of Hg^0 is inhibited

2. By consumption of active Lewis sites in the DeNOx reaction that must be oxidized to regain activity, the number of available sites for Hg^0 adsorption is reduced.

3. By the reduction of $HgCl_2$ by NH_3 at temperatures above T=325^{o}C, the overall Hg^0 oxidation is reduced.

The following three net reactions have therefore been identified as being relevant for the mercury chemistry over commercial SCR catalysts:

$$R1.\ \ 2\ HCl + Hg^0 + 1/2\ O_2 \ \leftrightarrow\ HgCl_2 + H_2O$$
$$R2.\ \ 2\ NH_3 + 3\ HgCl_2 \ \leftrightarrow\ N_2 + 3\ Hg^0 + 6\ HCl$$
$$R3.\ \ 2\ NO + 2\ NH_3 + 1/2\ O_2 \ \leftrightarrow\ 2\ N_2 + 3\ H_2O$$

Reaction R1 is the oxidation of Hg^0 by HCl, reaction R2 is the reduction of $HgCl_2$ by NH_3 and reaction R3 is the NO-reduction by NH_3. Based on the experimental data and microkinetic modelling, elementary steps have been derived for the mercury surface reactions R1 and R2.

The Hg^0 oxidation via reaction R1 is proposed to take place between adsorbed Hg^0 and HCl by a Langmuir-Hinshelwood mechanism. The rate of reaction R1 is proposed to be limited by the adsorption of Hg^0 on vanadia Lewis sites on the SCR catalyst. The number of available (oxidized) Lewis sites is dependent on the NH_3 concentration and the DeNOx reaction taking place.
The experimental data suggest that increasing HCl concentration (HCl$\geq$ 4 ppm) does not influence the rate of Hg^0 oxidation via reaction R1 indicating that sufficient HCl adsorbs for reaction with mercury. The rate of Hg^0 oxidation via reaction R1 increases with increasing V_2O_5 load, since more active sites are available for Hg^0 adsorption.

The $HgCl_2$ reduction via reaction R2 could not be studied separately from reaction R1 and so the mechanistic understanding of the reaction remains limited. The rate of R2 is promoted by increasing NH_3 until the SCR catalyst is saturated with adsorbed NH_3. The reaction is proposed to be coupled to TiO_2 sites on the catalyst, where $HgCl_2$ could be adsorbing. HCl inhibits the rate of $HgCl_2$ reduction, which possibly is due to scavenging of adsorbed $HgCl_2$. This means that increasing HCl will give an overall increasing rate of Hg^0 oxidation at temperatures above T=325^{o}C, where both reaction R1 and R2 are taking place.

10.2 Quantification and predictions

The experimental data suggests that two different mechanistic regimes exist, which control the surface reactivity towards Hg^0 oxidation on the SCR catalyst

- For T$\leq$ 300^{o}C: The catalytic Hg^0 oxidation is limited by the adsorption of Hg^0 on active Lewis sites on the catalysts. Both NH_3 alone and the DeNOx reaction is limiting the number of available Lewis sites.

- For T$\geq$ 350^{o}C: The overall Hg^0 oxidation is limited by the $HgCl_2$ reduction via reaction R2. A pseudo equilibrium mercury speciation may be established, where the rates of the Hg^0 oxidation and the $HgCl_2$ reduction are equal. As NH_3 is consumed in the DeNOx reaction, the pseudo equilibrium will shift towards more $HgCl_2$.

The temperature region T=300-350^{o}C represents a 'mixed regime'.

A kinetic model for the Hg^0 oxidation over monolithic SCR reactors has been built taking both external mass transfer, pore diffusion and reaction on the catalyst wall into account. The resulting model successfully reproduce the trends in Hg^0 oxidation over monolithic SCR reactors that have been observed in the laboratory experiments. This verifies that the relevant mercury chemistry has been incorporated in the model for describing the Hg^0 oxidation in the simulated flue gas. The validity of the model for describing the mercury chemistry in real flue gases is yet to be explored.

Model predictions suggest that the Hg^0 oxidation over high dust SCR reactors is limited by external mass transport, when the HCl concentration is sufficiently high. Only for T>350^{o}C and low HCl ($\approx$ 4 ppm) will the surface reactivity greatly limit the overall Hg^0 oxidation. This will be prevalent at high inlet fractions of $HgCl_2$. Means for improving the catalyst activity include increasing the V_2O_5 load, decreasing operating temperature or adding an additional catalyst layer, where the concentrations of NO and NH_3 will be negligible.

10.3 Future work

The kinetic model must be evaluated for describing the Hg^0 oxidation over full-scale SCR reactors in order to determine the predictive power of the current model, which is the ultimate aim of this Ph.D.-work.

The synergistic inhibition by NO and NH_3 on the Hg^0 oxidation needs further experimental investigation in order to determine the magnitude of the effect with greater certainty.

Other effects may come into play in real flue gases that will be important for the mercury chemistry over SCR catalysts. Examining the mercury chemistry in real flue gases is therefore the next pivotal step towards a fundamental understanding of the Hg^0 oxidation over full scale SCR reactors.

Appendix A

Details on experiments in simulated flue gases

Table A.1: Summary of laboratory experiments with simulated flue gases. STP is at T=25°C and P=1 atm. $LV = \frac{U(STP)}{a_c \cdot V}$ is the area velocity otherwise specified as AV in this report.

Reference	Bock et al. (2002)	Eom et al. (2008)	Eswaran and Stenger (2008)	He et al. (2009)
Catalyst				
Type	Commercial Ceramics GmbH Plate and honeycomb	Commercial Honeycomb	Commercial Plate and honeycomb	1 wt%V_2O_5/TiO_2 Powder
Dimensions	0.65 m^2	0.9x0.9x17.2cm	a_c=1022cm^2	3.6 mg
Gas composition				
Hg^0	22 $\mu g/m^3$	37 $\mu g/m^3$	20 $\mu g/m^3$	24 $\mu g/m^3$
$HgCl_2$	-	-	-	-
HCl	10-60 ppm	0-50 ppm	5-35 ppm	0-50 ppm
DeNOx	395-532 ppm NO	0-400 ppm NO	400 ppm NO	-
	395-532 ppm	0-360 ppm NH_3	360 ppm NH_3	-
SO_2/SO_3	500-540 ppm	-	-	-
Other	3%O_2, 3%H_2O, 50 ppm %CO	0-6%O_2	3%O_2, 8%H_2O, 12%CO_2	0-5%O_2
Operating conditions				
Flow	LV=1.7 m/s 4000 h^{-1}	2000 cm^3/min (STP) 411, 450 $cm^3(STP)/cm^2 \cdot h$	7 slpm	1L/min
Temperature	280-420°C	350°C	390°C	300°C
Comments		Stainless steel reactor, no background oxidation reported.		

Table A.2: Summary of laboratory experiments with simulated flue gases. $LV = \frac{U(STP)}{a_c \cdot V}$ is the area velocity otherwise specified as AV in this report.

Reference	Hocquel (2004)				Hong et al. (2010)
Catalyst					
Type	Pure V_2O_5, WO_3 or TiO_2		Commercial		Commercial
	Powder		Honeycomb and plate		Crushed honeycomb
Dimensions	100 mg		3 layers		1 g
Gas composition					
Hg^0	25-30 $\mu g/m^3$	7-13 $\mu g/m^3$	15-40 $\mu g/m^3$	15-40 $\mu g/m^3$	50 $\mu g/m^3$
$HgCl_2$	-	10-14 $\mu g/m^3$	-	-	-
HCl	200mg/m^3	1.4-2.8mg/m^3	0.4-155mg/m^3	0.5-100mg/m^3	0-50 mg/m^3
DeNOx	-	-	-	0-500 ppm NO	0-500 ppm NO
	-	-	-	0-500 ppm NH_3	0-500 ppm NH_3
SO_2/SO_3	-	0-76 ppm SO_2	-	0-1500 ppm SO_2	-
Other	10.5%O_2, 8.9%H_2O	10.5%O_2, 9.5%H_2O	1.8%O_2, 3.3%H_2O	2.3% O_2, 3.3% H_2O	3% O_2
				50-81 ppm CO	
Operating conditions					
Flow	-	-	LV=0.6 m/s	LV=1.7 m/s	2L/min
Temperature	170-350°C	330°C	250-310°C	280-420°C	250-350°C
Comments	Hg^0 oxidation	$HgCl_2$ reduction	Adsorption study	Hg^0 oxidation	

Table A.3: Summary of laboratory experiments with simulated flue gases. STP is at T=25°C and P=1 atm.

Reference	Kamata et al. (2008)	Struckmann et al. (2008)	Thorwarth (2007)	Zhuang et al. (2007)
Catalyst				
Type	0-15wt% V_2O_5/TiO_2	Commercial	0-1.8wt%V_2O_5/0-7wt%WO_3/TiO_2	Commercial
	Powder	Honeycomb and plate	-	Cormetech
Dimensions	30 mg	-	1-3 layers	-
Gas composition				
Hg^0	1.2 ppbv	50 $\mu g/m^3$	0-60 $\mu g/m^3$	13.3$\mu g/m^3$
$HgCl_2$	-	-	0-60 $\mu g/m^3$	-
HCl	10 ppm	60 ppm	0-20mg/m^3	0-50 ppm
DeNOx	-	0-400 ppm NO	690 ppm NO	600 ppm NO,18.5 ppm NO_2
	-	0-400 ppm NH_3	0-620 ppm NH_3	550 ppm NH_3
SO_2/SO_3	200 ppm SO_2	-	680 ppm SO_2	0-50 ppm SO_3
	-	-	-	0-2000 ppm SO_2
Other	2%O_2, 10%H_2O	4% O_2, 7% H_2O	4%O_2, 10.1%H_2O	6%O_2, 8%H_2O, 12%CO_2
Operating conditions				
Flow	2180 cc/min(STP)	AV=5.8-19.7 m/h	SV=7200 h^{-1}	'Typical SV'
Temperature	150°C	390°C	360°C	343°C
Comments				

Appendix B

Mercury analysis by RA-915+

Mercury is analyzed in the Lumex RA-915+ analyzer, which used cold vapor atomic absorption spectrometry to measure gaseous elemental mercury Hg^0 continuously. The analysis is based on differential Zeeman atomic absorption spectrometry using high frequency modulation of light polarisation. The analyzer produces real-time data.

The analyzer consists of a mercury lamp, which is placed in the gap of the poles of a magnet that is excited by a high-frequency generator. The light successively passes through a polarization modulator and the analysis cell (where the sample will flow through) and is detected by a photo detector.

The spectrometric method measures the attenuation of the light produced by the mercury vapor lamp as it passes through a cell that contains the sample gas. Mercury atoms (Hg^0) in the sample cell absorb light at their characteristic wavelength of 253.7 nm. The SO_2-molecule absorbs light across a wide spectrum including the 243.7 nm wavelength - thus interfering with mercury measurements. In order to remove the interference from SO_2, the radiation source is placed in a permanent magnetic field giving a slight shift the wavelength of the mercury vapor lamp (Zeeman modulation).

The Zeeman-effect is the splitting of a single spectral line into several components in the presence of a static magnetic field. In most atoms, several electron configurations with the same level of energy exists, so that transitions between these configurations correspond to a single spectral line. The presence of a magnet breaks this degeneracy, since the magnetic field interacts differently with electrons with different quantum numbers, slightly modifying their energy. The result is that the electron configurations now have slightly different energies giving rise to several very close spectral lines (Wikipedia, 21.07.2010).

The mercury resonance line (253.7 nm) is split into three polarized Zeeman components (Π, σ_- and σ_+) by the polarization modulator. The photo detector will only

detect radiation of the two σ-components, where only σ_- falls within the absorption line profile of mercury. When mercury is absent in the analytical cell, the radiation intensities of both σ-components are equal. The difference between the intensities of the σ-components increases as the mercury vapor concentration grows. The spectral shift of the σ-components is significantly smaller than the width of molecular absorption bands. This means that the broadband absorbers (such as SO_2) will attenuate the signal at both wavelength, and the difference between the signals is attributed to the mercury concentration.

Appendix C

Solving the equations by orthogonal collocation

The mass balances for $i = [NO, NH_3, Hg^0]$ in the monolith channel and wall have been derived in section 4.

The mass balance for component i in the monolith channel is

$$\frac{dy_{i,b}}{dz^*} + \frac{k_{g,i} \cdot a_c \cdot L}{v} \cdot (y_{i,b} - y_{i,s}) = 0 \tag{C.1}$$

with the initial condition $y_{i,b}(z* = 0) = y_{i0}$.

The mass balance for component i in the catalyst wall is

$$\frac{d^2 y_i}{dx^{*2}} - \phi_i^2 \cdot \frac{-r_{s,i}(y_i \cdot P_{i,0})}{-r_{s,i}(P_{i,0})} = 0 \tag{C.2}$$

with the following boundary conditions

1. Equal flux from the bulk gas to the catalyst surface ($x^* = 1$) and into the catalyst wall:

$$y_{i,s} = y_i|_{x^*=1} = y_{i,b} - \frac{1}{Bi_i} \cdot \left.\frac{dy_i}{dx^*}\right|_{x^*=1}$$

2. $\left.\frac{dy_i}{dx^*}\right|_{x^*=0} = 0$

where $Bi_i = \frac{k_{g,i} \cdot h}{D_i^e}$ and the Thiele modulus is given by

$$\phi_i^2 = \frac{R \cdot T \cdot h^2}{D_i^e \cdot P_{i,0}} \cdot (-r_{s,i}(P_{i,0})) \tag{C.3}$$

The differential equations will now be approximated by the orthogonal collocation method. The expansion

$$y_i(N) = \sum_{k=1}^{N+1} y_{i,k} l_k(u) \tag{C.4}$$

will be inserted in the differential equation for the catalyst wall yielding a set of algebraic equations to solve.

C.1 Catalyst wall

The following variable substitution is introduced:

$$u = x^{*2} \;\Rightarrow\; \frac{d}{dx^*} = \frac{d}{du} \cdot 2 \cdot \sqrt{u} \tag{C.5}$$

and equation (C.2) is rewritten

$$\begin{aligned}
2 \cdot \sqrt{u} \cdot \frac{d}{du}\left(\frac{dy_i}{du} 2 \cdot \sqrt{u}\right) - \phi_i^2 \cdot \frac{-r_{s,i}(y_i \cdot P_{i,0})}{-r_{s,i}(P_{i,0})} = 0 \Leftrightarrow \\
4 \cdot \frac{d}{du}\left(\frac{dy_i}{du}\sqrt{u}\right) - \frac{\phi_i^2}{\sqrt{u}} \cdot \frac{-r_{s,i}(y_i \cdot P_{i,0})}{-r_{s,i}(P_{i,0})} = 0 \Leftrightarrow \\
\frac{1}{\sqrt{u}}\left[4u\frac{d^2y_i}{du^2} + 2\frac{dy_i}{du} - \phi_i^2 \cdot \frac{-r_{s,i}(y_i \cdot P_{i,0})}{-r_{s,i}(P_{i,0})}\right] = 0 \Rightarrow \qquad \text{(C.6)} \\
4u\frac{d^2y_i}{du^2} + 2\frac{dy_i}{du} - \phi_i^2 \cdot \frac{-r_{s,i}(y_i \cdot P_{i,0})}{-r_{s,i}(P_{i,0})} = 0 \qquad \text{(C.7)}
\end{aligned}$$

The boundary conditions are

1.

$$\begin{aligned}
y_i|_{x^*=1} = y_{i,b} - \left(\frac{2 \cdot \sqrt{u}}{Bi_i} \cdot \frac{dy_i}{du}\right)\Bigg|_{x^*=1} \Leftrightarrow \\
0 = \frac{dy_i}{du}\Big|_{u=1} + \frac{Bi_i}{2}(y_i\Big|_{u=1} - y_{i,b})
\end{aligned}$$

where $Bi_i = \frac{k_{g,i} \cdot h}{D_i^e}$ and $K_i = \frac{Bi,i}{2}$.

2. $\left.\frac{dy_i}{du}\right|_{u=0} = 0$

The expansion in equation (C.4) is inserted in (C.7) giving the following residual at the j'th collocation point:

$$\begin{aligned} R_{i,N}(u_j) &= 4u_j \cdot \sum_{k=1}^{N+1} y_{i,k} l_k''(u_j) + 2 \cdot \sum_{k=1}^{N+1} y_{i,k} l_k'(u_j) - \phi_i^2 \cdot \frac{-r_{s,i}(y_{i,j} \cdot P_{i,0})}{-r_{s,i}(P_{i,0})} \\ &= \sum_{k=1}^{N+1} C_{jk} y_{ik} - \phi_i^2 \cdot \frac{-r_{s,i}(y_{i,j} \cdot P_{i,0})}{-r_{s,i}(P_{i,0})} \end{aligned} \tag{C.8}$$

where the discretization matrices A_{jk} and B_{jk} represents the weight given to the kth coefficient in the jth equations. Also:

$$C_{jk} = 4u_j B_{jk} + 2A_{jk} \ , \ A_{jk} = l_k'(u_j) \ , \ B_{jk} = l_k''(u_j) \tag{C.9}$$

The element $N+1$ is found from boundary condition 1:

$$\begin{aligned} \sum_{k=1}^{N+1} y_{i,k} l_k'(u_{N+1}) + K_i \cdot (\sum_{k=1}^{N+1} y_{i,k} l_k(u_{N+1}) - y_{i,b}) = 0 \ \Leftrightarrow \\ \sum_{k=1}^{N+1} A_{N+1,k} y_{i,k} + K_i \cdot (y_{i,N+1} - y_{i,b}) = 0 \Leftrightarrow \\ A_{N+1,N+1} y_{i,N+1} + \sum_{k=1}^{N} A_{N+1,k} y_{i,k} + K_i \cdot (y_{i,N+1} - y_{i,b}) = 0 \end{aligned} \tag{C.10}$$

A d-matrix is now defined as

$$d_{i,N+1} = \frac{K_i \cdot y_{i,b}}{A_{N+1,N+1} + K_i} \tag{C.11}$$

$$d_{ik} = \frac{-A_{N+1,k}}{A_{N+1,N+1} + K_i} \tag{C.12}$$

which gives the following expression for $y_{i,N+1}$:

$$y_{i,N+1} = d_{i,N+1} + \sum_{k+1}^{N} d_{i,k} y_{i,k} \tag{C.13}$$

The number of coupled equations are reduced to N by rewritting it

$$\begin{aligned}\sum_{k=1}^{N+1} C_{jk}y_{ik} &= \sum_{k=1}^{N} C_{jk}y_{ik} + C_{j,N+1}y_{i,N+1} \\ &= \sum_{k=1}^{N} E_{i,jk}y_{ik} + e_{ij} \end{aligned} \tag{C.14}$$

where

$$E_{i,jk} = C_{jk} + C_{j,N+1} \cdot d_{ik} \tag{C.15}$$

$$e_{i,j} = C_{j,N+1} \cdot d_{i,N+1} \tag{C.16}$$

The residual in equation (C.8) is now given as

$$R_{i,N}(u_j) = \sum_{k=1}^{N} E_{i,jk}y_{ik} + e_{ij} - \phi_i^2 \cdot \frac{-r_{s,i}(y_{i,j} \cdot P_{i,0})}{-r_{s,i}(P_{i,0})} \tag{C.17}$$

C.2 Catalyst channel

The surface concentration is given by $y_{i,s} = y_{i,N+1}$. From the mass balance for the catalyst wall $y_{i,N+1}$ is given as eq. C.13

$$y_{i,N+1} = d_{i,N+1} + \sum_{k+1}^{N} d_{i,k}y_{i,k}$$

If $KK_i = \frac{k_{g,i}a_cL}{v}$ is assumed constant along the length of the channel, the mass balance becomes

$$\begin{aligned} 0 =& \frac{dy_{ib}}{dz*} + KK_i \cdot (y_{ib} - d_{i,N+1} - \sum_{k=1}^{N} d_{i,k}y_{i,k}) \Leftrightarrow \\ \frac{dy_{ib}}{dz*} =& \, y_{ib} \cdot KK_i \cdot (g_{i,N+1} - 1) + KK_i \cdot \sum_{k=1}^{N} d_{i,k}y_{i,k} \end{aligned} \tag{C.18}$$

where $g_{i,N+1} = \frac{K_i}{A_{N+1,N+1}+K_i} = d_{i,N+1} \cdot \frac{1}{y_{ib}}$.

C.3 System of equations

The system of equations are now $3N$ coupled algebraic equations and 3 differential equations

$$
\begin{aligned}
R_{1:N}(u_j) &= \sum_{k=1}^{N} E_{NO,jk} \cdot y_k + C_{j,N+1} \cdot g_{NO,N+1} \cdot y_{3N+1} - \phi_{NO}^2 \cdot \frac{-r_{NO}(y_j \cdot P_{NO,0})}{-r_{NO}(P_{NO,0})} \\
R_{N+1:2N}(u_j) &= \sum_{k=1}^{N} E_{NH3,jk} \cdot y_{k+N} + C_{j,N+1} \cdot g_{NH3,N+1} \cdot y_{3N+2} - \phi_{NH3}^2 \cdot \frac{-r_{NO}(y_{j+N} \cdot P_{NH_3,0})}{-r_{NO}(P_{NH_3,0})} \\
R_{2N+1:3N}(u_j) &= \sum_{k=1}^{N} E_{Hg,jk} \cdot y_{k+2N} + C_{j,N+1} \cdot g_{Hg,N+1} \cdot y_{3N+3} - \phi_{Hg}^2 \cdot \frac{-r_{Hg}(y_{j+2N} \cdot P_{Hg^T})}{-r_{Hg}(P_{Hg^T})} \\
R_{3N+1}(u_j) &= y_{3N+1} \cdot KK_{NO}(g_{NO,N+1} - 1) + KK_{NO} \cdot \sum_{k=1}^{N} d_{NO,k} y_{j,k} \\
R_{3N+2}(u_j) &= y_{3N+2} \cdot KK_{NH_3}(g_{NH_3,N+1} - 1) + KK_{NH_3} \cdot \sum_{k=1}^{N} d_{NH_3,k} y_{j+N,k} \\
R_{3N+3}(u_j) &= y_{3N+3} \cdot KK_{Hg}(g_{Hg,N+1} - 1) + KK_{Hg} \cdot \sum_{k=1}^{N} d_{Hg,k} y_{j+2N,k}
\end{aligned} \tag{C.19}
$$

where

$$
\begin{aligned}
y(1:N) &= y_{NO} \\
y(N+1,2N) &= y_{NH3} \\
y(2N+1,3N) &= y_{Hg^0} \\
y(3N+1) &= y_{NO,b}(z*) \\
y(3N+2) &= y_{NH3,b}(z*) \\
y(3N+3) &= y_{Hg,b}(z*)
\end{aligned} \tag{C.20}
$$

Initial conditions for this system are the partial pressure profiles of NO, NH_3 and Hg^0 in the wall at $z* = 0$, where $y_{NO,0} = 1$, $y_{NH_3,0} = 1$ and $y_{Hg,0} = \frac{P_{Hg^0,0}}{P_{Hg^T}}$. The wall profiles are calculated from the bulk concentrations by solving the algebraic equations above.

C.4 Numerical solver and choice of collocation points

The equations are implemented in FORTRAN 95. A module of functions built by Michaelsen and Wedel (2006) is used for the numerical solution of the differential-algebraic equations. The differential equations are solved by a semi-implicit 3rd order Runge-Kutta ODE-solver.

The number of collocation points N necessary to achieve the necessary accuracy of the

solution is tested in the validation of the model. The Jacobi-polynomial $P_N^{(\alpha,\beta)}$ is chosen with exponents $\alpha = 0$ and $\beta = -0.5$, since the 3N integrands have a common factor of the form of $\frac{1}{\sqrt{u}}$. In this way, the collocation points becomes the quadrature points of the particular Gauss-Jacobi quadrature formula and optimal accuracy is achieved in the solution.

A numerical Jacobian has been applied in the solution as this makes the program more flexible to changes. The necessary accuracy is still achieved for the purpose.

C.5 Insertion of rate expressions

The reaction rate expressions for $i = [NO, NH_3, Hg^0]$ must be inserted in the following term in the system of equations (C.19):

$$\phi_i^2 \cdot \frac{-r_{s,i}(y_{i,j} \cdot P_{i,0})}{-r_{s,i}(P_{i,0})} \tag{C.21}$$

C.5.1 NO and NH_3

$$\phi_{NO}^2 = \frac{h^2 \cdot a_c \cdot k'_{NO}}{D_{NO}^e} \cdot \frac{K_{NH_3} \cdot P_{NH_3,0}}{1 + K_{NH_3} \cdot P_{NH_3,0}} \tag{C.22}$$

$$\phi_{NH}^2 = \frac{h^2 \cdot a_c \cdot k'_{NO}}{D_{NH_3}^e} \cdot \frac{K_{NH_3} \cdot P_{NO,0}}{1 + K_{NH_3} \cdot P_{NH_3,0}} \tag{C.23}$$

$$\frac{-r_{NO}(y_j \cdot P_{NO,0})}{-r_{NO}(P_{NO,0})} = \frac{y_j \cdot y_{j+N} \cdot (1 + K_{NH_3} \cdot P_{NH_3,0})}{1 + K_{NH_3} \cdot y_{j+N} \cdot P_{NH_3,0}} \tag{C.24}$$

where the reaction rate constant is $k'_{NO}[=]$m/s and given by $k'_{NO} = \frac{k_{NO} \cdot R \cdot T_N}{a_c}$. The adsorption coefficient of NH_3 is in units: $K_{NH_3}[=]1/atm$.

C.5.2 Hg

The conversion rate of Hg^0 is given by the difference in Hg^0 oxidation and $HgCl_2$ reduction:

$$-r_{s,Hg} = -r_{ox} + r_{red} \tag{C.25}$$

$$= \frac{k_1 \cdot P_{Hg^0}}{1 + \frac{P_{NO} \cdot \frac{K_{NH_3} \cdot P_{NH_3}}{1 + K_{NH_3} \cdot P_{NH_3}}}{k_{reox} \cdot P_{O_2}^{1/4}} + f_L \cdot K_{NH_3} \cdot P_{NH3}} \left(1 - \frac{1}{K_p} \cdot \frac{P_{HgCl_2}}{P_{HCl}^2 \cdot P_{Hg^0}} \cdot \frac{P_{H_2O}}{\sqrt{P_{O_2}}}\right) -$$

$$k_3 \cdot \left(\frac{K_{NH_3} \cdot P_{NH_3}}{1 + K_{NH_3} \cdot P_{NH_3}}\right)^{2/3} \cdot \frac{P_{HgCl_2}}{(1 + K_{HCl} \cdot P_{HCl})^{n_{HCl}}} \quad [mol/m^3 \cdot s] \tag{C.26}$$

The form of the term (C.21) for $i = Hg^0$ is shown on the next page.

$$\phi_{Hg}^2 = \frac{R \cdot T \cdot h^2}{D_{Hg}^e \cdot P_{Hg^T}} \cdot \left(-r_{s,Hg}(P_{Hg^T})\right) \tag{C.27}$$

$$-r_{s,Hg}(P_{Hg^T}) = \frac{k_1 \cdot P_{Hg^T}}{1 + \frac{P_{NO,0}}{k_{reox} \cdot P_{O_2}^{1/4}} \cdot \frac{K_{NH_3} \cdot P_{NH_3,0}}{1 + K_{NH_3} \cdot P_{NH_3,0}} + f_L \cdot K_{NH_3} \cdot P_{NH3,0}} \cdot \left(1 - \frac{1}{K_p} \cdot \frac{(1 - y_{Hg,0})}{y_{Hg,0}} \cdot \frac{P_{H_2O}}{P_{HCl}^2 \cdot \sqrt{P_{O_2}}}\right) -$$
$$k_3 \cdot \left(\frac{K_{NH_3} \cdot P_{NH_3,0}}{1 + K_{NH_3} \cdot P_{NH_3,0}}\right)^{2/3} \cdot \frac{(1 - y_{Hg,0}) \cdot P_{Hg^T}}{(1 + K_{HCl} \cdot P_{HCl})^{n_{HCl}}} \tag{C.28}$$

$$-r_{s,Hg}(y_{j+2N} \cdot P_{Hg^T}) = \frac{k_1 \cdot y_{j+2N} \cdot P_{Hg^T}}{1 + \frac{y_j \cdot P_{NO,0}}{k_{reox} \cdot P_{O_2}^{1/4}} \cdot \frac{K_{NH_3} \cdot y_{j+N} \cdot P_{NH_3,0}}{1 + K_{NH_3} \cdot y_{j+N} \cdot P_{NH_3,0}} + f_L \cdot K_{NH_3} \cdot y_{j+N} \cdot P_{NH3,0}} \cdot \left(1 - \frac{1}{K_p} \cdot \frac{(1 - y_{j+2N})}{y_{j+2N}} \cdot \frac{P_{H_2O}}{P_{HCl}^2 \cdot \sqrt{P_{O_2}}}\right) -$$
$$k_3 \cdot \left(\frac{K_{NH_3} \cdot y_{j+N} \cdot P_{NH_3,0}}{1 + K_{NH_3} \cdot y_{j+N} \cdot P_{NH_3,0}}\right)^{2/3} \cdot \frac{(1 - y_{j+2N}) \cdot P_{Hg^T}}{(1 + K_{HCl} \cdot P_{HCl})^{n_{HCl}}} \tag{C.29}$$

$$\phi_{Hg}^2 = \frac{a_c \cdot h^2}{D_{Hg}^e} \cdot$$
$$\left(\frac{k_{ox}}{1 + \frac{P_{NO,0}}{k_{reox} \cdot P_{O_2}^{1/4}} \cdot \frac{K_{NH_3} \cdot P_{NH_3,0}}{1 + K_{NH_3} \cdot P_{NH_3,0}} + f_L \cdot K_{NH_3} \cdot P_{NH3,0}} \left(1 - \frac{1}{K_p} \cdot \frac{(1 - y_{Hg,0})}{y_{Hg,0}} \cdot \frac{P_{H_2O}}{P_{HCl}^2 \cdot \sqrt{P_{O_2}}}\right) -\right.$$
$$\left. k_{red} \cdot \left(\frac{K_{NH_3} \cdot P_{NH_3,0}}{1 + K_{NH_3} \cdot P_{NH_3,0}}\right)^{2/3} \cdot \frac{(1 - y_{Hg,0})}{(1 + K_{HCl} \cdot P_{HCl})^{n_{HCl}}}\right) \tag{C.30}$$

where k_{ox} and k_{red} are in units m/s. They are given by $k_{ox} = \frac{k_1 \cdot R \cdot T}{a_c}$ and $k_{red} = \frac{k_3 \cdot R \cdot T}{a_c}$. The fitting parameter for the reoxidation of vanadia is given by $k_{reox}[=]atm^{3/4}$.

C.6 Validation of numerical solution

The numerical solutions for the mass balances of NO (and indirectly of NH_3) and Hg^0 have been tested for limiting cases, where analytical solutions exist.

C.6.1 NO concentration profile

For $K_{NH_3} \cdot P_{NH_3} >> 1$, then the surface reaction rate becomes

$$-r_{NO} = k_{NO} \cdot P_{NO} \tag{C.31}$$

The mass balance of NO can be solved analytically for this case. The value of the analytical solution is used for comparison with the numerical solution for a given set of conditions.
This comparison shows that the numerical solution for the NO concentration at the exit of the SCR ($y_{NO,b}(z = 1)$) is accurate up to the 3rd decimal.

C.6.2 Hg^0 concentration profile

For P_{NH_3}=0 and K_P very high, then

$$-r_{Hg} = k_1 \cdot P_{Hg^0} \tag{C.32}$$

The numerical solution for the Hg^0 concentration at the exit of the SCR ($y_{Hg,b}(z = 1)$) is accurate up to the 3rd decimal.

For $P_{NO} = 0$, k_{red}=0, and K_P very high, then

$$-r_{Hg} = \frac{k_1 \cdot P_{Hg^0}}{1 + f_L \cdot K_{NH_3} \cdot P_{NH_3}} \tag{C.33}$$

The numerical solution for the Hg^0 concentration at the exit of the SCR ($y_{Hg,b}(z = 1)$) is accurate up to the 3rd decimal.

For k'$_{NO}$=0, k_{red}=0, and K_P very high, then

$$-r_{Hg} = \frac{k_1 \cdot P_{Hg^0}}{1 + \frac{P_{NO} \cdot \frac{K_{NH_3} \cdot P_{NH_3}}{1 + K_{NH_3} \cdot P_{NH_3}}}{k_{reox} \cdot P_{O_2}^{1/4}} + f_L \cdot K_{NH_3} \cdot P_{NH3}} \tag{C.34}$$

The numerical solution for the Hg^0 concentration at the exit of the SCR ($y_{Hg,b}(z = 1)$) is accurate up to the 3rd decimal.

For $K_{NH_3} \cdot P_{NH_3} >> 1$, k_{ox}=0 and K_P very high, then

$$-r_{Hg} = -k_3 \cdot P_{HgCl_2} \cdot (\frac{1}{1 + 10^6 \cdot P_{HCl}})^3 \tag{C.35}$$

The numerical solution is found, when 100% $HgCl_2$ is added at the SCR entry. The numerical solution for the Hg^0 concentration at the exit of the SCR ($y_{Hg,b}(z = 1)$) is accurate up to the 3rd decimal.

The numerical solution has converged to this accuracy at 5 collocation points.

C.7 The Fortran program

Some rate constants and parameters have been removed from the program code.

```
      module variab
      parameter (ndn=100)
      DOUBLE PRECISION K1, K2, K3,KONST1,KONST2, KONST3, BROKEQ
      DOUBLE PRECISION KHCL, KNH4CL, KA, kred, ki3, kreox, ki
      DOUBLE PRECISION fL, nNH3,n2, KHCl
      DOUBLE PRECISION Q3, PHCL, PNO, PNH3, PO2
      Double precision EE1(NDn), EE2(NDn),EE3(NDn)
      DOUBLE PRECISION E1(ndn,ndn),E2(ndn,ndn),E3(ndn,ndn)
      double precision KK1,KK2,KK3,D1(NDN),D2(NDN),D3(NDN)
      double precision G1(NDN),G2(NDN),G3(NDN)
      double precision CG1(NDN),CG2(NDN),CG3(NDN)
      DOUBLE PRECISION LNO, LNH3, LHg
      double precision THIELE2_NO, THIELE2_NH3, THIELE2_HG
      end module

c*****SCRIPT***************************************************
      program ammoniak
      use colloc
      use variab

      IMPLICIT DOUBLE PRECISION (A-H,O-Z)
      INTEGER I, J, M, N, NT, MM, NN, II, JJ
      double precision T, v, DELTAG, vN
      PARAMETER (ND=100)
  777 FORMAT(F4.0, F6.0, F8.0, F8.2, F8.2)
  779 format(' T    PHCl    PNH3    XNO     XHG')


c     DEFINE VARIABLES
C     OPERATING CONDITIONS
      T=350d0+273.14d0
```

```
      vN=10.3d0
      v=vN*T/273.14d0

c     GAS COMPOSITION
      PHCL=4.3d-6
      PNO=100d-6
      PNH3=100d-6
      Q3=100d-2
      ANR=PNH3/PNO


      call KONT(T,v,PHCL,Q3)
      write(*,779)
      write(*,777) T-273d0, PHCl*1d6, PNH3*1d6, 1d0-lNO, 1d0-LHg


      end program
c*****************************************************************


c*****IN THIS SUBROUTINE THE SYSTEM IS SPECIFIED*******************
      SUBROUTINE KONT(T,v,PHCL,Q3)
      use colloc
      use variab

      IMPLICIT DOUBLE PRECISION (A-H,O-Z)
      INTEGER I, J, M, N, NT
      double precision kg1, kg2, kg3
      double precision k0, k03, KT, LE
      PARAMETER (ND=100)
      DIMENSION Y(ND),DT(ND), DEFF(ND)

C     COLLOCATION POINTS
      M=6
      N=3*M
      NT=3*M+3

C*****PARAMETERS TO BE DEFINED
C     OPERATING CONDITIONS and SPECIATION
C     T=[K], v=[m/S], q3=Hg0/HgT

c     FLUE GAS COMPOSITION mole fraction Pi/P [dim.less]
      PHG=1.3D-9
      PO2=39D-3
      PH2O=5D-2

c     Catalyst parameters
```

```
c     ac=m2/m3, h=m, LE=m, E(epsilon)=dimløs, dh=m
      ac=955d0
      LE=42d-2
      h=2d-4
      E=76d-2
      DH=32d-4

C*****FITTING PARAMETERS
c     PARAMETERS Hg
c     OXIDATION ki3[m/s], E3R=E/R=[K]
      k03= NA
      E3R= NA
      ki3=k03*exp(-E3R/T)
      KHCl=1d6

C     REVERSE OXIDATION =REDUCTION
      DELTAG=1674D-4*T-2648D-1
      KT=EXP(-DELTAG*1000D0/831447D-5/T)

c     Ammonia on Lewis sites
      fL=0.008
C     REOXIDATION OF VANADIA SITES
      kreox=2.296d-3*exp(-3203/T)

C     REDUCTION
      kred=1.751D16*exp(-21544.1d0/T)
      nNH3=0.667d0
      n2=3d0

c     PARAMETERS NO
c     Reduction k0=[m/s], EaR[=]K
      k0= NA
      EaR= NA
      ki=k0*exp(-EaR/T)*2d0

c     Adsorption kk0=[atm-1], QR[=]K
      B=NA
      QR= NA
      KA=B*exp(QR/T)

C*****CALCULATION OF PARAMETERS
c     1: NO, 2: NH3, 3: Hg
C     DIFFUSION COEFFICIENTS M2/S
      call DIFF(T,PNO,PNH3,PHG,DT,DEFF)
c     m2/s
      Die1=DEFF(1)
      Die2=DEFF(2)
```

```
      Die3=DEFF(3)

c     FILM GAS RESISTANCE m/s

      kg1= NA
      kg2= NA
      kg3= NA

C     OTHER CONSTANTS
      BROKEQ=PH2O/KT/PHCL**2D0/PO2**5D-1
      KONST1=(h**2)*ki*ac/Die1
      KONST2=(h**2)*ki*ac/Die2
      KONST3=(h**2)*ac/Die3
      K1=0.5*kg1*h/Die1
      K2=0.5*kg2*h/Die2
      K3=0.5*kg3*h/Die3
      KK1=kg1*ac*LE/v
      KK2=kg2*ac*LE/v
      KK3=kg3*ac*LE/v

c     THIELE MODULUS
      Thiele2_NO=KONST1*KA*PNH3/(1d0+KA*PNH3)
      Thiele2_NH3=KONST2*KA*PNO/(1d0+KA*PNH3)
      DAEK=(KA*PNH3/(1d0+KA*PNH3))**nNH3
      DAEK1=KA*PNH3/(1d0+KA*PNH3)
      PAREQ=1-BROKEQ*(1D0-Q3)/Q3
      Hg1=1d0+(PNO/kreox/PO2**0.25d0)*DAEK1+fL*KA*PNH3
      Hg2=ki3*Q3/Hg1*PAREQ-KRED*DAEK*(1d0-Q3)*
     &(3.5d0/(1d0+KHCl*PHCL))**n2
      Thiele2_HG=KONST3*Hg2

C*****CALL FOR MAIN SUBROUTINE
      CALL wall(NT,Y)
      END subroutine
c*************************************************************


c*****MAIN SUBROUTINE WITH EQUATIONS**********************

      SUBROUTINE wall(NT,Y)
      use colloc
      use variab

      IMPLICIT DOUBLE PRECISION (A-H,O-Z)
      INTEGER I, J, M, N, NT
      PARAMETER (ND=100)
      DIMENSION ROOTS(ND),A(ND), B(ND), C(nd,nd)
```

```
      DIMENSION Y(ND),W(4*ND),GAUSS(ND)
      EXTERNAL FUNCW, DERIVW, OUTW
      EXTERNAL FUNC,DERIV,OUTPUT
      N=NT-3
      M=N/3

c     GUESS
      DO J=1,N
      Y(J)=1D0
      ENDDO


C*****ZEROS
      ALFA=0D0
      BETA=-5D-1
      CALL Jacobi(M,0,1,ALFA,BETA,ROOTS)
C     For calc of effectiveness factor
      CALL QUADWT(GAUSS,0)
C*****A-,B- AND C-matrix
C     A,B OG C is the same for all coupled DEs
      DO J=1,M+1
      CALL Difopr(J,A,B)
      DO I=1,M+1
      C(J,I)=4*ROOTS(J)*B(I)+2*A(I)
      ENDDO
      ENDDO


C      D-MATRIX
      TERM1=A(M+1)+K1
      TERM2=A(M+1)+K2
      TERM3=A(M+1)+K3
      DO I=1,M
      D1(I)=-A(I)/TERM1
      D2(I)=-A(I)/TERM2
      D3(I)=-A(I)/TERM3
      ENDDO
      D1(M+1)=K1/TERM1
      D2(M+1)=K2/TERM2
      D3(M+1)=K3*Q3/TERM3

      DO J=1,M
      DO I=1,M
      E1(J,I)=C(J,I)+C(J,M+1)*D1(I)
      E2(J,I)=C(J,I)+C(J,M+1)*D2(I)
      E3(J,I)=C(J,I)+C(J,M+1)*D3(I)
      ENDDO
```

```
      EE1(J)=C(J,M+1)*D1(M+1)
      EE2(J)=C(J,M+1)*D2(M+1)
      EE3(J)=C(J,M+1)*D3(M+1)
      CG1(J)=C(J,M+1)*K1/TERM1
      CG2(J)=C(J,M+1)*K2/TERM2
      CG3(J)=C(J,M+1)*K3/TERM3
      ENDDO
      G1(M+1)=K1/TERM1
      G2(M+1)=K2/TERM2
      G3(M+1)=K3/TERM3

c*****START OF SOLVING e***********************************

      NPR=-1
c     numerical jacobi
      EPS=1D-4

c     CALCULATION OF INITIAL CONDITIONS
C     DEFINE W
      W(1:N)=1D0
      W(N+1)=0D0
      W(N+2)=1D1
      W(N+3)=EPS
      W(N+4)=1D-4
      W(N+5)=0


      CALL SIRUK_XT(N,NPR,FUNC,DERIV,OUTPUT,Y,W)
      Y1=0d0
      Y2=0d0
      Y3=0d0

C     PRINT OF WALL CONCENTRATIONS AT z=0
c      DO J=1,M
c      Y1=Y1+D1(J)*Y(J)
c      Y2=Y2+D2(J)*Y(J+M)
c      Y3=Y3+D3(J)*Y(J+2*M)
c      ENDDO
c  300 FORMAT('WALLSTART:U     YNO        YNH3   YHG')
c      WRITE (10,300)
c      WRITE (*,300)
c  301 FORMAT(F10.5, F10.5, F14.5, F10.5)
c      DO I=1,M
c      write (10,301) roots(I), y(I), y(I+M), Y(I+2*M)
c      write (*,301) roots(I), y(I), y(I+M), Y(I+2*M)
c      ENDDO
c      BB=1
```

```
c      write (*,301) BB, Y1, Y2, Y3
c      write (10,301) BB, Y1, Y2, Y3
C*****************************************************************

C     SOLVING OF 2M COUPLED ALGEBRAIC EQUATIONS
C                                        OG 2 DIFFERENTIALEQUATIONS
C     INITIAL CONDITIONS FOR DIFF.EQUATIONS
      Y(N+1)=1d0
      Y(N+2)=1d0
      Y(N+3)=Q3
C     DEFINERER W
      W(1:NT)=1D0
      W(NT+1)=0D0
      W(NT+2)=1D0
      W(NT+3)=EPS
      W(NT+4)=1D-4
      W(NT+5)=N

      NPR=-1

      CALL SIRUK_XT(NT,NPR,FUNCW,DERIVW,OUTW,Y,W)

C      PRINT OF WALL CONCENTRATIONS AT z=1
c  400 FORMAT('WALL_END:U     YNO        YNH3      YHG')
c      WRITE (10,400)
c      WRITE (*,400)
c  401 FORMAT(F10.5, F10.5, F14.5, F10.5)
c      DO I=1,M
c      write (10,401) roots(I), y(I), y(I+M), Y(I+2*M)
c      write (*,401) roots(I), y(I), y(I+M), Y(I+2*M)
c      ENDDO
c      Y1=G1(M+1)*Y(N+1)
c      Y2=G2(M+1)*Y(N+2)
c      Y3=G3(M+1)*Y(N+3)
c
c      DO J=1,M
c      Y1=Y1+D1(J)*Y(J)
c      Y2=Y2+D2(J)*Y(J+M)
c      Y3=Y3+D3(J)*Y(J+2*M)
c      ENDDO
c      write (*,401) BB, Y1, Y2, Y3
c      write (10,401) BB, Y1, Y2, Y3
      END SUBROUTINE
c*****************************************************************


C*****SOLVING COUPLED NON-LINEAR EQUATIONS VIA SIRUKE*****************
```

```
      SUBROUTINE FUNCW(NT,Y,F)
      use colloc
      use variab

      IMPLICIT DOUBLE PRECISION (A-H,O-Z)
      INTEGER I, J, M, N, NT
      PARAMETER (ND=100)
      DIMENSION Y(NT),f(nT)

      N=NT-3
      M=N/3
c     1: NO, 2: NH3, 3: Hg

      DO J=1,M
      F(J)=CG1(J)*Y(N+1)-Y(J)*Y(J+M)*KONST1*KA*PNH3/(1+KA*Y(J+M)*PNH3)
      DO I=1,M
      F(J)=F(J)+ E1(J,I)*Y(I)
      ENDDO
      ENDDO

      DO J=M+1,2*M
      F(J)=CG2(J-M)*Y(N+2)-Y(J)*Y(J-M)*KONST2*KA*PNO/(1+KA*Y(J)*PNH3)
      DO I=M+1,2*M
      F(J)=F(J)+ E2(J-M,I-M)*Y(I)
      ENDDO
      ENDDO

      DO J=2*M+1,N
      DAEK=(KA*Y(J-M)*PNH3/(1+KA*Y(J-M)*PNH3))**nNH3
      DAEK1=KA*Y(J-M)*PNH3/(1+KA*Y(J-M)*PNH3)
      PAREQ=1-BROKEQ*(1D0-Y(J))/Y(J)
      Hg1=1+(Y(J-2*M)*PNO/kreox/PO2**0.25d0)*DAEK1+fL*KA*Y(J-M)*PNH3
      Hg2=ki3*Y(J)/Hg1*PAREQ-KRED*DAEK*(1-Y(J))*
     &(3.5d0/(1d0+KHCl*PHCL))**n2
      F(J)=CG3(J-2*M)*Y(N+3)-KONST3*Hg2
      DO I=2*M+1,N
      F(J)=F(J)+ E3(J-2*M,I-2*M)*Y(I)
      ENDDO
      ENDDO

      F(N+1)=KK1*Y(N+1)*(G1(M+1)-1)
      F(N+2)=KK2*Y(N+2)*(G2(M+1)-1)
      F(N+3)=KK3*Y(N+3)*(G3(M+1)-1)
      DO I=1,M
      F(N+1)=F(N+1)+KK1*D1(I)*Y(I)
      F(N+2)=F(N+2)+KK2*D2(I)*Y(I+M)
```

```
      F(NT)=F(NT)+KK3*D3(I)*Y(I+2*M)
      ENDDO
      END SUBROUTINE


      SUBROUTINE DERIVW(NT,Y,DF)
      use variab
      use colloc
      IMPLICIT DOUBLE PRECISION (A-H,O-Z)
      INTEGER I, J, M, N, NT
      DIMENSION Y(NT), DF(NT,NT)
      END SUBROUTINE


      SUBROUTINE OUTW(NT,ZETA,Y)
      use colloc
      use variab
      IMPLICIT DOUBLE PRECISION (A-H,O-Z)
      INTEGER I, J, M, N, NT
      DIMENSION Y(Nt)

      IF (ZETA.EQ.1D0) THEN
      LNO=Y(NT-2)
      LNH3=Y(NT-1)
      LHg=Y(NT)
      ENDIF
      END SUBROUTINE
C*********************************************************************


C*****SOLVING EQUATIONS FOR WALL TO FIND INITIAL CONDITIONS************

      SUBROUTINE FUNC(N,Y,F)
      use colloc
      use variab

      IMPLICIT DOUBLE PRECISION (A-H,O-Z)
      INTEGER I, J, M, N
      PARAMETER (ND=100)
      DIMENSION Y(N),f(n)
      M=N/3

c     1: NO, 2: NH3, 3: Hg
      DO J=1,M
      F(J)=EE1(J)-Y(J)*Y(J+M)*KONST1*KA*PNH3/(1+KA*Y(J+M)*PNH3)
      DO I=1,M
      F(J)=F(J)+ E1(J,I)*Y(I)
```

```
      ENDDO
      ENDDO

      DO J=M+1,2*M
      F(J)=EE2(J-M)-Y(J)*Y(J-M)*KONST2*KA*PNO/(1+KA*Y(J)*PNH3)
      DO I=M+1,2*M
      F(J)=F(J)+ E2(J-M,I-M)*Y(I)
      ENDDO
      ENDDO


      DO J=2*M+1,N
      DAEK=(KA*Y(J-M)*PNH3/(1+KA*Y(J-M)*PNH3))**nNH3
      DAEK1=KA*Y(J-M)*PNH3/(1+KA*Y(J-M)*PNH3)
      PAREQ=1-BROKEQ*(1D0-Y(J))/Y(J)
      Hg1=1+(Y(J-2*M)*PNO/kreox/PO2**0.25d0)*DAEK1+fL*KA*Y(J-M)*PNH3
      Hg2=ki3*Y(J)/Hg1*PAREQ-KRED*DAEK*(1-Y(J))*
     &(3.5d0/(1d0+KHCl*PHCL))**n2
      F(J)=EE3(J-2*M)-KONST3*Hg2
      DO I=2*M+1,N
      F(J)=F(J)+ E3(J-2*M,I-2*M)*Y(I)
      ENDDO
      ENDDO
      END SUBROUTINE


      SUBROUTINE DERIV(N,Y,DF)
      use variab
      use colloc
      IMPLICIT DOUBLE PRECISION (A-H,O-Z)
      INTEGER I, J, M, N
      DIMENSION Y(N)
      DIMENSION  DF(N,N)
      END SUBROUTINE


      SUBROUTINE OUTPUT(N,ZETA,Y)
      use colloc
      IMPLICIT DOUBLE PRECISION (A-H,O-Z)
      INTEGER I, J, M, N
      DIMENSION Y(N)
      END SUBROUTINE
C***********************************************************************


C*****DIFFUSION*********************************************************
      SUBROUTINE DIFF(T,PNO,PNH3,PHG,DT,DEFF)
```

```
      IMPLICIT DOUBLE PRECISION (A-H,M,O-Z)
      INTEGER I, J, N
      PARAMETER (ND=15)
      DOUBLE PRECISION KT1,P,RHOP, LAB
C      DOUBLE PRECISION
      DIMENSION MW(ND), SIGMA(ND), EPSK(ND), VP(ND)
      DIMENSION MW_A(ND),SIGMA_A(ND), EPSK_A(ND)
      DIMENSION MWT(ND), SIGMAT(ND), DK(ND,ND)
      DIMENSION OHM(ND), EPSKT(ND), TSTAR(ND)
      DIMENSION Y(ND), Y_A(ND), TRM(ND), D_AB(ND)
      DIMENSION DT(3),TRM2(ND), RP(ND)
      DIMENSION ESPI(ND), Dp(ND,ND), Deffi(ND,ND)
      Dimension DEFF(3), sumb(ND)
C     Y_A; 1: NO, 2: NH3, 3: HG
C     Y(1): N2

C     PARAMETERS TO BE DEFINED
      Y_A(1)=PNO
      Y_A(2)=PNH3
      Y_A(3)=PHG
      Y(1)=1d0
C     p=[ATM]
      P=1D0
C**** CONSTANTS FOR BULK DIFFUSION**********************
C     [G/MOL]
      MW_A(1)=3000D-2
      MW_A(2)=1703D-2
      MW_A(3)=20059D-2
      MW(1)=2801D-2

C     COLLISION DIAMETER
C     [Å]
      SIGMA_A(1)=3492D-3
      SIGMA_A(2)=2900D-3
      SIGMA_A(3)=2969D-3
      SIGMA(1)=3798D-3

C     CHARACTERISTIC LENNARD-JONES ENERGY DIVIDED BY KB
C     [K]
      EPSK_A(1)=1167D-1
      EPSK_A(2)=5583D-1
      EPSK_A(3)=750D0
      EPSK(1)=714D-1

C     LENNARD JONES POTENTIAL BY NEUFIELD ET AL.
      A=106036D-5
```

```
      B=15610D-5
      C=19300D-5
      D=47635D-5
      E=103587D-5
      F=152996D-5
      G=176474D-5
      H=389411D-5
      KT1=0.0018583D0

c*****CONSTANTS FOR EFFECTIVE DIFFUSION*****************************
c     [kg/m3]
      RHOP=1D3
c     Turtuosity via labyrinth factor
      LAB=333D-3
c     PORE SIZES [Å]
      RP(1)=173911.5d0
      RP(2)=123361.9d0
      RP(3)=71898.6d0
      RP(4)=36970.2d0
      RP(5)=4343.5d0
      RP(6)=820.3d0
      RP(7)=191.8d0
      RP(8)=31.1d0


C     PORE SIZE DISTRIBUTION vol [m3/kg]
      Vp(1)=NA
      Vp(2)=NA
      Vp(3)=NA
      Vp(4)=NA
      Vp(5)=NA
      Vp(6)=NA
      Vp(7)=NA
      Vp(8)=NA

C*****CALCULATIONS**************************************************

      DO I=1,3
      MWT(I)=1/MW_A(I)+1/MW(1)
      SIGMAT(I)=(SIGMA_A(I)+SIGMA(1))/2
      EPSKT(I)=SQRT(EPSK_A(I)*EPSK(1))
      TSTAR(I)=T/EPSKT(I)
      OHM(I)=A/(TSTAR(I)**B)+C/(EXP(D*TSTAR(I)))
     &+E/(EXP(F*TSTAR(I)))+G/(EXP(H*TSTAR(I)))
      TRM(I)=P*(SIGMAT(I))**2*OHM(I)
      TRM2(I)=SQRT(MWT(I)*(T**3))
      D_AB(I)=KT1*TRM2(I)/TRM(I)
```

```
c     BULK DIFF-COEFFICIENT [m2/s]
      DT(I)=D_AB(I)/1d4
      ENDDO

      sumb(1:3)=0d0
      DO I=1,8
      ESPI(I)=RHOP*Vp(I)
      DO J=1,3
      DK(I,J)=3.493D-5*RP(I)*SQRT(T/MW_A(J))
      Dp(I,J)=1/(1/DK(I,J)+1/DT(J)/3600d0)
      Deffi(I,J)=LAB*ESPI(I)*Dp(I,J)
      sumb(J)=sumb(J)+Deffi(I,J)
      ENDDO
      ENDDO
c     [m2/s]
      Deff(1:3)=sumb(1:3)/3600d0

      END SUBROUTINE

c**********************************************************************
```

Appendix D

List of acronyms

Symbol	Description
APCD	Air pollution control device
EPA	U.S. Environmental Protection Agency
FGD	Flue gas desulfurisation
ICR	Information collection request
PCD	Particulate control device
SCR	Selective catalytic reduction

Appendix E

List of symbols and abbreviations

Symbol	Description
Dependent variables	
P_i	Partial pressure of component i in the catalyst wall [atm]
P_{ib}	Partial pressure of component i in the catalyst channel [atm]
P_{is}	Partial pressure of component i on the catalyst external surface [atm]
y_i	Dimensionless partial pressure of component $i = NO, NH_3$ in the catalyst wall: $y_i = \frac{P_i}{P_{i,0}}$
y_{Hg}	Dimensionless partial pressure of Hg in the catalyst wall: $y_{Hg} = \frac{P_{Hg^0}}{P_{Hg^T,0}}$
y_{ib}	Dimensionless partial pressure of component i in the catalyst channel
y_{is}	Dimensionless partial pressure of component i on the catalyst external surface
Independent variables	
x	Distance from catalyst wall center [m]
z	Distance in the catalyst channel [m]
$x*$	Dimensionless distance from catalyst wall center: $x* = \frac{x}{h}$

Continued on next page...

Symbol	Description
u	Dimensionsless variable: $u = x*^2 = (\frac{x}{h})^2$
$z*$	Dimensionless distance in the catalyst channel: $z* = \frac{z}{L}$
Catalyst parameters	
h	Half catalyst wall thickness [m]
L	Length of catalyst channel [m]
a_c	Geometric surface area of catalyst $[\frac{m^2}{m^3}]$
A_z	Cross-sectional area of monolith $[m^2]$
ϵ	Void fraction in monolith [dim.less]
Operating conditions	
$P_{i,0}$	Inlet partial pressure of component i [atm]
y_{i0}	Dimensionless inlet partial pressure of component i
v	Linear flow rate of gas in the channel ('empty tower') $v = \frac{U}{A_z}$ $[\frac{m}{s}]$
v_{eff}	Effective linear flow rate in monolith channel $v = \frac{U}{A_z \cdot \epsilon}$ $[\frac{m}{s}]$
F_i	Molar flow of component i in the gas $[\frac{mol}{s}]$
U	Convective flow of gas $[\frac{m^3}{s}]$
Parameters in model	
Bi_i	Dimensionless Biot number for component i: $Bi_i = \frac{k_i^g h}{D_i^e}$
D_i	Bulk diffusion coefficient of component i $[\frac{m^2}{s}]$
D_i^e	Effective diffusion coefficient in catalyst wall for component i $[\frac{m^2}{s}]$
f_L	Fraction of NH_3 adsorbing on Lewis sites to Brønsted sites: $K_{L,NH3} = f_L \cdot K_{NH3}$
k_1, k_3	Reaction rate constants for reaction R1 and R2 $[\frac{mol}{m^3 \cdot atm \cdot s}]$
$k_{g,i}$	Mass transfer coefficient across film layer for component i $[\frac{m}{s}]$
k_{NO}	Reaction rate constant for reaction R3 $[\frac{mol}{m^3 \cdot atm \cdot s}]$
k'_{NO}	Reaction rate constant for reaction R3 $[\frac{m}{s}]$
k_{ox}, k_{red}	Reaction rate constants for reaction R1 and R2 $[\frac{m}{s}]$
k_{reox}	Rate of vanadia reoxidation to rate of DeNOx reaction $[atm^{3/4}]$

Continued on next page...

Symbol	Description
K_i	Adsorption coefficient for component i $[atm^{-1}]$
K_P	Equilibrium constant for Hg^0 oxidation via reaction R1
$K1, K2, K3$	Dimensionless constant for component 1:NO, 2: NH_3 and 3: Hg^0: $K1, K2, K3 = \frac{Bi_{1-3}}{2}$
$KK1, KK2, KK3$	Dimensionless constant for component 1:NO, 2: NH_3 and 3: Hg^0: $KK1, KK2, KK3 = \frac{k_{g,1-3} \cdot a_c \cdot L}{v}$
n_{HCl}	Dim.less order of HCl dependency in the reaction rate for R2 via $\left(\frac{1}{1+K_{HCl} \cdot P_{HCl}}\right)^{n_{HCl}}$
r_i	Rate of production of component i in the catalyst wall $[\frac{mol}{m^3 \cdot s}]$
ϕ_i	Dim.less Thiele modulus for component i: $\phi_i^2 = \frac{h^2}{P_{i,b} \cdot D_i^e} \cdot (-r_{s,i}(P_{i,b}))$
θ_i	Coverage of adsorbed component i on the catalyst: $\theta_i = \frac{K_i \cdot P_i}{1+K_i \cdot P_i}$
Parameters in calculation of properties	
$T*$	Dimensionless temperature $T* = \frac{\kappa \cdot T}{\in}$
$\in$	Lennard-Jones characteristic energy $[J]$
$\Omega_{D,AB}$	Collision integral
σ	Collision diameter $[\mathring{A}]$
Physical constants	
R	Universal gas constant $R = 8.2057 \cdot 10^{-5} {}^{atm \cdot m^3}/_{mol \cdot K}$
κ	Boltzmann's constant $\kappa = 1,38066 \cdot 10^{-23} {}^{J}/_{K}$
Normal conditions	
P_N	P=1 atm
T_N	T=273.14K

Bibliography

AMAP/UNEP (2008). Technical background report to the global atmospheric mercury assessment. Arctic monitoring and assessment programme /UNEP Chemicals Branch, 159 pp. http://www.chem.unep.ch/mercury/Atmospheric_Emissions/Technical_background_report.pdf (accessed July 18, 2011) .

Beeckman, J. and L. Hegedus (1991). Design of monolith catalysts for power plant NOx emission control. *Industrial & Engineering Chemistry Research 30*, 969–978.

Beretta, A., C. Orsenigo, N. Ferlazzo, E. Tronconi, and P. Forzatti (1998). Analysis of the performance of plate-type monolithic catalysts for selective catalytic reduction DeNOx applications. *Industrial & Engineering Chemistry Research 37*, 2623–2633.

Bird, R., W. Stewart, and E. Lightfoot (2002). *Transport Phenomena - Second Edition*. University of Wisconsin-Madison, USA: John Wiley and Sons, Inc.

Bock, J., M. Hocquel, S. Unterberger, and K. Hein (2002). Mercury oxidation across SCR catalysts of flue gas with varying HCl concentrations. *Proceedings for Air Quality III, Arlington, VA, September 9-12*.

Castellino, F. (2008). *Deactivation of SCR Catalysts by Additives* . Copenhagen, Denmark (ISBN: 978-87-91435-81-1): Frydenberg A/S.

Chu, P., D. Laudal, L. Brickett, and C. Lee (2003). Power plant evaluation of the effect of SCR technology on mercury. *Combined Power Plant Air Pollutant Control Mega Symposium, Washington, DC, May 19-22*.

Dumesic, J., N. Topsøe, H. Topsøe, Y. Chen, and T. Slabiak (1996). Kinetics of selective catalytic reduction of nitric oxide by ammonia over vanadia/titania. *Journal of Catalysis 163*, 409–417.

Dunham, G., R. DeWall, and C. Senior (2003). Fixed-bed studies of the interactions between mercury and coal combustion fly ash. *Fuel Processing Technology 82*, 197–213.

Eom, Y., S. Jeon, T. A. Ngo, J. Kim, and T. G. Lee (2008). Heterogeneous mercury reaction on a selective catalytic reduction (SCR) catalyst. *Catalyst Letters 121*, 219–225.

EPA (2011a). Health effects of mercury. From homepage of the US Environmental Protection Agency: http://www.epa.gov/mercury/effects.htm (accessed July 18) .

EPA (2011b). Mercury and air toxics standards (MATS) for power plants. From homepage of the US Environmental Protection Agency on 18^{th} of July: http://www.epa.gov/airquality/powerplanttoxics/actions.html .

Eswaran, S. and H. Stenger (2008). Effect of halogens on mercury conversion in SCR catalysts. *Fuel Processing Technology 89(11)*, 1153–1159.

Evans, R., G. Watson, and E. Mason (1961). Gaseous diffusion in porous media at uniform pressure. *Journal of Chemical Physics 35*, 2076–2083.

Frandsen, F., K. Dam-Johansen, and P. Rasmussen (1994). Trace elements from combustion and gasification of coal - an equilibrium approach. *Progress in Energy and Combustion Science 20*, 115–138.

Gabrielsson, P. and H. G. Pedersen (2008). *Handbook of Heterogeneous Catalysis- 2nd Edition, Flue Gases from Stationary Sources*. Germany: Wiley-VCH.

Gale, T. K., B. W. Lani, and G. R. Offen (2008). Mechanisms governing the fate of mercury in coal-fired power systems. *Fuel Processing Technology 89*, 139–151.

Ghorishi, S. B., C. Lee, and J. D. Kilgroe (1999). Mercury speciation in combustion systems: Studies with simulated flue gases and model fly ashes . *Proceedings of the AWMA 92nd Annual Conference and Exhibition, St. Louis, MO, June 20-24*.

Giakoumelou, I., C. Fountzoula, C. Kordulis, and S. Boghosian (2006). Molecular structure and catalytic activity of V_2O_5/TiO_2 catalysts for the SCR of NO by NH3: In situ Raman spectra in the presence of O_2, NH_3, NO, H_2, H_2O, and SO_2. *Journal of Catalysis 239*, 1–12.

Granite, E., H. Pennline, and R. Hargis (2000). Novel sorbents for mercury removal from flue gas. *Industrial & Engineering Chemistry Research 39*, 1020–1029.

He, S., J. Zhou, Y. Zhu, Z. Luo, M. Ni, and K. Cen (2009). Mercury oxidation over a vanadia-based selective catalytic reduction catalyst. *Energy & Fuels 23*, 253–259.

Hocquel, M. (2004). *The behaviour and fate of mercury in coal-fired power plants with downstream air pollution control devices*. Düsseldorf, Germany (ISBN: 3-18-325115-9): VDI Verlag.

Hong, H., S. Ham, M. Kim, S. Lee, and J. Lee (2010). Characteristics of commercial selective catalytic reduction catalyst for the oxidation of gaseous elemental mercury with respect to reaction conditions. *Korean Journal of Chemical Engineering 27(4)*, 1117–1122.

Huggins, F., N. Yap, and G. Huffman (2000). Investigation of mercury adsorption on Cherokee fly-ash using XAFS spectroscpy. *Proceedings of the AWMA 93rd Annual Conference and Exhibition, Salt Lake City, UT, June 18-22*.

Huggins, F., N. Yap, G. Huffman, and C. Senior (2003). XAFS characterization of mercury captured from combustion gases on sorbents at low temperatures. *Fuel Processing*

Technology 82, 167–196.

Kamata, H., S. Ueno, T. Naito, A. Yamaguchi, and S. Ito (2008). Mercury oxidation by hydrochloric acid over a VOx/TiO2 catalyst. *Catalysis Communications 9*, 2441–2444.

Kolker, A., C. Senior, and J. Quick (2006). Mercury in coal and the impact of coal quality on mercury emissions from combustion systems. *Applied geochemistry 21*, 1821–1836.

Lee, C., J. D. Kilgroe, and S. B. Ghorishi (2000). Speciation of Mercury in the Presence of Coal and Waste. *Proceedings of the AWMA 93rd Annual Conference and Exhibition, Salt Lake City, UT, June 18-22*.

Lee, C., R. Srivastava, S. B. Ghorishi, J. Karwowski, T. Hastings, and J. Hirschi (2004). Effect of SCR catalyst on mercury speciation. *Combined Power Plant Air Pollutant Control Mega Symposium, Washington, DC, August 30 - September 2*.

Lietti, L., P. Forzatti, and F. Bregani (1996). Steady-state and transient reactivity study of TiO_2-supported V_2O_5-WO_3 De-NOx catalysts: Relevance of the vanadium-tungsten interaction on the catalytic activity. *Industrial & Engineering Chemistry Research 35*, 3884–3892.

López-Antón, M., P. Abad-Valle, M. Díaz-Somoano, I. Suárez-Ruiz, and M. R. Martínez-Tarazona (2009). The influence of carbon particle type in fly ashes on mercury adsorption. *Fuel 88*, 1194–1200.

Machalek, T., M. Ramavajjala, M. Richardson, C. Richardson, C. Dene, B. Goeckner, H. Anderson, and A. Morris (2003). Pilot evaluation of flue gas reactions across an SCR unit. *Combined Power Plant Air Pollutant Control Mega Symposium, Washington, DC, May 19-22*.

Michaelsen, M. and S. Wedel (2006). Fortran program. Department of Chemical and Biochemical Engineering, Technical University of Denmark.

Miller, C., T. Feeley, W. Aljoe, B. Lani, K. Schroeder, C. Kairies, A. McNemar, A. Jones, and J. Murphy (2006). Mercury capture and fate using wet FGD at coal-fired power plants - DOE/NETL Mercury and wet FGD R&D, August. http://www.netl.doe.gov/technologies/coalpower/ewr/coal_utilization_byproducts/pdf/mercury_%20FGD%20white%20paper%20Final.pdf (accessed July 18, 2011).

Niksa, S. and N. Fujiwara (2005). A predictive mechanism for mercury oxidation on selective catalytic reduction catalysts under coal-derived flue gas. *Journal of the Air & Waste Management Association 55*, 1866–1875.

Niksa, S., J. Helble, and N. Fujiwara (2001). Kinetic modeling of homogeneous mercury oxidation: The importance of NO and H_2O in predicting oxidation in coal-derived systems. *Environmental Science & Technology 35*, 3701–3706.

Norton, G., H. Yang, R. Brown, D. Laudal, G. Dunham, and J. Erjavec (2003). Heterogeneous oxidation of mercury in simulated post combustion conditions. *Fuel 82*, 107–116.

Nova, I., C. Ciardelli, E. Tronconi, D. Chatterjee, and B. Bandl-Konrad (2006). NH_3-SCR of NO over a V-based Catalyst: Low-T Redox Kinetics with NH_3 Inhibition. *AIChE Journal 52*, 3222–3233.

Pavlish, J., E. Sondreal, M. Mann, E. Olson, K. Galbreath, D. Laudal, and S. Benson (2003). Status review of mercury control options for coal-fired power plants. *Fuel Processing Technology 82*, 89–165.

Reid, R., J. Prausnitz, and B. Poling (1987). *The properties of gases and liquids - 4th edition*. Massachusetts Institute of Technology, USA: McGraw Hill.

Richardson, C., T. Machalek, S. Miller, C. Dene, and R. Chang (2002). Effect of NOx control processes on mercury speciation in utility flue gas. *Journal of the Air & Waste Management Association 52*, 941–947.

Satterfield, C. (1980). *Heterogeneous catalysis in practice* . Massachusetts Institute of Technology, USA: McGraw-Hill Book Company.

Senior, C. (2001). Behavior of mercury in air pollution control devices on coal-fired utility boilers, Prepared for power production in the 21st century: Impacts of fuel quality and operations. *Engineering Foundation Conference, Snowbird, UT, October 28-November 2*.

Senior, C. (2004a). Oxidation of Mercury across SCR catalysts in coal-fired power plants burning low rank fuels, Quarterly progress report - DOE cooperative agreement no: DE-FC26-03NT41728, April 30.

Senior, C. (2004b). Oxidation of Mercury across SCR catalysts in coal-fired power plants burning low rank fuels, Quarterly progress report - DOE cooperative agreement no: DE-FC26-03NT41728, July 30.

Senior, C. (2004c). Oxidation of Mercury across SCR catalysts in coal-fired power plants burning low rank fuels, Quarterly progress report - DOE cooperative agreement no: DE-FC26-03NT41728, October 29.

Senior, C. (2006). Oxidation of mercury across selective catalytic reduction catalysts in coal-fired power plants. *Journal of the Air & Waste Management Association 56*, 23–31.

Senior, C., A. Sarofim, T. Zeng, J. Helble, and R. Mamani-Paco (2000). Gas-phase transformations of mercury in coal-fired power plants. *Fuel Processing Technology 63*, 197–213.

Serre, S., C. Lee, P. Chu, and T. Hastings (2008). Evaluation of the impact of chlorine on mercury oxidation in a pilot-scale coal combustor - the effect of coal blending. *Combined Power Plant Air Pollutant Control Mega Symposium, Baltimore, MD, August 25-28*.

Sibley, A., W. Hinton, A. Jimenez, and C. Dene (2008). Pilot scale studies of mercury oxidation by SCR catalysts. *Combined Power Plant Air Pollutant Control Mega Symposium, Baltimore, MD, August 25-28*.

Slabiak, T. (2005). DeNOx med SCR. *Brændsels- og Energiteknisk Selskab, Hvidovre,*

Denmark, April 12-13.

Sliger, R., J. Kramlich, and N. Marinov (2000). Towards the development of a chemical kinetic model for the homogeneous oxidation of mercury by chlorine species. *Fuel Processing Technology 65-66*, 423–438.

Struckmann, P., H. Gutberlet, R. Stolle, and H. Köser (2008). Determining the mercury oxidation capability of SCR catalyst, EPRI's 2008 Workshop on SCR, Charlotte, North Carolina, November 11-13.

Thorwarth, H. (2007). *Trace element behaviour in pulverized fuel fired power plants - Impact of fuels and emission control technologies*. Göttingen, Germany (ISBN: 978-3-86727-343-5): Cuvillier Verlag.

Tillman, D., D. Duong, and B. Miller (2009). Chlorine in solid fuels fired in pulverized fuel boilers - Sources, forms, reactions, and consequences: A literature review. *Energy & Fuels 23*, 3379–3391.

TOMERED - Deliverable D08 (2006). Project number ENK5-CT-2002-00699: Development of theoretical and CFD models for prediction of ToMe behaviour during combustion and flue gas treatment in large scale plants, April 11.

Topsoe, N. (1994). Mechanism of the selective catalytic reduction of nitric oxide by ammonia elucidated by in situ on-line fourier transform infrared spectroscopy. *Science 265*, 1217–1219.

UNECE (2011). The 1998 Aarhus Protocol on Heavy Metals. From homepage of the United Nations Economic Commission for Europeon 18^{th} of July: http://www.unece.org/env/lrtap/full%20text/1998.Heavy.Metals.e.pdf .

Vassilev, S., G. Eskenazyb, and C. Vassileva (2000). Contents, modes of occurrence and origin of chlorine and bromine in coal. *Fuel 79*, 903–921.

Withum, J. A. (2006). Evaluation of mercury emissions from coal-fired facilities with SCR and FGD systems - DOE/NETL Cooperative Agreement DE-FC26-02NT41589, Project Final Report - April 2006 .

Zhuang, Y., J. Laumb, R. Liggett, M. Holmes, and J. Pavlish (2007). Impacts of acid gases on mercury oxidation across SCR catalyst. *Fuel Processing Technology 88*, 929–934.